NETHERLANDS GEODETIC COMMISSION
PUBLICATIONS ON GEODESY
NEW SERIES
NUMBER 35

THE GEODETIC BOUNDARY VALUE PROBLEM IN TWO DIMENSIONS AND ITS ITERATIVE SOLUTION

by

MARTIN VAN GELDEREN

1991

NEDERLANDSE COMMISSIE VOOR GEODESIE, THIJSSEWEG 11, DELFT, THE NETHERLANDS

PRINTED BY W. D. MEINEMA B.V., DELFT, THE NETHERLANDS

ISBN 90 6132 241 3

Contents

Abstract

In this thesis, the geodetic boundary value problem (GBVP) for a completely hypothetical earth is developed. As already shown in (Gerontopoulos, 1978), the complete GBVP for a 2D earth can be set up. It can serve as an example for the real 3D one, with the advantage of less complex mathematics and better performable numerical simulations.

In chapter *one*, the points of departure of this thesis are discussed. It is underlined that we do not seek for a strict mathematical solution of the GBVP, as done by Gerontopoulos, but investigate aspects of the 2D GBVP that have correspondence with the 3D case. This introductory chapter is concluded by an overview of the history of the problem of the determination of the figure of the earth.

Chapter *two* serves as preparation for the formulation and solution of the GBVP. Some points of the potential theory in the plane are treated and special attention is paid to the series solution of the potential for a circular boundary, which is an ordinary Fourier series. Finally expressions are derived for the integral kernels appearing in the solution of the GBVP.

In chapter *three*, the linear observation equations are derived for the classical observations potential, gravity and astronomical latitude, and for the components of the gravity gradient tensor. From several combinations of these observables, the potential, and the position are solved with the observation equations in circular, and constant radius approximation. For their solution, closed integral expressions are given. The systems of equations can be either uniquely determined or overdetermined. This yields solutions for the disturbing potential which are almost identical to the 3D problem. It is also possible to solve, in this approximation, the GBVP analytically from discrete measurements. The analytical expression derived for the inverse normal matrix can be used for error propagation. It is shown that the integral of astronomical leveling can be derived from the solution of the GBVP with observations of astronomical latitude. Furthermore, attention is paid to the zeroth and first degree coefficients, and to the application of the theory of reliability to the GBVP.

In chapter *four*, first the effect of the neglect of the topography and the ellipticity is analysed. It follows an iteration method can be applied in order to obtain solutions of the GBVP without, or with only little, approximation. Then, five levels of approximation are defined: three linear approximations (with or without the

topography and/or the ellipticity taken into account), a quadratic model and the exact, non-linear equations. In the iteration the analytical solutions of the GBVP's in circular, constant radius approximation are used for the solution step. For the backward substitution the model is applied for which the solution is sought for. The problems are solved numerically by iteration in chapter five. The iterative solution of the problem in circular approximation, occasionally referred to as the simple problem of Molodensky, is also given as a series of integrals. For the convergence of the iteration criteria are derived.

In chapter *five*, the generation of a synthetical world is presented. The features of the real world, with respect to the topography and the gravity field, are used to determine its appearance. The observations are computed, from which the potential and the position are solved by the iteration, for all five levels of approximation defined. The fixed, scalar and vectorial problem are considered. It turns out that, in case band limited observations without noise are used, the ellipticity of the earth, not taken into account in the solution step of the iteration, is the main obstacle for convergence. This can be overcome by the use of a potential series with elliptical coordinates, instead of the polar coordinates usually applied. The theoretical condition for convergence of the iteration is tested, and for several circumstances the accuracy of the solution of the potential and position unknowns is computed. We mention: uniquely determined and overdetermined problems, band limited observations, block averages and point values, number of points etc. Finally, the error spectra of the solved coefficients are compared to the error estimates obtained by error propagation with the analytical expression for the inverse normal matrix of the GBVP in circular, constant radius approximation, and a simple noise model for the observations. If the data noise is the dominant error source, this error estimation turns out to work very well.

Acknowledgments

In the first place I like to thank Reiner Rummel for his ideas, support and his encouraging enthusiasm. I also thank my friend and colleague Radboud Koop, and the other members of our section, for the discussions, both scientific and not, and the atmosphere necessary for writing a thesis. The discussions with Prof. Teunissen and Prof. Krarup are gratefully acknowledged.

1 |

Introduction

ALTHOUGH THE NAME currently used to indicate the problem of the determination of the figure of the earth and its gravity field, the *geodetic boundary value problem*, was introduced only in this century, the interest of mankind in the shape of the earth is already very old. A brief overview of its history, from antiquity up to the recent developments, is given in the last section of this chapter. But first the motives and the points of departure of this thesis are discussed.

About this thesis

In (Rummel & Teunissen, 1982) a new approach to the geodetic boundary value problem (GBVP) was presented. This was elaborated in (Rummel & Teunissen, 1986) and (Rummel et al., 1989). A solution is found of the free boundary value problem for the exterior domain, from data given on the earth's surface. Like with Molodensky's approach, there is no need for reduction towards the geoid. The results were promising. The formulation can be applied to uniquely determined as well as overdetermined GBVP's, 'horizontal' observations (which depend on a horizontal derivative of the potential in spherical approximation) can be included easily, error propagation is straightforward and iteration seems feasible. But a number of aspects demand further consideration. We mention *sampling* (discrete observations vs. the requirement of continuous data), *noise modeling* (how to define a suitable noise model for discrete observations which can be used with the continuous formulation of the GBVP), the implementation of an *iteration* procedure and *numerical verification* of the theoretical results.

It seemed attractive to try out the same concept on a two-dimensional earth. This 2D earth is *not* a planar approximation of the curved boundary of the real earth, but a complete 2D world with an one-dimensional boundary, as used in (Sansò, 1977) and (Gerontopoulos, 1978). This hypothetical earth can be imagined as an infinitely thin slice of the real earth through its center and poles (see figure 1.1). The 2D earth has a number of advantages over the 3D one. The reduction of the dimension by

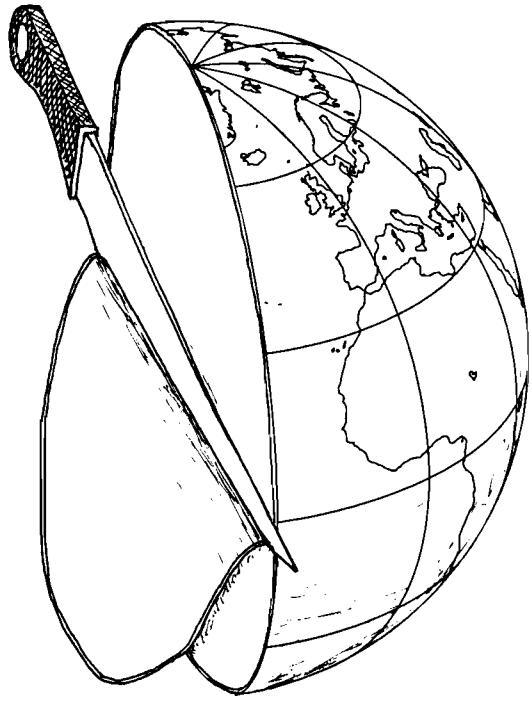

Figure 1.1 *The preparation of a two dimensional earth.*

one releases us from awkward things such as meridian convergence, azimuths and Legendre functions. Strong mathematical tools are available: conformal mapping, used by Gerontopoulos for his solutions to the 2D GBVP, the theory of complex numbers and Fourier series. One can expect that the extensive literature on time series, with well-formulated theorems on sampling, discrete and continuous signals, averaging and noise modeling, can be applied to the GBVP. The formulae are simpler and more compact, because of the reduction of the number of parameters. This facilitates not only the interpretation of the formulae, but also the implementation of numerical tests.

Unfortunately, the examination of the 2D earth does not only bring advantages. As long as the real world is still three-dimensional, we are ultimately interested in the properties of the 3D GBVP. This brings up the question to which extent the results obtained by considering the 2D problem, are valid for 3D. Although we are rather confident the results cannot be very different, some doubts about the validity of the conclusions drawn for 2D, when applied to 3D, remain. Another drawback is the need for derivation of all kinds of relations well-known for 3D, such as elliptical harmonics and their transformation to polar series and the exact formulation of the observation equations.

The potential of a point mass in 2D is the *logarithm* of the inverse distance, in contrast with the function of the inverse distance for 3D. The logarithm becomes a

separate term in the series expansion of the 2D potential; the zero degree component only represents the potential constant. Although this does not bring any theoretical problem, it yields some confusion when comparing the results for 2D with 3D.

What can be expected in this thesis? Not all aspects mentioned in the introduction could be included in full detail. Emphasis was put on iteration and convergence.

First some general properties of the logarithmic potential, its series representation, and auxiliary formulas are discussed. This is basically a condensed treatise of potential theory for our 2D earth. In the following chapter, the linear model for the 2D GBVP is presented. The solutions to various GBVP's are derived in circular, constant radius approximation. Next, in chapter 4, GBVP's in higher approximations are considered, and their possible solution by iteration. Finally, the iterative solutions are tested numerically for various GBVP's.

The points of departure

Some properties of the 2D earth, and the topics to be investigated, are already mentioned above. Here the principal choices made, and the points on which we focus our attention, are listed:

- 2D earth, flattened at the poles, with a logarithmic potential.
- No rotation. The reason for this is not only a simplification of the formulae but also the impossibility to define a meaningful rotation axis in combination with flattening.
- The observations are located on the earth's surface. Solution of the potential for the exterior domain.
- We try to be as close as possible to 3D; not only by considering a 2D earth with properties derived from the 3D earth, but also by refraining from techniques that do not have a 3D counterpart, such as conformal mapping. This in contrast with Gerontopoulos, who derived mathematically strict solutions to the 2D problem using specific 2D techniques. We do apply the techniques from time series analysis. Although not all properties can be directly translated from our 1D boundary to the sphere, the behavior of the functions on the sphere is expected to be, more or less, similar.
- We do not aim for mathematical perfection, but consider the problems from a geodetic point of view. On the other hand, practical aspects, such as computer time, are not taken into account.
- Local solutions and accuracies are not considered. We only focus to *global* solutions and properties of the GBVP.

And now something completely different.

History of the problem

As far as known, the Greek scientist *Pythagoras* was one of the first to propose a spherical shape for the earth in the sixth century BC. Aristoteles picked up this idea and gave it a better basis by noting the apparent movement of the stars, the circular shadow of the earth during a lunar eclipse and the depression of the horizon. Since Greek science was merely philosophically oriented, it took about three centuries before a serious attempt was made to measure the radius of the earth. It was the director of the famous library of Alexandria, *Eratosthenes*, who estimated the earth's radius by observing the elevation of the sun on june 21th at noon in Alexandria. Since at that time the sun was in zenith position in Aswan, and since he was aware of the relative position of the two cities (Aswan is situated one thousand kilometers south of Alexandria and approximately on the same meridian), Eratosthenos was able to calculate the radius of the earth. Remarkably, considering his poor measuring tools, his solution was only 16% too large.

With the fall of the Greek empire and the introduction of Christianity in Europe, scientific study declined. It was not before the end of the Middle Ages, that discoveries by da Gama and Columbus revived the interest for the face of the earth. The idea of a flat earth was finally rejected and new attempts were made to measure the earth's circumference. The Frenchman *Fernel* was in 1525 the first to give a new estimate. He observed the elevation of the sun in Paris and Amiens. By the use of astronomic tables and the distance between the two cities, measured by an odometer, he obtained a value for the earth's radius 1% wrong. The development of new instruments made other, and more accurate, techniques possible. The most important for geodesy was the invention of the theodolite. *Willibrord Snel van Royen*, a professor of mathematics in Leiden, used it in 1615 for the measurement of the distance between the Dutch cities Alkmaar and Bergen op Zoom by triangulation. The scale of the network was determined from a baseline, observed with a surveyor's chain. With astronomic latitude observations in the end points of the network, the earth's circumference was determined with an error of 3%. Although Snel's result was not very accurate, he introduced a technique of measuring distance still in practice.

The discovery of his mechanical laws, led *Newton* to the conclusion that gravity, as observed by a pendulum, must be of decreasing magnitude from the poles towards the equator, due to the centrifugal force. Furthermore, he, or Picard, hypothesized that the earth is an oblate spheroid, instead of a perfect sphere; supposing the earth being an equilibrium figure. This undermined the major premise taken for the computation of the size of the earth. To test this hypothesis, the French Academy of Science asked *Cassini*, with his son, to make triangulations running from Dunkerque to the Pyrenees. The division of the trajectory in two would show whether the length of a degree was dependent on latitude, as is the case on a spheroid. Surprisingly, Cassini came to a conclusion opposite to Newton's: the earth would be a prolate spheroid, flattened at the equator. To dispel this contradiction, the French Academy

sent out in 1736 two expeditions, one to Lapland and the other to Peru, to determine the length of a degree at two different latitudes. From these expeditions, and from many others that followed, Newton's hypothesis of an oblate spheroidal earth, was confirmed.

With the Peru expedition also another geodetic discovery was made. *Bouguer* noticed variations in gravity that could not be contributed to elevation or latitude. This was the first time evidence was found for a non-uniform density distribution in the earth, causing regional variations in gravity.

Clairaut published in 1738 the relation between the gravity flattening and the geometrical flattening of the ellipsoid. This connection between gravity and geometry can be identified as the first step towards the solution to the geodetic boundary value problem (GBVP): by observing the length of the gravity vector, the flattening of the earth can be determined. Clairaut adopted for his relation some hypothesis on the density distribution of the earth. *Stokes* derived a far more general expression in 1849. He showed that gravity, up to a constant, can be determined from the shape of the earth, and vice versa, if it is a surface of equilibrium, close to a sphere; without any assumptions on the density distribution. He also proved that the determination of this surface is sufficient to obtain a unique solution to the gravity in the space external to the surface.

Stokes' publication marked the start of the third period in the history of the knowledge of the earth's shape. After the hypotheses of a spherical and ellipsoidal earth, the suggestion of Laplace, an earth which is only *approximately* spheroidal, could be tested by gravity observations, reduced to sea level, and Stokes' formula. In geodetic terminology introduced later, Stokes' integral connects, in a linear approximation, gravity anomalies reduced to sea level with geoid heights above the reference ellipsoid. The integrals of *Vening Meinesz* (1928), relate the deflections of the vertical to the gravity anomalies. Together with Stokes' integral, they establish the relationship between gravity and the coordinates of the earth's surface.

The major drawback of the integrals of Stokes' and Vening Meinesz is the assumption of a mass free space outside the geoid and the need for reduction of the gravity anomalies from the surface to the geoid. To fulfil these requirements, and to keep the errors small, usually a terrain correction is applied, which requires information about the density structure above the geoid. In 1945, *Molodensky et al.* devised a method for the determination of the figure of the earth and its gravity field from the surface observations of the potential and the gravity vector, free of assumptions on the density. For the geodetic boundary value problem in spherical approximation, i.e. the ellipticity of the reference surface is neglected, a series solution is given. A large number of papers were published on this so-called *Molodensky problem*. At risk of doing no justice to other authors, we mention the contributions (Krarup, 1971), (Krarup, 1981), (Moritz, 1968) and (Moritz, 1972).

The next major step forward in the theory of the geodetic boundary value problem, was taken by *Hörmander* in 1975. He investigated the existence and uniqueness of the solution of the linear and the *non-linear* boundary value problem. A solu-

tion of the non-linear problem was found by means of a modified Nash iteration combined with smoothing. His results were improved by *Sansò* in 1977. By the transformation of the problem to the gravity space, a fixed boundary value problem could be obtained at the expense of a more complicated Laplace equation . The conditions on the shape of the boundary and the gravity field to guarantee uniqueness and existence of the solution, are less severe than required for Hörmanders solution. Various aspects of the non-linear problem are also considered in (Moritz, 1969), (Grafarend & Niemeier, 1971), (Witsch, 1985), (Witsch, 1986) and (Heck, 1989a), among others.

Although solutions are proposed for the linear and the non-linear problem, almost always Stokes' solution is used in practice because of its computational simplicity. To overcome, partially, the approximations made with Stokes', several techniques can be applied. The most important is *iteration*, as used in (Hörmander, 1976), (Molodensky et al., 1962) or (Rummel et al., 1989). Pursuing this to the end can lead to the solution to the linear or non-linear problem. But usually one iteration is sufficient, regarding the data accuracy and density. To account for the ellipticity of the earth, often *ellipsoidal corrections* are applied, which are computed from Stokes' solution. See e.g. (Lelgemann, 1970), (Hotine, 1969) or (Cruz, 1986). This method can also be considered as an iteration. Another approach is the use of ellipsoidal harmonics for the disturbing potential. The ellipticity is already contained in the coordinate system. Afterwards, the ellipsoidal potential coefficients are transformed to coefficients with respect to the polar coordinates, we refer to (Gleason, 1988) and (Jekeli, 1988).

The problems of Stokes and Molodensky require a continuous coverage of the entire boundary of the earth with observations. This is far from reality, not only will measurements always be discrete, but restrictions also exist concerning the type, e.g. leveling observations are not available in ocean areas. On the other hand, new types of observations became available, such as sea surface heights from satellite altimetry. The combination of gravity and potential observations on the continents, and altimetry in ocean areas, results in the *altimetry-gravimetry* boundary value problem. A large variety of papers on this topic can be found. We mention (Sacerdote & Sansò, 1983), (Holota, 1982), (Svensson, 1983) and (Baarda, 1979). Baarda discusses the GBVP from the operational point of view and reaches the conclusion that a separate solution needs to be applied for sea and land areas.

The introduction of new kinds of observables, in addition to the classical observations leveling, gravimetry and astronomical observations, gave an impulse for the development of *overdetermined* boundary value problems. More observations than unknowns are available; the abundance of data is used to improve the precision of the solution. See e.g. (Sacerdote & Sansò, 1985), (Grafarend & Schaffrin, 1986) and (Rummel et al., 1989).

Nowadays precise satellite positioning, such as GPS, provides station coordinates without knowledge of the (local) gravity field. Then the so-called *fixed* GBVP, with a known earth's surface, is composed to determine the gravity field from e.g.

gravimetry, see (Backus, 1968), (Koch & Pope, 1972) or (Heck, 1989a). Since the astronomical observations of latitude and longitude are scarce and not very accurate, the horizontal position is usually provided by triangulation. The combination of leveling and gravimetry can supply the topographic heights and the gravity field. The latter is is the *scalar* GBVP. See (Sacerdote & Sanso, 1986) or (Heck, 1989b).

Several mathematical techniques are applied for the formulation of the GBVP's. The most common is the use of one or more boundary conditions containing derivatives of the disturbing potential. Close to potential theory is the use of integral equations, see (Molodensky et al., 1962) or (Lelgemann, 1970). Sacerdote and Sansò use functional analysis to treat the GBVP. An alternative formulation is given in (Rummel & Teunissen, 1982). There the GBVP is presented as a classical linear system, which can be solved by least squares.

In the previous paragraphs a brief description of the development of the GBVP was given. It is far from complete, we only tried to provide the history that led to the invention of Stokes' solution and the further key steps of the development of physical geodesy. In the first half of the section, no references to literature were given. This is made up here. A general introduction into the history of surveying can be found in (Wilford, 1981). A discussion of the work of Snel van Royen (Snellius) is given in (Haasbroek, 1968). Details of ancient arc and gravity-survey expeditions were found in (Baeyer, 1861), (Mayer, 1876) and (Clark, 1880). For the proof of uniqueness by Stokes, Kellogg refers in his book of 1929 to (Stokes, 1854).

2 |

Potential theory of a two-dimensional mass distribution

POTENTIAL THEORY , in particular the solution to Laplace's equation in the exterior of a distribution of solid matter, allows for the computation of the gravitational potential and all its derivatives in the exterior space, given its boundary values. It can therefore considered to be the basis of physical geodesy.

We start with some elementary two-dimensional potential theory. The purpose here is to derive some formulas that are useful for the subsequent sections and to show how close the potential theory for the plane is to that for the three-dimensional space. We certainly do not aim for completeness. More can be found in (Mikhlin, 1970), (Rikitake et al., 1987) or (Kellogg, 1929). Often, for the potential a series expansion is used. In section 2.2 it is shown that the Fourier base functions satisfy the two-dimensional Laplace equation and can be used as a series expansion for the potential. Finally, some integral formulas are derived and their properties are discussed.

2.1 The logarithmic potential

The restriction to the two-dimensional plane violates reality since the world is three-dimensional. It can be argued, however, that certain features associated with the geodetic boundary value problem are common with the two- and three-dimensional cases. The Green's function of the Laplace equation in the two-dimensional space contains the logarithm of the distance from the source point and the observation point. For a line mass of strength M per length we have, see (Kellogg, 1929),

$$V(P) = GM \ln \frac{1}{|\ell|} + constant, \tag{2.1}$$

where G is the gravitational constant and $\boldsymbol{\ell}$ the vectorial distance from the line mass to the point of observation. This potential has two singularities: at the location of the mass ($\ell = 0$) and at infinity ($\ell \to \infty$). The corresponding attraction is given by (ibid.)

$$\boldsymbol{g} = -G\frac{M\boldsymbol{\ell}}{|\boldsymbol{\ell}|^2}.$$

A superposition of line masses yields the potential for a general two-dimensional mass distribution:

$$V(P) = G\int_{\Sigma} \rho(Q) \ln \frac{1}{|\boldsymbol{\ell}_{PQ}|} d\sigma_Q + constant \tag{2.2}$$

with Σ the domain occupied by the mass, and ρ the linear mass density (see also figure 2.1). It satisfies Laplace equation outside the domain Σ. The corresponding attraction is given by

$$\boldsymbol{g}(P) = -G\int_{\Sigma} \frac{\rho(Q)\boldsymbol{\ell}_{PQ}}{|\boldsymbol{\ell}_{PQ}|^2} d\sigma_Q \tag{2.3}$$

and is related to the potential with $\boldsymbol{g} = \operatorname{grad} V$.

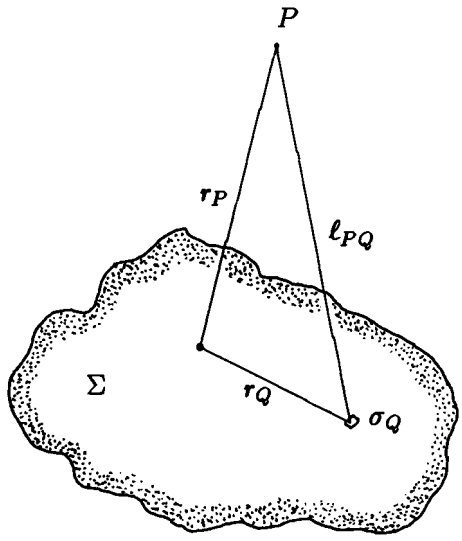

Figure 2.1 *The attraction of a mass Σ in a point P.*

In the entire plane, V yields a solution to Poisson's equation (Kellogg, 1929):

$$\Delta V(P) = -2\pi G\rho. \tag{2.4}$$

2.2 Series expansion of the potential

When solving for the potential from the boundary values, usually a sequence of orthogonal functions is introduced and its coefficients are determined. Here a series expansion will be derived either by expanding $\ln \frac{1}{\ell}$ into a series or by solving the Laplace equation. Both methods yield the same result.

2.2.1 Expansion of the inverse distance

For the distance

$$\ell = \sqrt{r_P^2 + r_Q^2 - 2r_P r_Q \cos\psi_{PQ}} = \sqrt{r_P - r_Q e^{i\psi}}.\sqrt{r_P - r_Q e^{-i\psi}}$$

we write

$$\ln \frac{1}{\ell} = -\frac{1}{2}\ln(1 - \frac{r_Q}{r_P}e^{i\psi}) - \frac{1}{2}\ln(1 - \frac{r_Q}{r_P}e^{-i\psi}) - \ln r_P. \tag{2.5}$$

Expansion into a Taylor series (convergent for $r_P > r_Q$, hence P must be located outside the Brillouin sphere) yields

$$\ln \frac{1}{\ell} = \frac{1}{2}\sum_{\substack{n=-\infty \\ n\neq 0}}^{\infty} \left(\frac{r_Q}{r_P}\right)^{|n|} \frac{1}{|n|} e^{in\psi} - \ln r_P. \tag{2.6}$$

Inserting (2.6) into (2.2) gives a series expression for the potential (the uniform convergence of the series (2.6) permits interchanging of summation and integration)

$$\begin{aligned} V(P) &= G\int_\Sigma \left[\frac{1}{2}\sum_{\substack{n=-\infty \\ n\neq 0}}^{\infty} \left(\frac{r_Q}{r_P}\right)^{|n|} \frac{1}{|n|} e^{in\psi_{PQ}} - \ln r_P\right] \rho(Q) d\sigma_Q + constant \\ &= \sum_{\substack{n=-\infty \\ n\neq 0}}^{\infty} \frac{1}{2}\frac{G}{|n|}\int_\Sigma \rho(Q) e^{-in\phi_Q} r_Q^{|n|} d\sigma_Q \frac{1}{r_P^{|n|}} e^{in\phi_P} + \mu \ln\frac{1}{r_P} + constant \\ &= \mu \ln\frac{1}{r_P} + \sum_{n=-\infty}^{\infty} a_n \left(\frac{1}{r_P}\right)^{|n|} e^{in\phi_P}. \end{aligned} \tag{2.7}$$

with

$$\begin{aligned} \mu &= GM = G\int_\Sigma \rho(Q) d\sigma_Q \\ a_n &= \frac{G}{2|n|}\int_\Sigma \rho(Q) e^{-in\phi_Q} r_Q^{|n|} d\sigma_Q \qquad n \neq 0 \\ a_0 &\quad arbitrary \end{aligned} \tag{2.8}$$

The constant is represented by $n = 0$ in (2.7). Since the constant is arbitrary, a_0 is arbitrary.

2.2.2 Solution of the Laplace equation

Series (2.6) can also be derived from Laplace's equation. This partial differential equation can be solved by a separation of variables (see e.g. (Walter, 1971)). Inserting

$$V(r,\phi) = \alpha(r)\beta(\phi)$$

into the Laplace equation $\Delta V = 0$ yields

$$\frac{r^2}{\alpha}(\alpha'' + \frac{1}{r}\alpha') = -\frac{\beta''}{\beta} = constant \equiv n^2 \qquad (n \in \mathrm{Z}). \tag{2.8}$$

(other choices of the constant lead to solutions β not periodic with 2π). The solutions for the two differential equations are

$$\alpha(r) = r^{\pm n},\ \beta(\phi) = e^{in\phi},$$

for $n \neq 0$ and $\alpha(r) = \ln r$, $\beta(\phi) = 1$ for $n = 1$, with periodicity laid upon β. In the exterior space, V tends asymptotically to $-\mu \ln r$ as $r \to \infty$. Hence no positive powers of r are allowed:

$$V = \mu \ln \frac{1}{r} + O(\frac{1}{r}) \quad \text{as } r \to \infty, \quad \text{uniformly in } \phi.$$

It can be shown that in an exterior domain $V - \mu \ln \frac{1}{r}$ is uniquely determined by the Laplace equation, the boundary values and the prescribed behavior at infinity.

Since Laplace equation is linear, the sum of all particular solutions is a solution too. Thus the general solution to Laplace in the outer area is

$$V(P) = a \ln \frac{1}{r_P} + \sum_{n=-\infty}^{\infty} a_n \left(\frac{1}{r_P}\right)^{|n|} e^{in\phi_P}. \tag{2.9}$$

We observe that (2.9) agrees with (2.6), derived along a different path, if $a = \mu$.

2.2.3 Determination of the coefficients

The coefficients a_n can be determined either from (2.7), if the density distribution of Σ is known, or from a function given on a known boundary enclosing all masses. This leads to one of the three classical boundary value problems of potential theory. If the given function is the potential at that boundary it is Dirichlet's problem (the other two are Neumann's and Robin's problem). The determination from the boundary data is especially simple when this boundary is a circle. Then, the potential coefficients can be determined as follows.

Specializing (2.6) or (2.9) to $r = R$ and writing $a = GM = \mu$, we have

$$V(R,\phi) = \mu \ln \frac{1}{R} + \sum_{n=-\infty}^{\infty} a_n \left(\frac{1}{R}\right)^{|n|} e^{in\phi}. \tag{2.10}$$

The given potential function on the boundary is expanded into a Fourier series as

$$f = \sum_{n=-\infty}^{\infty} c_n e^{in\phi}. \tag{2.11}$$

From a comparison of (2.10) and (2.11) the unknown coefficients a_n are found to be:

$$\begin{cases} c_0 = \mu \ln \frac{1}{R} + a_0 \\ c_n = a_n \left(\frac{1}{R}\right)^{|n|} \quad n \neq 0 \end{cases} \Leftrightarrow \begin{cases} a_0 = c_0 - \mu \ln \frac{1}{R} \\ a_n = R^{|n|} c_n \quad n \neq 0. \end{cases} \tag{2.12}$$

From (2.12) it can be seen that the combination of the potential constant a_0 and the logarithmic term on the circle $\mu \ln \frac{1}{R}$ together constitute the zero order coefficient c_0 of the series (2.11). For practical purposes we like to keep them separated and define $c_0 = a_0$. Inserting in (2.9) gives, with $a = \mu$, the modified series for V

$$V(r,\phi) = \mu \ln \frac{1}{r} + \sum_{n=-\infty}^{\infty} c_n \left(\frac{R}{r}\right)^{|n|} e^{in\phi}. \tag{2.13}$$

The coefficients c_n are computed with the inverse of (2.11) (Papoulis, 1962), with a modification for $n = 0$,

$$\begin{aligned} c_0 &= \frac{1}{2\pi} \int_{-\pi}^{\pi} f d\phi - \mu \ln \frac{1}{R}, \\ c_n &= \frac{1}{2\pi} \int_{-\pi}^{\pi} f e^{-in\phi} d\phi \qquad (n \neq 0). \end{aligned} \tag{2.14}$$

Since we deal with GBVP's, with the density ρ unknown, the above derivation is appropriate for our purposes. We used here the complex Fourier base functions $e^{in\phi}$ because they lead to more compact formulas. Naturally, also the $\sin n\phi$ and $\cos n\phi$ functions are solutions to (2.8).

2.3 Kernel operators

In physical geodesy integral kernel operators play an important role. They connect, in circular approximation, the various quantities of the gravitational field in the exterior domain. Also in the planar GBVP such operators apply.

The relevant integral kernel operator can be written as

$$f(x) = \int_{\mathcal{D}} g(\xi) K(x - \xi) d\sigma_\xi$$

where K and g are two square integrable functions. K is the kernel of the operator equation. The domain of integration $\mathcal{D}$ and the area element $d\sigma_\xi$ depend on the space the operator is applied. The special position of operators of this type is brought by

their easy diagonalization. Before showing this, first the concept of diagonalization in linear algebra is considered. A matrix $\boldsymbol{A}$, which is regular and Hermitian, can be written as:

$$\boldsymbol{A} = \boldsymbol{S}\boldsymbol{\Lambda}\boldsymbol{S}^*.$$

(the asterisk denotes transpose and complex conjugate). The columns of $\boldsymbol{S}$ contain the (orthogonal) eigenvectors of $\boldsymbol{A}$, such that $\boldsymbol{S}\boldsymbol{S}^* = \boldsymbol{S}^*\boldsymbol{S} = \boldsymbol{I}$; the diagonal matrix $\boldsymbol{\Lambda}$ its eigenvalues. Then for an arbitrary vector $\boldsymbol{x}$ we have

$$\boldsymbol{y} = \boldsymbol{A}\boldsymbol{x} = \boldsymbol{S}\boldsymbol{\Lambda}\boldsymbol{S}^*\boldsymbol{x} \Leftrightarrow \boldsymbol{S}^*\boldsymbol{y} = \boldsymbol{\Lambda}\boldsymbol{S}^*\boldsymbol{x}$$

$$\Leftrightarrow \tilde{\boldsymbol{y}} = \boldsymbol{\Lambda}\tilde{\boldsymbol{x}} \quad \text{with} \quad \tilde{\boldsymbol{x}} = \boldsymbol{S}^*\boldsymbol{x}, \quad \tilde{\boldsymbol{y}} = \boldsymbol{S}^*\boldsymbol{y}.$$

By the transformation of the vectors $\boldsymbol{x}$ and $\boldsymbol{y}$ by means of their multiplication by $\boldsymbol{S}^*$, the original operator attains a diagonal form. If the same reasoning is now applied to an infinite dimensional space with $\boldsymbol{A}$ a self-adjoint operator in a function space, and $\boldsymbol{x}$ and $\boldsymbol{y}$ as functions, the equation $\boldsymbol{y} = \boldsymbol{A}\boldsymbol{x}$ represents the integral kernel equation of above. The diagonalization procedure can also be applied to this operator. First a set of orthogonal base functions ϕ_k, assumed to be complete in the domain $\mathcal{D}$, is introduced through the property

$$\int_{\mathcal{D}} \phi_k(\xi) K(x-\xi) d\sigma_\xi = \lambda_k \phi_k(x).$$

So the ϕ_k functions are the *eigenfunctions* of the operator, and λ_k the *eigenvalues*. We define the inner product as

$$(f,g) = \int_{\mathcal{D}} f(x) g^*(x) d\sigma_x$$

Functions that are elements of $\mathcal{D}$, are decomposed with respect to the base functions as

$$f(x) = \sum_k f_k \phi_k(x), \quad f_k = \int_{\mathcal{D}} f(x) \phi_k^*(x) d\sigma_x$$

$$g(x) = \sum_k g_k \phi_k(x), \quad g_k = \int_{\mathcal{D}} g(x) \phi_k^*(x) d\sigma_x.$$

These equations are the analogous expansions to what was written in the finite case as $\boldsymbol{x} = \boldsymbol{S}\tilde{\boldsymbol{x}}$, $\tilde{\boldsymbol{x}} = \boldsymbol{S}^*\boldsymbol{x}$. $\boldsymbol{S}$ is the operator from the frequency to the original domain, $\boldsymbol{S}^*$ its inverse, and $\tilde{\boldsymbol{x}}$ the spectrum of $\boldsymbol{x}$. Substitution in the integral equation yields

$$f(x) = \sum_k f_k \phi_k(x) = \int_{\mathcal{D}} \sum_k g_k \phi_k(\xi) K(x-\xi) d\sigma_\xi = \sum_k \lambda_k g_k \phi_k(x)$$

or

$$f_k = \lambda_k g_k.$$

Which corresponds to $\tilde{\boldsymbol{y}} = \boldsymbol{\Lambda}\tilde{\boldsymbol{x}}$. When the domain $\mathcal{D}$ is the (unit) sphere, the system of eigenfunctions ϕ_k are the *surface spherical harmonics*. On the circle, the eigenfunctions are the *Fourier functions*.

2.3.1 Fourier kernels

From Fourier theory we know (Papoulis, 1962) that functions on the circle can be expanded as

$$x(t) = \sum_n x_n e^{int}, \quad y(t) = \sum_n y_n e^{int}, \quad h(t) = \sum_n h_n e^{int}.$$

When these expansions are inserted into the convolution integral

$$y(t) = x(t) * h(t) \quad \text{or} \quad y(t) = \frac{1}{2\pi}\int_{-\pi}^{\pi} h(t-\tau)x(\tau)d\tau \tag{2.15}$$

the relation

$$y_n = x_n h_n, \tag{2.16}$$

holds for their Fourier coefficients. In the GBVP application we will write (2.15) as

$$f(\phi_P) = \frac{1}{2\pi}\int_{-\pi}^{\pi} K(\psi_{PQ})g(\phi_Q)d\phi_Q \tag{2.17}$$

with $\psi_{PQ} = \phi_Q - \phi_P$. $K(\psi)$ is expanded as

$$K(\psi) = \sum_{n=-\infty}^{\infty} \lambda_n e^{in\psi} \tag{2.18}$$

and, as in (2.16), it is

$$f_n = g_n \lambda_n \tag{2.19}$$

(f_n and g_n are the spectral components of f and g in (2.17)).

Since the complex expansions do not permit an easy interpretation we show how to write them as cosine or sine series. Kernels with an even and real-valued spectrum ($\lambda_n \in \mathrm{R}, \lambda_\mathrm{n} = \lambda_{-\mathrm{n}}, \forall \mathrm{n} \in \mathrm{Z}$) can be written as cosine series

$$\begin{aligned} K(\psi) &= \sum_{n=-\infty}^{\infty} \lambda_n e^{in\psi} \\ &= \lambda_0 + \sum_{n=1}^{\infty} \lambda_n (e^{in\psi} + e^{-in\psi}) = \lambda_0 + 2\sum_{n=1}^{\infty} \lambda_n \cos n\psi \end{aligned} \tag{2.20}$$

A kernel with an odd imaginary spectrum ($i\lambda_n \in \mathrm{R}, \lambda_\mathrm{n} = -\lambda_{-\mathrm{n}}, \forall \mathrm{n} \in \mathrm{Z}$) can be written as sine series

$$\begin{aligned} K(\psi) &= \sum_{n=-\infty}^{\infty} \lambda_n e^{in\psi} \\ &= \lambda_0 + \sum_{n=1}^{\infty} \lambda_n (e^{in\psi} - e^{-in\psi}) = \lambda_0 + 2i\sum_{n=1}^{\infty} \lambda_n \sin n\psi \end{aligned} \tag{2.21}$$

In both cases the function $K(\psi)$ is real. Complex kernels do not occur in our BVP's.

2.3.2 Analytical expressions for the kernels

In the previous section it was shown how the kernel operators are expressed in terms of the spectrum (2.18). Often this is the representation in which the kernels are used in the GBVP applications. In this section it is shown how an analytical, closed from, can be derived from the eigenvalues. Since only real-valued kernels are used, the derivation is decomposed into a part for cosine kernels and in a part for sine kernels. At the end, an example of the use of these formulas will be given.

Later we will see that all the eigenvalues λ_n of the kernels appearing in GBVP can be written either as

$$\frac{1}{n+A} \qquad (A \in \mathrm{Z}) \qquad \text{or as} \qquad \frac{1}{\mathrm{n}^2}, \tag{2.22}$$

or as a linear combination of these. As the expansion (2.18) is linear, a linear combination of eigenvalues gives a linear combination of the corresponding kernels, and the evaluation of kernels with the eigenvalues (2.22) is sufficient.

Cosine kernels

In (Gradshteyn & Ryzhik, 1980) it is found that

$$\sum_{n=1}^{\infty} \frac{\cos n\psi}{n^2} = \frac{\pi^2}{6} - \frac{\pi\psi}{2} + \frac{\psi^2}{4} \qquad (0 \le \psi \le 2\pi). \tag{2.23}$$

So the cosine kernel for $\lambda_n = 1/n^2$ is easily found. For the other eigenvalues we have some more work to do. We will follow a procedure analogous to (Moritz, 1980, ch. 23).

First we start with two general functions which contain an additional factor σ. After deriving the analytical expressions for these functions σ is simply put to 1 to get the desired kernel functions. These general functions are defined as

$$F_A(\sigma,t) = \sum_{n=1}^{\infty} \sigma^n \frac{\cos n\psi}{n+A} \qquad (A \ge 0),$$

$$F_A(\sigma,t) = \sum_{n=1-A}^{\infty} \sigma^n \frac{\cos n\psi}{n+A} \qquad (A \le 0). \tag{2.24}$$

Furthermore we define

$$L = \sqrt{1+\sigma^2-2\sigma t}, \qquad t = \cos\psi.$$

From (Gradshteyn & Ryzhik, 1980) we have

$$\sum_{n=1}^{\infty} \sigma^n \cos n\psi = \frac{\sigma t - \sigma^2}{L^2} \qquad (0 < \psi < 2\pi, \quad 0 \le \sigma < 1). \tag{2.25}$$

First the function F_A for $A > 0$ is analyzed. We have with (2.24) and (2.25)

$$\sigma^A F_A(\sigma,t) = \sum_{n=1}^{\infty} \sigma^{n+A} \frac{\cos n\psi}{n+A}$$

$$\Rightarrow \frac{\partial}{\partial\sigma}(\sigma^A F_A(\sigma,t)) = \sum_{n=1}^{\infty} \sigma^{n+A-1} \cos n\psi = \sigma^{A-1} \frac{\sigma t - \sigma^2}{L^2} = \sigma^A \frac{t-\sigma}{L^2}. \tag{2.26}$$

Integration of (2.26) results in

$$\sigma^A F_A(\sigma,t) = \int_0^{\sigma} \sigma^A \frac{t-\sigma}{L^2} d\sigma + c_A. \tag{2.27}$$

The integration constant c_A has to be chosen such that the condition $F_A(0,t) = 0$ is fulfilled, as can be seen from (2.24). We solve the integral (2.27) with (ibid.). Defining the auxiliary function

$$G_A = \int_0^{\sigma} \frac{\sigma^A}{L^2} d\sigma$$

we obtain

$$\sigma^A F_A(\sigma,t) = tG_A(\sigma,t) - G_{A+1}(\sigma,t) + c_A. \tag{2.28}$$

For G_A it is (ibid.)

$$\begin{aligned}
G_0 &= \frac{1}{\sin\psi} \arctan \frac{\sigma - t}{\sin\psi} \\
G_1 &= \ln L + tG_0 \\
G_2 &= \sigma + 2t \ln L + (2t^2 - 1)G_0 \\
G_3 &= \tfrac{1}{2}\sigma^2 + 2t\sigma + (4t^2 - 1)\ln L + t(4t^2 - 3)G_0.
\end{aligned}$$

Inserting in (2.28) gives for $A = 1$

$$\sigma F_1(\sigma,t) = -\cos\psi \ln L - \sigma + \sin\psi \arctan \frac{\sigma - \cos\psi}{\sin\psi} + c_1. \tag{2.29}$$

From the condition $\sigma F_1 = 0$ for $\sigma = 0$ it follows from (2.29) for c_1

$$c_1 = (\frac{\pi}{2} - \psi)\sin\psi.$$

Upon putting $\sigma = 1$ to get the expressions we are looking for, (2.29) gives

$$F_1(1,t) = -\cos\psi \ln(2\sin\psi/2) - 1 + \sin\psi(\pi - \psi)/2.$$

Analogously we find for $A = 2$ from (2.28)

$$F_2(1,t) = -\tfrac{1}{2} - \cos\psi - \cos 2\psi \ln(2\sin\psi/2) + \sin 2\psi(\pi - \psi)/2.$$

For $A < 0$ we only compute F_A for $A = -1$. With (2.24) and (2.25) it is

$$\sigma^{-1} F_{-1}(\sigma, t) = \sum_{n=2}^{\infty} \sigma^{n-1} \frac{\cos n\psi}{n-1} \Rightarrow$$

$$\frac{\partial}{\partial \sigma}(\sigma^{-1} F_{-1}(\sigma, t)) = \sum_{n=2}^{\infty} \sigma^{n-2} \cos n\psi = \sigma^{-1} \frac{t-\sigma}{L^2} - \frac{1}{\sigma} \cos\psi.$$

Integration yields

$$\sigma^{-1} F_{-1}(\sigma, t) = \int_0^{\sigma} \sigma^{-1} \frac{t-\sigma}{L^2} d\sigma - \ln\sigma \cos\psi + c_{-1}.$$

The integral can be found in (Gradshteyn & Ryzhik, 1980). We get

$$\sigma^{-1} F_{-1}(\sigma, t) = t \ln \frac{\sigma}{L} + (t^2 - 1) \frac{1}{\sin\psi} \arctan \frac{\sigma - \cos\psi}{\sin\psi} - \ln\sigma \cos\psi + c_{-1}.$$

The condition $\sigma^{-1} F_{-1} = 0$ for $\sigma = 0$ gives

$$c_{-1} = (\psi - \frac{\pi}{2}) \sin\psi.$$

For $\sigma = 1$ it is

$$F_{-1}(1, t) = -\cos\psi \ln(2 \sin\psi/2) - \sin\psi(\pi - \psi)/2.$$

In (Gradshteyn & Ryzhik, 1980) we directly find

$$F_0(1, t) = \sum_{n=1}^{\infty} \frac{\cos n\psi}{n} = \ln \frac{1}{L}.$$

The validity of the derived expressions for F_A for $\sigma = 1$ or $\psi = 0$ or $\psi = \pi$ will be discussed below.

Summarizing we have found the functions

$$F_A = \sum_{n=1}^{\infty} \frac{1}{n+A} \cos n\psi \qquad A \in \{-1, 0, 1, 2\}$$

as

$$\begin{aligned}
F_0 &= -\ln(2 \sin\psi/2) \\
F_1 &= -\cos\psi \ln(2 \sin\psi/2) - 1 + \sin\psi(\pi - \psi)/2 \\
F_2 &= -\tfrac{1}{2} - \cos\psi - \cos 2\psi \ln(2 \sin\psi/2) + \sin 2\psi(\pi - \psi)/2 \\
F_{-1} &= -\cos\psi \ln(2 \sin\psi/2) - \sin\psi(\pi - \psi)/2
\end{aligned} \tag{2.30}$$

The functions F_A for other values of A can be derived analogously.

Sine kernels

The expressions for the sine kernels are derived analogously to those for the cosine kernels. We start with (Gradshteyn & Ryzhik, 1980)

$$\sum_{n=1}^{\infty} \sigma^n \sin n\psi = \frac{\sigma u}{L^2} \qquad (\sigma < 1, 0 < \psi < \pi),$$

where the substitution $u = \sin\psi$ is used. The general functions we are looking for are

$$E_A(\sigma, u) = \sum_{n=1}^{\infty} \sigma^n \frac{\sin n\psi}{n+A} \qquad (A \geq 0)$$

$$E_A(\sigma, u) = \sum_{n=1-A}^{\infty} \sigma^n \frac{\sin n\psi}{n+A} \qquad (A \leq 0). \tag{2.31}$$

The functions E_A are determined in the same way as the F_A functions. We only give the results.

$$\begin{aligned}
E_0 &= (\pi - \psi)/2 \\
E_1 &= \sin\psi \ln(2\sin\psi/2) + \tfrac{1}{2}(\pi - \psi)\cos\psi \\
E_2 &= \sin\psi + \sin 2\psi \ln(2\sin\psi/2) + \tfrac{1}{2}(\pi - \psi)\cos 2\psi \\
E_3 &= \tfrac{1}{2}\sin\psi + \sin 2\psi + \ln(2\sin\psi/2)\sin 3\psi + \tfrac{1}{2}(\pi - \psi)\cos 3\psi \\
E_{-1} &= -\sin\psi \ln(2\sin\psi/2) + \tfrac{1}{2}(\pi - \psi)\cos\psi.
\end{aligned} \tag{2.32}$$

Validity for $\sigma = 1$ or $\psi = 0$

All the formulas for the cosine kernels are derived with (2.25). But (2.25) is not valid outside $(0, \pi)$ and for $\sigma = 1$. We show that the derived formulas, however, are correct for these situations, too.

First the $\sigma = 1$ problem. This is a problem of convergence. The series (2.25) do not converge for $\sigma = 1$. That is not a problem in itself as we are not interested in this series. What we like to know is whether the series F_A, derived with (2.25), converge.

We know that the series F_A are convergent, i.e. have a certain limit, from the fact that (Gradshteyn & Ryzhik, 1980)

$$\ln\frac{1}{L} = \sum_{n=1}^{\infty} \sigma^n \frac{\cos n\psi}{n}$$

is convergent for $(0 \leq \sigma \leq 1, 0 < \psi < 2\pi)$. This can be proven as follows. We define

$$a_n = \frac{\cos n\psi}{n+A} \qquad \text{and} \qquad b_n = \frac{\cos n\psi}{n}.$$

The series $\sum_n b_n$ ($\sigma = 1$) converges. With

$$\lim_{n\to\infty} \frac{a_n}{b_n} = \frac{n}{n+A} = 1 \Rightarrow \exists n \quad \text{such that} \quad \tfrac{1}{2} < \frac{a_n}{b_n} < \tfrac{3}{2} b_n \qquad \forall n > N$$

$$\Rightarrow \begin{cases} \frac{1}{2}b_n < a_n < \frac{3}{2}b_n & \forall\, n > N \quad (a_n > 0) \\ \frac{1}{2}b_n > a_n > \frac{3}{2}b_n & \forall\, n > N \quad (a_n < 0) \end{cases}$$

Since $\sum_n \frac{1}{2}b_n$ and $\sum_n \frac{3}{2}b_n$ are convergent $\sum_n a_n$ is convergent, too.

Now we have to know whether the limit of the series (2.24) equals the value from the derived formulas (2.30) or not. We are sure that they are correct for $\sigma < 1$. Also it is known that both the series and the analytical formulas are continuous functions of σ up to $\sigma = 1$. Hence the F_A formulas as stated in (2.30) and (2.24) have to yield an identical value for $\sigma = 1$. So F_A is convergent for $\sigma \leq 1$. This proof also applies to the sine series.

From (2.24) it is seen that for $\sigma = 1$ all series diverge for $\psi = 0$. This means that all the functions $F_A(1,t)$ must be infinite for $\psi = 0$. It is easy to see that this is the case in (2.30). The sine series (2.32) are zero for $\psi = 0$. The logarithmic terms vanish:

$$\lim_{\psi\downarrow 0} \sin\psi \ln(2\sin\psi/2) \leq \lim_{\psi\downarrow 0} \psi \ln(2\psi/2) = 0,$$

but the cosine functions do not. So the functions $E_A(1,u)$ in (2.32) are only valid for $0 < \psi < \pi$.

Example

Derive with the formulas of the last section the analytical function of the kernel

$$K(\psi) = \sum_{n=2}^{\infty} \frac{1}{(|n|+2)(|n|-1)} e^{in\psi} = \tfrac{2}{3} \sum_{n=2}^{\infty} \left(\frac{1}{n-1} - \frac{1}{n+2}\right) \cos\psi, \tag{2.33}$$

where (2.20) was used and

$$\frac{1}{(n-1)(n+2)} = \frac{1}{3}\frac{1}{n-1} - \frac{1}{3}\frac{1}{n+2}.$$

From (2.24) and (2.33) it is

$$K(\psi) = \tfrac{2}{3} F_{-1}(1,t) - \tfrac{2}{3} F_2(1,t) + \tfrac{2}{9}\cos\psi.$$

Inserting (2.30) yields

$$K(\psi) = \tfrac{2}{3}\left[(\sin\psi + \sin 2\psi)(\psi - \pi)/2 + \tfrac{1}{2} + \tfrac{4}{3}\cos\psi + (\cos 2\psi - \cos\psi)\ln(2\sin\psi/2)\right].$$

3

The linear geodetic boundary value problem by least squares

THE GEODETIC BOUNDARY VALUE PROBLEM describes the relation between the unknown potential, in our case in the exterior domain, and the shape of the earth and the measurable quantities given on that surface. The exact relation between unknowns and the observations is non-linear, at least for all relevant quantities. The first step to a solution is usually a linearization. Then the linearized problem is solved, if necessary with some approximations.

In this chapter we start with the general formulation of the linear GBVP. Then it is shown how the GBVP can be solved analytically, by the introduction of the *circular constant radius approximation*. This is the 2D counterpart of the spherical constant radius approximation of the 3D problem. It leads to Stokes' solution to the classical GBVP with potential and gravity being given. For different kinds of observations, and combinations of them, in determined and overdetermined problems, the solution will be given too. The approximations made here, and the formulation of models of higher order, will be described in chapter 4.

For the derivation of the solution, the GBVP is formulated as a system of linear equations, and solved by least squares, as introduced in (Rummel & Teunissen, 1986) and (Rummel et al., 1989) for the 3D problem. This method is applied since it yields brief and clear formulas, it allows a simple error propagation and a direct way to attack overdetermined problems. Furthermore, the change from the discrete formulation, appropriate for a practical situation, to the formulation with continuous observations, which is required for the 3D problem in order to be able to derive analytical solutions, can be taken smoothly. At this point, we meet one of the advantages of the 2D problem. As the discrete problem can also be solved analytically, the step discrete to continuous can be described well.

After the treatment of the solutions to the different GBVP's, attention is paid to

the role and the interpretation of the logarithmic, zero and first degree term in the series expansion of the potential. Finally, it is shown how the concept of astronomic leveling can be coupled to the GBVP, and how the Delft theory of reliability is implemented into the GBVP.

3.1 The linear model

We start with one of the theoretical cornerstones, the linear model. First it is presented in a general formulation. Then the model is worked out as a system of linear equations in each point, using local coordinates. In the subsequent sections the model is further specified with different degrees of approximation.

As the observables the ***gravity vector***, later decomposed in its length (the scalar gravity) and its orientation with respect to an equatorial frame, the ***potential***, associated with the attraction field and the ***second derivatives***, or curvatures, of the potential are considered. The formulation of the GBVP for the plane is very close to the formulas for the 3D-earth. In (Gerontopoulos, 1978) we find for the classical problem, for the non-rotating earth:

$$\begin{aligned} \Delta W(\boldsymbol{x}) \equiv W(\boldsymbol{x}) - U(\boldsymbol{x}') &= U_{i'}(\boldsymbol{x}')\Delta x^{i'} + T(\boldsymbol{x}') \\ \Delta W_{i'}(\boldsymbol{x}) \equiv W_{i'}(\boldsymbol{x}) - U_{i'}(\boldsymbol{x}') &= U_{i'j'}(\boldsymbol{x}')\Delta x^{j'} + T_{i'}(\boldsymbol{x}'). \end{aligned} \tag{3.1}$$

The principles of the notation used in this chapter are outlined in appendix A. As kernel letters we introduced in (3.1):

W : Gravitational potential
U : Normal potential
T : Disturbing potential.

Furthermore, we used $\boldsymbol{x}$ for the position vector of the observation, and $\boldsymbol{x}'$ for the approximate position. For the coordinates we anticipated on the detailed formulation of (3.1) in local coordinates by using the index letters of a local frame. Essentially this choice is arbitrary, but we have to choose a frame anyway. The local frame is the most suitable one for our purposes as it reflects the situation that most of our measurements are directed along the local vertical or refer to it. With the potential-related quantities we have to be careful with the notation. The derivatives of the potential are obtained by means of covariant differentiation, resulting in *covariant* components, denoted with subscripts. Superscripts are used to denote *contravariant* components, for example, the familiar components of the displacement vector. As long as cartesian frames are applied, either can be used since they coincide. Here, the covariant components are used where possible.

Since also the gravity gradients will be considered as the observables in the forthcoming sections, their linear observation equations will be treated together with those of Stokes' problem. By the same procedure as used for (3.1), by linearization

with respect to potential and position, we have

$$\Delta W_{i'j'} \equiv W_{i'j'}(\boldsymbol{x}) - U_{i'j'}(\boldsymbol{x}') = U_{i'j'k'}(\boldsymbol{x}')\Delta x^{k'} + T_{i'j'}(\boldsymbol{x}'). \tag{3.2}$$

In the equations (3.1) and (3.2) we indicate the use of local coordinates by writing $W_{i'}$, etc. The prime is used to discriminate between the *normal* local frame $\boldsymbol{e}_{i'}$, with $\boldsymbol{e}_{i'=3}$ directed parallel to the vector of normal gravity $\boldsymbol{\gamma} = U_{i'=2}\,\boldsymbol{e}_{i'=3}$, and the *actual* normal frame $\boldsymbol{e}_i$, with $\boldsymbol{e}_{i=3}$ directed parallel to the vector of actual gravity $\boldsymbol{g} = W_{i=2}\,\boldsymbol{e}_{i=3}$. The latter frame is convenient to use for the observations, since they are all derivatives of the potential along the axes of the actual local frame. The normal frame is used for the equations since the orientation of the actual frame is unknown. The use of the normal local frame in the models (3.1) and (3.2) makes it necessary to convert the components with respect to the actual frame to the ones of the normal local frame.

We start with the conversion of the elements of $\boldsymbol{g}$. For a tensor of rank one we have the transformation (A.3):

$$W_{i'} = \frac{\partial x^{i'}}{\partial x^i} W_i = \frac{\partial x^{i'}}{\partial x^I}\frac{\partial x^I}{\partial x^i} W_i. \tag{3.3}$$

The elements of this transformation can be found in (A.10). For the first transformation, from the actual local frame to the equatorial frame, $\omega = \Phi$ has to be substituted (Φ is the astronomical latitude), for the second transformation, from the equatorial to the normal local frame, $\omega = \phi$ (geodetic latitude) has to be taken. Multiplication and linear approximation yields for (3.3) in matrix notation:

$$\begin{pmatrix} W_{x'} \\ W_{z'} \end{pmatrix}_{|P} = \begin{pmatrix} 1 & \xi \\ -\xi & 1 \end{pmatrix} \begin{pmatrix} W_x \\ W_z \end{pmatrix}_{|P},$$

with the deflection of the vertical $\xi = \Phi(\boldsymbol{x}) - \phi(\boldsymbol{x})$. The problem with this formula is that Φ is observed in $\boldsymbol{x}$ and ϕ can only be computed in $\boldsymbol{x}'$. So we replace the disturbance ξ by the anomaly $\Delta\Phi = \Phi(\boldsymbol{x}) - \phi(\boldsymbol{x}')$ and get

$$\begin{pmatrix} W_{x'} \\ W_{z'} \end{pmatrix}_{|P'} = \begin{pmatrix} 1 & \Delta\Phi \\ -\Delta\Phi & 1 \end{pmatrix} \begin{pmatrix} W_x \\ W_z \end{pmatrix}_{|P}. \tag{3.4}$$

Now we can write, with (3.4) and

$$\boldsymbol{g}(\boldsymbol{x}) = -g(\boldsymbol{x})\,\boldsymbol{e}_z \equiv W_z\,\boldsymbol{e}_z,$$

the components of $\boldsymbol{g}$ as

$$\begin{aligned} W_{i'=1} &\equiv W_{x'} = -g(\boldsymbol{x})\Delta\Phi \approx -\gamma(\boldsymbol{x}')\Delta\Phi \\ W_{i'=2} &\equiv W_{z'} = -g(\boldsymbol{x}). \end{aligned}$$

Inserting in (3.1) gives, with $\gamma = -\gamma(\boldsymbol{x}')\, \boldsymbol{e}_{i'=3}$,

$$\begin{pmatrix} \Delta W \\ -\gamma\Delta\Phi \\ -\Delta g \end{pmatrix} = \begin{pmatrix} U_{x'} & U_{z'} \\ U_{x'x'} & U_{x'z'} \\ U_{z'x'} & U_{z'z'} \end{pmatrix} \begin{pmatrix} \Delta x' \\ \Delta z' \end{pmatrix} + \begin{pmatrix} T \\ T_{x'} \\ T_{z'} \end{pmatrix};$$

where the anomaly $\Delta g = g(\boldsymbol{x}) - \gamma(\boldsymbol{x}')$, is introduced. Rewriting gives finally (omitting the primes)

$$\begin{pmatrix} \Delta W \\ \Delta g \\ \Delta\Phi \end{pmatrix} = \begin{pmatrix} U_x & U_z \\ -U_{zx} & -U_{zz} \\ -\frac{1}{\gamma}U_{xx} & -\frac{1}{\gamma}U_{xz} \end{pmatrix} \begin{pmatrix} \Delta x \\ \Delta z \end{pmatrix} + \begin{pmatrix} T \\ -T_z \\ -\frac{1}{\gamma}T_x \end{pmatrix}. \tag{3.5}$$

For the tensor of the second derivatives of the potential W_{ij} a similar procedure has to be followed to get an expression for the transformation of the actual components of W_{ij} to the normal local frame.

For a second order tensor the transformation to another coordinate frame is computed as (A.3):

$$W_{i'j'} = \frac{\partial x^{i'}}{\partial x^i}\frac{\partial x^{j'}}{\partial x^j}W_{ij} = \frac{\partial x^{i'}}{\partial x^I}\frac{\partial x^I}{\partial x^i}\frac{\partial x^{j'}}{\partial x^J}\frac{\partial x^J}{\partial x^j}W_{ij}. \tag{3.6}$$

Here we have the same transformation elements as in (3.3). Writing (3.6) as a matrix equation, using the approximate rotation matrix from (3.4) and using the symmetry and tracelessness of W_{ij} it is:

$$\begin{pmatrix} -W_{z'z'} & W_{x'z'} \\ W_{x'z'} & W_{z'z'} \end{pmatrix} = \begin{pmatrix} 1 & \Delta\Phi \\ -\Delta\Phi & 1 \end{pmatrix} \begin{pmatrix} -W_{zz} & W_{xz} \\ W_{xz} & W_{zz} \end{pmatrix} \begin{pmatrix} 1 & -\Delta\Phi \\ \Delta\Phi & 1 \end{pmatrix}.$$

Omitting the squares of $\Delta\Phi$, the transformation becomes

$$\begin{pmatrix} W_{x'z'} \\ W_{z'z'} \end{pmatrix} = \begin{pmatrix} 1 & 2\Delta\Phi \\ -2\Delta\Phi & 1 \end{pmatrix} \begin{pmatrix} W_{xz} \\ W_{zz} \end{pmatrix}. \tag{3.7}$$

The anomalies are defined as

$$\begin{aligned} \Delta\Gamma_{xz} &= W_{xz}(\boldsymbol{x}) - U_{x'z'}(\boldsymbol{x}') \\ \Delta\Gamma_{zz} &= W_{zz}(\boldsymbol{x}) - U_{z'z'}(\boldsymbol{x}'). \end{aligned} \tag{3.8}$$

In contrast with (3.2), the derivatives taken here for the computation of the anomalies are not with respect to the same frame! With (3.7) and (3.8), (3.2) is rewritten

as

$$\begin{pmatrix} \Delta\Gamma_{xz} \\ \Delta\Gamma_{zz} \end{pmatrix} = \begin{pmatrix} U_{xxz} & U_{xzz} \\ U_{xzz} & U_{zzz} \end{pmatrix} \begin{pmatrix} \Delta x \\ \Delta z \end{pmatrix} + \begin{pmatrix} T_{xz} \\ T_{zz} \end{pmatrix} + 2\Delta\Phi \begin{pmatrix} -W_{xz} \\ W_{zz} \end{pmatrix}.$$

We take the approximation $W = U$ for the last term on the right hand side. This can be done safely since that vector is multiplied by a small anomaly. We insert the linear model for $\Delta\Phi$ from (3.5), and finally the model for the gradients is obtained:

$$\begin{pmatrix} \Delta\Gamma_{xz} \\ \Delta\Gamma_{zz} \end{pmatrix} = \begin{pmatrix} U_{xxz} - \frac{2}{\gamma}U_{xz}^2 & U_{xzz} + \frac{2}{\gamma}U_{xz}U_{xz} \\ U_{xzz} + \frac{2}{\gamma}U_{xz}U_{xz} & U_{zzz} - \frac{2}{\gamma}U_{xz}^2 \end{pmatrix} \begin{pmatrix} \Delta x \\ \Delta z \end{pmatrix} + \begin{pmatrix} T_{xz} + \frac{2}{\gamma}U_{xz}T_x \\ T_{zz} - \frac{2}{\gamma}U_{xz}T_z \end{pmatrix}. \tag{3.9}$$

In some literature, the rotation over $\Delta\Phi$ is omitted from the model for the second derivatives. It entered the equations by the use of two different coordinate frames in the definition of the anomaly. This choice was made to get the same kind of anomalies as for the potential and gravity vector. In case of *satellite gradiometry*, the orientation of the actual local frame, to which the measurements are related, will be known by star-tracking. Attitude control ensures the satellite is oriented e.g. radially. Hence, a rotation to compensate for the unknown direction of the frame of observation is not required and the second term of all elements of (3.9) is omitted for satellite gradiometry.

3.2 Circular approximation

In the last section the general linear model was derived using the local coordinates. For this formulation we have to know the coefficients, which are derivatives of the normal potential U. Also the direction of the normal local frame has to be defined (usually it is connected to the choice of the normal potential by taking $e_{i'=3}$ parallel to the normal gravity vector γ). One can take a very sophisticated normal potential for this purpose. However, if the approximate values for the observations are good, the position correction vector and the disturbing potential are small, consequently a simple choice of the function U for the coefficient matrix does only introduce a small error. In this section we will work out the GBVP by taking the simplest normal potential: the potential of a point mass. We call it the linear model in *circular approximation*. A further simplification is obtained by computing all the coefficients at the same radius: *constant radius approximation*. The solution in this approximation for the classical GBVP is Stokes' integral. It has to be underlined that only for the coefficients of the model a simple normal potential is used. For the approximate values of the observations, usually the elliptical potential or an earth model is used. In section 4.4 more attention is paid to this.

The potential of a point mass is, see (2.1),

$$U = \mu' \ln \frac{1}{r}. \tag{3.10}$$

The equipotential lines of the potential of a point mass are circles. This implies that the normal gravity vector is pointing to the origin of the equatorial coordinate frame and the $\boldsymbol{e}_z$-axis is directed radial.

Because the potential is given as a function of r and the series expression we will substitute for T are written in polar coordinates too, the use of polar coordinates is convenient. So the derivatives with respect to the local frame have to be expressed as (covariant) derivatives with respect to r and ϕ. These relations can be found using (A.3) and (A.4):

$$\begin{aligned} W_i &= \frac{\partial x^I}{\partial x^i}\frac{\partial x^\alpha}{\partial x^I} W_\alpha \\ W_{ij} &= \frac{\partial x^I}{\partial x^i}\frac{\partial x^J}{\partial x^j}\frac{\partial x^\alpha}{\partial x^I}\frac{\partial x^\beta}{\partial x^J} W_{\alpha\beta} \\ W_{ijk} &= \frac{\partial x^I}{\partial x^i}\frac{\partial x^J}{\partial x^j}\frac{\partial x^K}{\partial x^k}\frac{\partial x^\alpha}{\partial x^I}\frac{\partial x^\beta}{\partial x^j}\frac{\partial x^\gamma}{\partial x^k} W_{\alpha\beta\gamma}. \end{aligned} \tag{3.11}$$

As explained in appendix A, $W_{\alpha=1}$ denotes $\frac{\partial W}{\partial r}$, $W_{\alpha=2} = \frac{\partial W}{\partial \phi}$ etc. The transformations are computed via the equatorial frame $\boldsymbol{e}_I$. Using (A.9)–(A.10) with $\omega = \phi$, the following partial derivatives are found in the origin of the local frame (the distinction between $\bar{\phi}$ and ϕ is omitted here since we work in circular approximation):

$$\begin{aligned} \frac{\partial W}{\partial x} &= \frac{1}{r}\frac{\partial W}{\partial \phi}, \\ \frac{\partial W}{\partial z} &= \frac{\partial W}{\partial r}, \\ \frac{\partial^2 W}{\partial x^2} &= \frac{1}{r}\frac{\partial W}{\partial r} + \frac{1}{r^2}\frac{\partial^2 W}{\partial \phi^2}, \\ \frac{\partial^2 W}{\partial z^2} &= \frac{\partial^2 W}{\partial r^2}, \\ \frac{\partial^2 W}{\partial x \partial z} &= -\frac{1}{r^2}\frac{\partial W}{\partial \phi} + \frac{1}{r}\frac{\partial^2 W}{\partial r \partial \phi}, \\ \frac{\partial^3 W}{\partial x^3} &= -\frac{2}{r^3}\frac{\partial W}{\partial \phi} + \frac{3}{r^2}\frac{\partial^2 W}{\partial r \partial \phi} + \frac{1}{r^3}\frac{\partial^3 W}{\partial \phi^3}, \\ \frac{\partial^3 W}{\partial x^2 \partial z} &= -\frac{1}{r^2}\frac{\partial W}{\partial r} + \frac{1}{r}\frac{\partial^2 W}{\partial r^2} - \frac{2}{r^3}\frac{\partial^2 W}{\partial \phi^2} + \frac{1}{r^2}\frac{\partial^3 W}{\partial r \partial \phi^2}, \\ \frac{\partial^3 W}{\partial x \partial z^2} &= -\frac{2}{r^2}\frac{\partial^2 W}{\partial r \partial \phi} + \frac{2}{r^3}\frac{\partial W}{\partial \phi} + \frac{1}{r}\frac{\partial^3 W}{\partial r^2 \partial \phi}, \\ \frac{\partial^3 W}{\partial z^3} &= \frac{\partial^3 W}{\partial r^3}. \end{aligned} \tag{3.12}$$

Now the elements of the coefficient matrix of (3.5) can be computed by differentiating the normal potential (3.10) analogously with the differential operators of (3.12). They are

$$U_x = 0, \qquad U_z = -\frac{\mu'}{r} \equiv -\gamma$$

$$U_{xx} = -\frac{\gamma}{r}, \qquad U_{xz} = 0, \qquad U_{zz} = \frac{\gamma}{r}. \tag{3.13}$$

$$U_{xxz} = \frac{2\gamma}{r^2}, \qquad U_{zzz} = -\frac{2\gamma}{r^2}, \qquad U_{xzz} = 0.$$

Inserting these into the system of equations (3.5), and taking all $r = R \Rightarrow \gamma = \gamma_0 = \mu'/R$, yields the linear model for vectorial Stokes in *circular constant radius approximation*:

$$\begin{pmatrix} \Delta W \\ \Delta g \\ \Delta \Phi \end{pmatrix} = \begin{pmatrix} 0 & -\gamma_0 \\ 0 & -\frac{\gamma_0}{R} \\ \frac{1}{R} & 0 \end{pmatrix} \begin{pmatrix} \Delta x \\ \Delta z \end{pmatrix} + \begin{pmatrix} T \\ -\frac{\partial T}{\partial r} \\ -\frac{1}{R\gamma}\frac{\partial T}{\partial \phi} \end{pmatrix}_{|r=R} . \tag{3.14}$$

For the gradiometric GBVP in *circular constant radius approximation* we get:

$$\begin{pmatrix} \Delta \Gamma_{xz} \\ \Delta \Gamma_{zz} \end{pmatrix} = \begin{pmatrix} 0 & 0 \\ 0 & -\frac{2\gamma_0}{R^2} \end{pmatrix} \begin{pmatrix} \Delta x \\ \Delta z \end{pmatrix} + \begin{pmatrix} \frac{1}{R^2}\frac{\partial T}{\partial \phi} + \frac{1}{R}\frac{\partial^2 T}{\partial r \partial \phi} \\ \frac{\partial^2 T}{\partial r^2} \end{pmatrix}_{|r=R} . \tag{3.15}$$

The systems of equations (3.14) and (3.15) are set up for each point of observation. Because at an individual point, T and its various derivatives have to be considered independent unknowns, the equations cannot be solved point by point. The number of unknowns can be balanced with the number of observations by linking the unknown disturbing potential to its derivatives and solving the systems simultaneously. This connection is established by Laplace's equation; T is written as a series of harmonic functions. The coefficients of the series replace the potential and its derivatives as unknowns. The number of coefficients that can be used, depends on the number of observations: if the number of coefficients equals the number of points, the system is well-determined, provided that the coefficient matrix has full rank. A series like (2.13) is used with dimensionless Fourier coefficients :

$$T = \mu'(\Delta c \ln\left(\frac{1}{r}\right) + \sum_{n=-\infty}^{\infty} \Delta c_n \left(\frac{R}{r}\right)^{|n|} e^{in\phi}), \tag{3.16}$$

where $\Delta c = (\mu - \mu')/\mu$: the relative difference of the GM values of the earth and the normal field. The other coefficients, Δc_n, are the Fourier coefficients of the

potential of the earth minus the coefficients of the normal field, divided by μ'. For the derivatives of T we obtain from (3.16)

$$\begin{aligned}
\frac{\partial T}{\partial r} &= \frac{-\mu'}{R}(\Delta c \left(\frac{R}{r}\right) + \sum_{n=-\infty}^{\infty} |n| \Delta c_n \left(\frac{R}{r}\right)^{|n|+1} e^{in\phi}), \\
\frac{\partial T}{\partial \phi} &= \mu' \sum_{n=-\infty}^{\infty} in \Delta c_n \left(\frac{R}{r}\right)^{|n|} e^{in\phi}, \\
\frac{\partial^2 T}{\partial r \partial \phi} &= -\frac{\mu'}{R} \sum_{n=-\infty}^{\infty} in|n| \Delta c_n \left(\frac{R}{r}\right)^{|n|+1} e^{in\phi}, \\
\frac{\partial^2 T}{\partial r^2} &= \frac{\mu'}{R^2}(\Delta c \left(\frac{R}{r}\right)^2 + \sum_{n=-\infty}^{\infty} |n|(|n|+1) \Delta c_n \left(\frac{R}{r}\right)^{|n|+2} e^{in\phi}).
\end{aligned} \tag{3.17}$$

For notational simplicity the coefficient Δc is omitted in the remainder of this section. More attention to this coefficient shall be given in section 3.8. Just as in (Rummel & Teunissen, 1986) dimensionless quantities are introduced to get more compact formulas. We have

$$dW = \frac{\Delta W}{\mu'}, \qquad dT = \frac{T}{\mu'}, \qquad dg = \frac{\Delta g}{\gamma_0}, \qquad d\Phi = \Delta\Phi,$$

$$d\Gamma_{xz} = \frac{R\Delta\Gamma_{xz}}{\gamma_0}, \qquad d\Gamma_{zz} = \frac{R\Delta\Gamma_{zz}}{\gamma_0}, \qquad dx = \frac{\Delta x}{R}, \qquad dz = \frac{\Delta z}{R}.$$

Inserting (3.17), with $r = R$, in (3.14) gives the model for potential and gravity in dimensionless quantities:

$$\begin{pmatrix} dW \\ dg \\ d\Phi \end{pmatrix} = \begin{pmatrix} 0 & -1 \\ 0 & -1 \\ 1 & 0 \end{pmatrix} \begin{pmatrix} dx \\ dz \end{pmatrix} + \begin{pmatrix} \sum_n \Delta c_n e^{in\phi} \\ \sum_n |n| \Delta c_n e^{in\phi} \\ -\sum_n in \Delta c_n e^{in\phi} \end{pmatrix}, \tag{3.18}$$

and for the gradiometric observations

$$\begin{pmatrix} d\Gamma_{xz} \\ d\Gamma_{zz} \end{pmatrix} = \begin{pmatrix} 0 & 0 \\ 0 & -2 \end{pmatrix} \begin{pmatrix} dx \\ dz \end{pmatrix} + \begin{pmatrix} -\sum_n in(|n|-1) \Delta c_n e^{in\phi} \\ \sum_n |n|(|n|+1) \Delta c_n e^{in\phi} \end{pmatrix}. \tag{3.19}$$

3.3 Stokes' problem

In this, and the following sections, the solution to Stokes' problem is considered, i.e., the computation of the disturbing potential from observations of the potential and the gravity vector, which are directly related to the combination of leveling,

gravimetry, and observation of astronomic latitude. First the matrices of (3.18) are rewritten and some general remarks are made about the solution. Then it is shown how the scalar Stokes problem (potential and gravity observations) can be solved by different approaches. As the solutions to the other possible problems run completely analogously, their solution is only given for continuous observations.

First, the observation equations (3.18) are written in one system for all measurement points. When all the unknowns, coordinate differences and potential coefficients, are written in one vector we have the linear system

$$\boldsymbol{y} = \boldsymbol{A}\boldsymbol{x} \tag{3.20}$$

with

$$\underset{3I \times 1}{\boldsymbol{y}} = \begin{pmatrix} [dW_i] \\ [dg_i] \\ [d\Phi_i] \end{pmatrix}, \qquad \underset{(2I+N) \times 1}{\boldsymbol{x}} = \begin{pmatrix} [dx_i] \\ [dz_i] \\ [\Delta c_n] \end{pmatrix},$$

$$\underset{3I \times (2I+N)}{\boldsymbol{A}} = \begin{pmatrix} [0] & [-\delta_{ij}] & \left[e^{in\phi}\right] \\ [0] & [-\delta_{ij}] & \left[|n|e^{in\phi}\right] \\ [\delta_{ij}] & [0] & \left[-ine^{in\phi}\right] \end{pmatrix}.$$

where δ_{ij} is the Kronecker delta. The index i is used to indicate the points of observation, the square brackets indicate sub-matrices. Below the matrices their size is given. The number of points is called I, the number of potential coefficients N. If the limit $I \to \infty$ is taken, $\boldsymbol{y}$ becomes a combination of three continuous functions, $\boldsymbol{x}$ a combination of two continuous functions and an infinite, countable sequence. Furthermore, a weight matrix for the observations is introduced. If no correlation is assumed between the measurements, and the weight of each measurement type is homogeneous, i.e. independent of the location of the point of observation, this matrix can be written as

$$\boldsymbol{P}_y = \begin{pmatrix} [p_w\delta_{ij}] & [0] & [0] \\ [0] & [p_g\delta_{ij}] & [0] \\ [0] & [0] & [p_\Phi\delta_{ij}] \end{pmatrix},$$

where p_w, p_g and p_Φ denote the weights for potential, gravity and astronomic latitude observations, respectively.

For the solution to (3.20), the commonly applied method for a system of linear equations is used: least squares. Although also an ordinary inversion of the matrix

$\boldsymbol{A}$ can be used here, if $\boldsymbol{A}$ is assumed to be regular, least squares has two major advantages: in case of overdetermined systems, which can be obtained by e.g. adding another type of observations to the system, the same method of solution can be applied. Secondly, the inverse normal matrix of a least squares problem is the a-posteriori error variance-covariance matrix of the unknowns, if the introduced weight matrix can be interpreted as the a-priori variance-covariance matrix of the observations.

The system (3.20) can be solved by least squares for every combination of observations and unknowns as long as $\boldsymbol{A}$ is regular. But our goal in this chapter is to show that an ***analytical*** expression for the least squares solution can be found if the data and unknowns satisfy certain conditions.

First we recall that the least squares solution $\hat{\boldsymbol{x}}$ is defined by the minimization problem

$$\min \|\boldsymbol{y} - \boldsymbol{A}\hat{\boldsymbol{x}}\|_P^2$$

(the minimization of the residuals with respect to the norm induced by $\boldsymbol{P}$), which leads to the normal equations

$$\boldsymbol{A}^*\boldsymbol{P}\boldsymbol{A}\hat{\boldsymbol{x}} = \boldsymbol{A}^*\boldsymbol{P}\boldsymbol{y}, \tag{3.21}$$

with the solution

$$\hat{\boldsymbol{x}} = \boldsymbol{Q}_x\boldsymbol{A}^*\boldsymbol{P}_y\boldsymbol{y}, \tag{3.22}$$

with

$$\boldsymbol{Q}_x = \boldsymbol{N}^{-1} = (\boldsymbol{A}^*\boldsymbol{P}_y\boldsymbol{A})^{-1},$$

where $\boldsymbol{A}^*$ means the Hermitian conjugate matrix of $\boldsymbol{A}$. $\boldsymbol{P}$ can be seen as a reproducing kernel of the Hilbert space $\mathcal{H}$, spanned by the columns of $\boldsymbol{A}$, and with an inner product given by

$$(\boldsymbol{a}, \boldsymbol{b}) = \boldsymbol{a}^*\boldsymbol{P}\boldsymbol{b}.$$

The minimum principle leads to minimum variance of the estimated unknowns if $\boldsymbol{P}$ equals the inverse variance-covariance matrix of the observations $\boldsymbol{y}$. In case of a finite system of equations, $\mathcal{H}$ is the R_n, the n–dimensional Euclidean space, (n is the dimension of $\boldsymbol{y}$). In case $\boldsymbol{y}$ is a function, $\mathcal{H}$ will be a Hilbert space, e.g. of square integrable functions.

Looking for explicit expressions for $\hat{\boldsymbol{x}}$, fulfilling the normal equations (3.21), implies that the inverse of the normal matrix has to be computed analytically. The first $2I$ columns of $\boldsymbol{A}$ consist of zero's and one's; they do not give any difficulty in the inversion. The second part of the matrix consists of N vectors containing the base functions. If either the points of observation are distributed such that they have constant separation (taken in ϕ), or the observations are given as continuous functions, orthogonality relations can be applied and an analytical expression for the inverse normal matrix can be given (see next sections).

For the three dimensional GBVP the situation is less fortunate. Only for the continuous case straightforward orthogonality relations are available. So only for

(hypothetical) continuous observations an analytical solution can be given. In (Rummel et al., 1989) and earlier in (Rummel & Teunissen, 1986) the least squares formulas and the observation equations are given for a finite dimensional space. Later on, when the application of the orthogonality relations of spherical harmonics is required to obtain a solution, the limits $I \to \infty$ and $N \to \infty$ were taken. This approach let to some questions about the convergence of the solution in this limit case. But, as shown above, the least squares approach could as well immediately be applied to continuous functions, and lead to the solutions given in (ibid.). Then it should be feasible to proof convergence for $I \to \infty$ and $N \to \infty$ in case we can guarantee for instance the maximum distance between two adjacent points to be less than every arbitrary value greater than zero. It seems to be not too difficult to give a full proof of this, but I did not try. But a convergence problem may exist when we do not apply spherical approximation but consider the observations to be located on the real boundary, which has a very nasty shape. See e.g. (Sansò, 1988).

In the coming sections it is shown how the scalar Stokes problem can be solved. The same problem is treated four times: for discrete and continuous data and in the space and the frequency domain. All these approaches finally lead to Stokes' integral. By working in the frequency domain, it can be shown nicely how the formulation of the discrete problem converges to the continuous problems when the number of points and potential coefficients tends to infinity. For all the other BVP's treated here, only the continuous solutions will be derived.

3.3.1 Discrete scalar Stokes

We assume here that we have a determined system of equations. This implies $I = N$. We have from (3.20)

$$\boldsymbol{y} = \begin{pmatrix} [dW_i] \\ [dg_i] \end{pmatrix}, \qquad \boldsymbol{A} = \begin{pmatrix} [-\delta_{ij}] & \left[e^{in\phi_i}\right] \\ [-\delta_{ij}] & \left[|n|e^{in\phi_i}\right] \end{pmatrix}, \qquad \boldsymbol{P_y} = \begin{pmatrix} [p_w\delta_{ij}] & [0] \\ [0] & [p_g\delta_{ij}] \end{pmatrix}. \tag{3.23}$$

We directly observe that the matrix $\boldsymbol{A}$ is singular. In the sequel, $|n| = 1$ will be excluded from the system of equations, which removes the singularity. See also section 3.8. For the normal matrix we get

$$\boldsymbol{N} = \begin{pmatrix} [(p_w + p_g)\delta_{ij}] & \left[-(p_w + |n|p_g)e^{in\phi_i}\right] \\ \left[-(p_w + |n|p_g)e^{-in\phi_j}\right] & [N(p_w + n^2p_g)\delta_{nm}] \end{pmatrix}.$$

Thereby use has been made of the orthogonality

$$\sum_{j=0}^{N-1} e^{i(n-m)\phi_j} = N\delta_{nm}, \qquad (\phi_j = \frac{2\pi}{N}j). \tag{3.24}$$

We invert N by the well known relations

$$\begin{aligned} Q_{22} &= (N_{22} - N_{21}N_{11}^{-1}N_{12})^{-1}, \\ Q_{12} &= -N_{11}^{-1}N_{12}Q_{22}, \\ Q_{11} &= N_{11}^{-1} + N_{11}^{-1}N_{12}Q_{22}N_{21}N_{11}^{-1}. \end{aligned} \tag{3.25}$$

For the sub-matrices of Q we obtain with (3.25)

$$\begin{aligned} Q_{22} &= \frac{1}{N}\left(\frac{p_w + p_g}{(|n|-1)^2 p_w p_g}\right)\delta_{nm}, \\ Q_{12} &= \frac{1}{N}\frac{p_w + |n|p_g}{(|n|-1)^2 p_w p_g}e^{in\phi}, \\ Q_{11} &= \frac{1}{p_w + p_g}\left(\delta_{ij} + \frac{1}{N}\sum_n \frac{(p_w + |n|p_g)^2}{(|n|-1)^2 p_w p_g}e^{in\phi_i}e^{-in\phi_j}\right). \end{aligned} \tag{3.26}$$

Furthermore we have

$$\boldsymbol{A}^* \boldsymbol{P}_y \boldsymbol{y} = \begin{pmatrix} [-p_w dW_i - p_g dg_i] \\ [N(p_w dW_n + |n|p_g dg_n)] \end{pmatrix}. \tag{3.27}$$

By dg_n we denote here the Fourier coefficients of dg

$$dg_n = \frac{1}{N}\sum_{j=0}^{N-1} dg_j e^{-in\phi_j}. \tag{3.28}$$

With (3.22), (3.26) and (3.27) we find the solution

$$\begin{aligned} \Delta c_n &= \frac{1}{|n|-1}(dg_n - dW_n) \qquad |n| \neq 1 \\ dz_i &= -dW_i + \sum_{n=-N/2+1}^{N/2} \frac{1}{|n|-1}e^{in\phi}(dg_n - dW_n). \end{aligned} \tag{3.29}$$

Or, writing (3.29) in the space domain,

$$\begin{aligned} dT_i &= \frac{1}{N}\sum_{j=0}^{N-1}(dg_j - dW_j)St(\psi_{ij}) \\ dz_i &= -dW_i + \frac{1}{N}\sum_{j=0}^{N-1}(dg_j - dW_j)St(\psi_{ij}) \end{aligned} \tag{3.30}$$

with

$$St(\psi_{ij}) = \sum_{n=-N/2+1}^{N/2} \frac{1}{|n|-1}e^{in(\phi_i - \phi_j)}. \tag{3.31}$$

Equation (3.31) is the discrete Stokes kernel for the plane.

Next, we solve again Stokes' problem, but now we write the equations in the spectral domain. This is done to show that the solution in the frequency domain is the same as in the space domain. It will lead to a simple connection to the continuous boundary value problem. We obtain the spectral equations by taking linear combinations of the observation equations (3.23). The first was

$$dW_i = -dz_i + \sum_n \Delta c_n e^{in\phi}. \tag{3.32}$$

With (3.24) and (3.28) we find

$$\frac{1}{N}\sum_i dW_i e^{-im\phi_i} = -\frac{1}{N}\sum_i dz_i e^{-im\phi_i} + \frac{1}{N}\sum_i\sum_n \Delta c_n e^{i(n-m)\phi_i}$$

$$\Leftrightarrow\ dW_n = -dz_n + \Delta c_n. \tag{3.33}$$

The same procedure is applied to dg_i. Now we have (3.23) in the spectral domain as

$$\begin{pmatrix} [dW_n] \\ [dg_n] \end{pmatrix} = \begin{pmatrix} [-\delta_{nm}] & [\delta_{nm}] \\ [-\delta_{nm}] & [|n|\delta_{nm}] \end{pmatrix} \begin{pmatrix} dz_n \\ \Delta c_n \end{pmatrix}. \tag{3.34}$$

We define the weight matrix as

$$\boldsymbol{P}_y = \begin{pmatrix} [p'_w\delta_{nm}] & [0] \\ [0] & [p'_g\delta_{nm}] \end{pmatrix}.$$

Solving the system (3.34) by least squares we get

$$\boldsymbol{N} = \begin{pmatrix} [(p'_w + p'_g)\delta_{nm}] & [-(p'_w + |n|p'_g)\delta_{nm}] \\ [-(p'_w + |n|p'_g)\delta_{nm}] & [(p'_w + n^2p'_g)\delta_{nm}] \end{pmatrix},$$

$$Q_{22} = \left(\frac{p'_w + p'_g}{(|n|-1)^2 p'_w p'_g}\right)\delta_{nm},$$

$$Q_{12} = \frac{p'_w + np'_g}{(|n|-1)^2 p'_w p'_g}\delta_{nm},$$

$$Q_{11} = \frac{1}{p'_w + p'_g}\left(1 + \frac{(p'_w + np'_g)^2}{(|n|-1)^2 p'_w p'_g}\delta_{nm}\right),$$

$$\Delta c_n = \frac{1}{|n|-1}(dg_n - dW_n), \qquad |n| \neq 1$$

$$dz_n = -dW_n + \frac{1}{|n|-1}(dg_n - dW_n).$$

The same solution as obtained by the space domain approach (3.29). Naturally this is no surprise as the only change made here was to take a linear combination of the observation equations before solving for the unknowns.

3.3.2 Continuous Stokes in the spectral domain

So far we used the quantities dW_i, etc. as discrete functions. But the observation equations like (3.32) are also valid for a continuous function of observations. The continuous problem will be considered in this section. To express the fact that dW is continuous we write (3.32) as

$$dW(\phi) = -dz(\phi) + \sum_n \Delta c_n e^{in\phi}.$$

Just as we did in (3.33) we take linear combinations of the observations. Because of the continuity of the functions integrals instead of sums are used. We have

$$\frac{1}{2\pi}\int_{-\pi}^{\pi} dW(\phi)e^{-im\phi}d\phi = -\frac{1}{2\pi}\int_{-\pi}^{\pi} dz(\phi)e^{-im\phi}d\phi + \sum_n \frac{1}{2\pi}\Delta c_n \int_{-\pi}^{\pi} e^{in\phi}e^{-im\phi}d\phi$$

$$\Leftrightarrow \quad dW_n = -dz_n + \Delta c_n. \tag{3.35}$$

The relation for the Fourier coefficients

$$dW_n = \frac{1}{2\pi}\int_{-\pi}^{\pi} dW(\phi)e^{-in\phi}d\phi \tag{3.36}$$

is applied and the orthogonality

$$\frac{1}{2\pi}\int_{-\pi}^{\pi} e^{in\phi}e^{-im\phi}d\phi = \delta_{nm}. \tag{3.37}$$

We see that we have in (3.35) the same spectral relation as in (3.33) for the discrete problem. So also the continuous problem leads to the solution (3.29).

When converting the continuous functions to the spectral domain the continuous system of equations is transformed to a discrete system with an infinite number of equations. This transformation is allowed when the integrals in (3.35) are finite. From Fourier theory we know that every function $f \in L^2[0, 2\pi]$ can be represented by its (finite) Fourier coefficients f_n, such that

$$\lim_{N\to\infty} \|f(\phi) - \sum_{n=-N}^{N} f_n e^{in\phi}\| = 0$$

Hence, if all the boundary functions are element of $L^2[0, 2\pi]$, the integrals are finite and the transformation is allowed.

3.3.3 Continuous Stokes in the space domain

In the previous section the continuous Stokes problem was solved by transformation to the spectral domain. In this section it is shown how it can be formulated in the space domain, as was done in section 3.3.1 for the discrete problem.

Since the weight matrix used for the solution to the GBVP is a unit matrix, multiplied by a constant weight factor, the inner product applied here is the standard inner product of linear algebra. In order to prepare the step from discrete to continuous, the inner product

$$(\boldsymbol{a}, \boldsymbol{b}) = \sum_i \frac{1}{N} a_i b_i$$

is introduced. Then the reproducing kernel becomes the scaled unit matrix: $N.\boldsymbol{I}$. Applying this to the observation equations (3.32) we get:

$$\begin{aligned} dW_i &= -dz_i + \sum_n \Delta c_n e^{in\phi} \\ &= -\sum_{j=0}^{N-1} \delta_{ij} dz_j + \sum_n \Delta c_n e^{in\phi} \qquad (3.38) \\ &= -\frac{1}{N} \sum_{j=0}^{N-1} (N\delta_{ij}) dz_j + \sum_n \Delta c_n e^{in\phi}. \qquad (3.39) \end{aligned}$$

Equation (3.38) can be read as the first equation of the matrix equation (3.18) with the standard inner product $\sum_i f_i.g_i$ and the reproducing kernel δ_{ij}. In (3.39), the newly defined inner product and reproducing kernel were used.

Now (3.23) is written as

$$\begin{pmatrix} [dW_i] \\ [dg_i] \end{pmatrix} = \begin{pmatrix} [-N\delta_{ij}] & \left[e^{in\phi}\right] \\ [-N\delta_{ij}] & \left[|n|e^{in\phi}\right] \end{pmatrix} \begin{pmatrix} [dz_i] \\ [\Delta c_n] \end{pmatrix}, \qquad (3.40)$$

$$\boldsymbol{P}_y = \begin{pmatrix} [Np_w\delta_{ij}] & [0] \\ [0] & [Np_g\delta_{ij}] \end{pmatrix}.$$

For the normal matrix we have

$$\boldsymbol{N} = \begin{pmatrix} [N(p_w + p_g)\delta_{ij}] & \left[-(p_w + |n|p_g)e^{in\phi}\right] \\ \left[-(p_w + |n|p_g)e^{-in\phi_j}\right] & [(p_w + n^2 p_g)\delta_{nm}] \end{pmatrix}.$$

Solving (3.40) leads to the solution (3.29). Although this formulation of the discrete problem is not the most natural one, it is correct. The charm of formulating the

problem in this way is that taking the limit $N \to \infty$ leads directly to the solution to the continuous problem. The inner product for the space domain becomes

$$\lim_{N\to\infty} \frac{1}{N} \sum_{j=0}^{N-1} f(\frac{2\pi}{N}j).g(\frac{2\pi}{N}j) = \lim_{N\to\infty} \frac{1}{2\pi} \sum_{j=0}^{N-1} f(\phi_j).g(\phi_j)\,\Delta\phi = \frac{1}{2\pi}\int_{-\pi}^{\pi} f(\phi).g(\phi)\,d\phi. \tag{3.41}$$

This yields for the orthogonality (3.24) the relation (3.37)

$$\lim_{N\to\infty} \frac{1}{N} \sum_{j=0}^{N-1} e^{i(n-m)\frac{2\pi}{N}j} = \frac{1}{2\pi}\int_{-\pi}^{\pi} e^{i(n-m)\phi}d\phi = \delta_{nm}$$

and for the equation for the coefficients (3.28) we get (3.36)

$$dg_n = \lim_{N\to\infty} \frac{1}{N} \sum_{j=0}^{N-1} dg(\frac{2\pi}{N}j).e^{-in\frac{2\pi}{N}j} = \frac{1}{2\pi}\int_{-\pi}^{\pi} dg(\phi)e^{-in\phi}d\phi.$$

See (Jenkins & Watts, 1968).

This requires some explanation. With the discrete problem we had discrete functions given on the circle; i.e. periodic functions. Their spectra are therefore periodic and discrete too. By taking more and more points on the interval $[0, 2\pi]$, the point density increases and the number of coefficients in the spectrum too. In the limit $N \to \infty$ the function becomes continuous, so summations over points become integrals, and the number of Fourier coefficients gets infinite but countable. Since the spectrum remains a discrete function in this limit, the functions are periodic, all the operations on the spectral variables do not change. Thus matrix multiplications involving summations over the spectral index n or m and also the identity operation δ_{nm} do not change when taking the limit. As said before the space domain functions become continuous. Since we worked with equidistantly spaced functions in the discrete case, this transition runs smoothly. The integrals just replace the summations. The only functions we have to take a closer look at are the identity functions (reproducing kernels). For the discrete problem the Kronecker delta δ_{ij} was used. Now we have to show what happens to the $N\delta_{ij}$, as used in (3.39), when $N \to \infty$. We compute this limit in the spectral domain. The spectrum of δ_{ij} is (Papoulis, 1962)

$$a'_n = \begin{cases} \frac{1}{N} & n \in \{-\frac{N}{2}+1, \ldots, -1, 0, 1, \ldots, \frac{N}{2}\} \\ 0 & \text{else} \end{cases}$$

This yields for the spectrum of $\lim_{N\to\infty} N\delta_{ij}$

$$a_n = 1 \qquad \forall n \in \mathrm{Z}.$$

This is the spectrum of the Dirac function $2\pi\delta(\phi_P - \phi_Q)$ (Papoulis, 1962). So we have

$$\lim_{N\to\infty} N\delta_{ij} = 2\pi\delta(\phi_P - \phi_Q). \tag{3.42}$$

Hence, $2\pi\delta$ is the reproducing kernel for the continuous problem. This can also be shown by using the well known reproducing property of the Dirac function

$$\int_{-\pi}^{\pi} f(\tau)\delta(\phi-\tau)d\tau = f(\phi)$$

or, with the inner product (3.41),

$$\frac{1}{2\pi}\int_{-\pi}^{\pi}[2\pi\delta(\phi_P-\phi_Q)]\,f(\phi_P)d\phi_P = f(\phi_Q).$$

Now we finally have (3.23) for the continuous situation

$$\begin{pmatrix}[dW(\phi_P)]\\ [dg(\phi_P)]\end{pmatrix} = \begin{pmatrix}[-2\pi\delta_{PQ}] & \left[e^{in\phi_P}\right]\\ [-2\pi\delta_{PQ}] & \left[|n|e^{in\phi_P}\right]\end{pmatrix}\begin{pmatrix}[dz(\phi_Q)]\\ [\Delta c_n]\end{pmatrix}. \tag{3.43}$$

In the sequel we will omit the argument ϕ whenever convenient. The weight matrix is

$$\boldsymbol{P}_y = \begin{pmatrix}[2\pi p_w\delta] & [0]\\ [0] & [2\pi p_g\delta]\end{pmatrix}.$$

We do not give a solution to this problem, it will again be Stokes' integral, but continue in the next section with the vectorial problem.

Before proceeding with the other GBVP's, one remark about convergence should be made. As shown in this section, the potential coefficients can be determined either from discrete observations or from continuous data. This brings us to the question how the potential coefficients, computed from these different kind of data sources, are related to each other. The answer is found in signal theory. There we find the *sampling theorem*, which shows how the spectrum of a continuous function and the spectrum derived from samples of that function are related, see e.g. (Jenkins & Watts, 1968). Because the discrete boundary data are obtained by sampling a continuous function on that boundary, this theorem can be applied to the GBVP. It gives the opportunity to relate the spectrum of the discrete observations to the spectrum of the continuous function. Since the potential coefficients are directly related to the coefficients of the same degree of the boundary data, the effects of sampling on the solved potential coefficients can be computed easily. To come back to the convergence, it is obvious from the theorems concerning sampling, that the error introduced by taking discrete data instead of continuous, can be made arbitrary small by taking a large enough amount of samples.

3.3.4 Vectorial Stokes

Now we continue with the vectorial Stokes problem we started with, i.e. potential, gravity and astronomical latitude are assumed to be observed. In this case the

design matrix, with the definition of the inner product (3.41) for continuous data, becomes,

$$\boldsymbol{A} = \begin{pmatrix} [0] & [-2\pi\delta] & \left[e^{in\phi}\right] \\ [0] & [-2\pi\delta] & \left[|n|e^{in\phi}\right] \\ [2\pi\delta] & [0] & \left[-ine^{in\phi}\right] \end{pmatrix}.$$

For the normal matrix we get

$$\boldsymbol{N} = \begin{pmatrix} [2\pi p_\Phi \delta] & [0] & \left[-p_\Phi ine^{in\phi}\right] \\ [0] & [2\pi(p_w + p_g)\delta] & \left[-(p_w + |n|p_g)e^{in\phi}\right] \\ \left[p_\Phi ine^{-in\phi}\right] & \left[-(p_w + |n|p_g)e^{-in\phi}\right] & [(p_w + n^2 p_g + n^2 p_\Phi)\delta_{nm}] \end{pmatrix}.$$

The sub-matrices of the inverse normal matrix are

$$Q_{11} = \begin{pmatrix} \left[\frac{2\pi}{p_\Phi}\delta + \sum_n n^2 \frac{p_w+p_g}{(|n|-1)^2 p_w p_g} e^{in\phi_i} e^{-in\phi_j}\right] & \left[\sum_n \frac{in(p_w+|n|p_g)}{(|n|-1)^2 p_w p_g} e^{in\phi_i} e^{-in\phi_j}\right] \\ \left[-\sum_n \frac{in(p_w+|n|p_g)}{(|n|-1)^2 p_w p_g} e^{in\phi_i} e^{-in\phi_j}\right] & \left[\frac{2\pi}{p_w+p_g}\delta + \sum_n \frac{(p_w+|n|p_g)^2}{p_w+p_g} \frac{e^{in\phi_i} e^{-in\phi_j}}{(|n|-1)^2 p_w p_g}\right] \end{pmatrix},$$

$$Q_{12} = \begin{pmatrix} [in(p_w + p_g)] \\ [p_w + |n|p_g] \end{pmatrix} \frac{e^{in\phi}}{(|n|-1)^2 p_w p_g},$$

$$Q_{22} = \frac{p_w + p_g}{(|n|-1)^2 p_w p_g} \delta_{nm}.$$

For $\boldsymbol{A}^* \boldsymbol{P}\boldsymbol{y}$ we have

$$\boldsymbol{A}^* \boldsymbol{P}\boldsymbol{y} = \begin{pmatrix} [p_\Phi d\Phi] \\ [-p_w dW - p_g dg] \\ [p_w dW_n + |n|p_g dg_n + inp_\Phi d\Phi_n] \end{pmatrix}.$$

This finally yields the solution

$$\Delta c_n = \frac{1}{|n|-1}(dg_n - dW_n) \qquad (|n| \neq 0, 1) \qquad \text{(Stokes)}, \tag{3.44}$$

and

$$dx_P = d\Phi_P + \sum_{n=-\infty}^{\infty} \frac{in}{|n|-1}(dg_n - dW_n)e^{in\phi_P} \qquad (|n| \neq 0, 1) \qquad \text{(Vening Meinesz)},$$

$$dz_P = -dW_P + \sum_{n=-\infty}^{\infty} \frac{1}{|n|-1}(dg_n - dW_n)e^{in\phi_P} \qquad (|n| \neq 0, 1) \qquad \text{(Stokes - Bruns)}$$

As mentioned before, as in the 3D case, a singularity problem arises for $|n| = 1$. The unknown $\Delta c_{|n|=1}$ can not be solved for. Its introduction as unknown, yields a singular system of equations. The reason for this, and how to handle this problem, is discussed in section 3.8. With (2.18) the corresponding integral formulas become

$$dT_P = \Delta c \ln \frac{1}{R} + \frac{1}{2\pi} \int_{-\pi}^{\pi} St(\psi_{PQ})(dg - dW)_Q d\phi_Q, \tag{3.45}$$

$$dx_P = d\Phi_P - \frac{1}{2\pi} \int_{-\pi}^{\pi} \frac{\partial St(\psi_{PQ})}{\partial \psi}(dg - dW)_Q d\phi_Q, \tag{3.46}$$

$$dz_P = -dW_P + \Delta c \ln \frac{1}{R} + \frac{1}{2\pi} \int_{-\pi}^{\pi} St(\psi_{PQ})(dg - dW)_Q d\phi_Q. \tag{3.47}$$

In order to have a complete solution for the unknowns the logarithmic term is added to the Stokes integral. For the Stokes kernel St the analytical expression can be derived from (2.30). It is

$$St(\psi) = \sin\psi(\psi - \pi) - 2\cos\psi \ln(2\sin\psi/2) \qquad (0 \leq \psi \leq \pi),$$

which is in agreement with (Gerontopoulos, 1978). For the derivative (Vening Meinesz function) we have by differentiation

$$\frac{\partial St}{\partial \psi} = \sin\psi - \cos\psi\cot\psi/2 + 2\sin\psi\ln(2\sin\psi/2) + \cos\psi(\psi - \pi) \qquad (0 < \psi < \pi).$$

See figure 3.1 for a graph of the two functions. Apart from some constants and the logarithmic function, the Stokes integral found here is identical to Stokes' integral of 3D. For the Vening Meinesz integral one major difference occurs: the absence of the azimuth. This is not surprising since our boundary is not a surface but a line, such that the orientation of the line connecting the point of integration and the point of computation is fixed.

3.4 The gradiometric problem

The solution of the system of equations (3.19) for the gradiometric problem is straightforward: since the Γ_{zz} component does not depend on the position corrections we directly find:

$$\Delta c_n = \frac{1}{n} \frac{1}{|n| - 1}(d\Gamma_{zz})_n$$
$$dz = \tfrac{1}{2}(T_{rr} - d\Gamma_{zz}).$$

The horizontal shift cannot be determined, obviously.

The independence of Γ_{zz} of the position, is introduced by the definition of the anomalies (see 3.1). Nevertheless, the combination with the other second derivative, Γ_{zz} is sufficient to replace e.g. the potential and gravity as observations: from both combinations potential and vertical position can be solved.

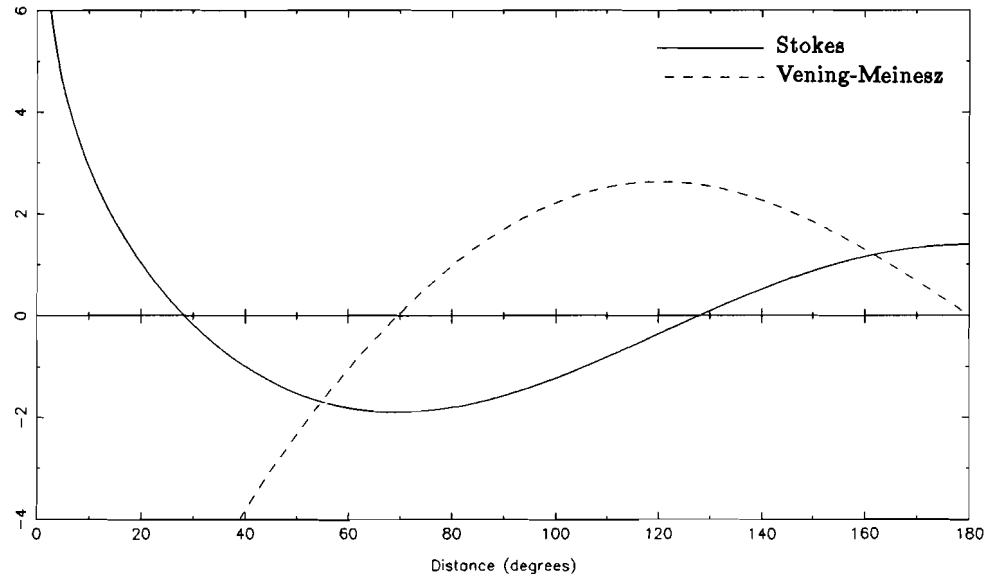

Figure 3.1 *The Stokes and the Vening Meinesz kernel.*

3.5 Overdetermined vertical problem

Up to now, uniquely determined systems of equations were considered. By adding more observations to these systems, they become overdetermined if no additional unknowns are introduced. First we take all observations from (3.18)–(3.19) which only depend on the vertical position and the disturbing potential. Also the observation of vertical position dz, which can be observed by means of satellite altimetry (on sea) or GPS, is included. The disturbance dz is the projection of the distance between the approximate point on the telluroid and the point on the surface onto the local normal gravity vector. The dz can serve as observation for these kinds of measurements since the coordinates of the surface point are the observables. In this system there are four observables and only two unknowns for each point, hence it is overdetermined.

The system is, from (3.18) and (3.19),

$$\begin{pmatrix} dW \\ dg \\ d\Gamma_{zz} \\ dz \end{pmatrix} = \begin{pmatrix} -1 \\ -1 \\ -2 \\ 1 \end{pmatrix} \left(dz \right) + \begin{pmatrix} \sum_n \Delta c_n e^{in\phi} \\ \sum_n |n| \Delta c_n e^{in\phi} \\ \sum_n |n|(|n|+1) \Delta c_n e^{in\phi} \\ 0 \end{pmatrix}. \tag{3.48}$$

Solving this system in the same way as was done for Stokes' problem we get

$$Q_{11} = \frac{1}{p_w + p_g + 4p_\Gamma + p_z}\left(2\pi\delta_{ij} + \sum_n \frac{(p_w + |n|p_g + |n|(|n|+1)p_\Gamma)^2}{E_n} e^{in\phi_i} e^{-in\phi_j}\right),$$

$$Q_{12} = \frac{p_w + |n|p_g + |n|(|n|+1)p_\Gamma}{E_n} e^{in\phi},$$

$$Q_{22} = \frac{p_w + p_g + 4p_\Gamma + p_z}{E_n}\delta_{nm},$$

where

$$\begin{aligned} E_n =& p_w p_g(|n|-1)^2 + p_w p_\Gamma(|n|-1)^2(|n|+2)^2 + p_w p_z + p_g p_\Gamma(|n|-1)^2 n^2 + \\ &+ p_g p_z n^2 + p_\Gamma p_z(|n|+1)^2 n^2. \end{aligned} \tag{3.49}$$

For the coefficients Δc_n we find

$$\begin{aligned} \Delta c_n =& \frac{1}{E_n}(p_w p_g(|n|-1)(dg_n - dW_n) + p_w p_\Gamma(|n|-1)(|n|+2)(d\Gamma_n - 2dW_n) + \\ & p_w p_z(dz_n + dW_n) + p_g p_\Gamma(|n|-1)|n|(d\Gamma_n - 2dg_n) + p_g p_z|n|(dz_n + dg_n) + \\ & p_\Gamma p_z(|n|+1)|n|(d\Gamma_n + 2dz_n)), \end{aligned} \tag{3.50}$$

and for the vertical position

$$\begin{aligned} dz_i = \frac{1}{p_w + pg + 4p_\Gamma + p_z}\{&-p_w dW_i - p_g dg_i - 2p_\Gamma d\Gamma_i + p_z dz_i + \\ &+ \sum_n (p_w + |n|p_g + 2|n|(|n|+1)p_\Gamma)\Delta c_n e^{in\phi_i}\Big\} \end{aligned} \tag{3.51}$$

The integral form of (3.50) is written as a combination of six kernel integrals:

$$\begin{aligned} dT(P) = \Delta c \ln\frac{1}{R} + \frac{1}{2\pi}\int_{-\pi}^{\pi} [\, & K_a(\psi_{PQ})(dg - dW)_Q + \\ & K_b(\psi_{PQ})(d\Gamma - 2dW)_Q + \\ & K_c(\psi_{PQ})(dz + dW)_Q + \\ & K_d(\psi_{PQ})(d\Gamma - 2dg)_Q + \\ & K_e(\psi_{PQ})(dz + dg)_Q + \\ & K_f(\psi_{PQ})(d\Gamma + 2dz)_Q \,]\, d\phi_Q. \end{aligned} \tag{3.52}$$

The kernels of this integral are defined as

$$\left.\begin{matrix} K_a(\psi) \\ K_b(\psi) \\ K_c(\psi) \\ K_d(\psi) \\ K_e(\psi) \\ K_f(\psi) \end{matrix}\right\} = \sum_n \frac{1}{E_n} e^{in\psi} \left\{\begin{matrix} p_w p_g(|n|-1) \\ p_w p_\Gamma(|n|-1)(|n|+2) \\ p_w p_z \\ p_g p_\Gamma(|n|-1)|n| \\ p_g p_z |n| \\ p_\Gamma p_z(|n|+1)|n| \end{matrix}\right. .$$

In contrast with the solutions to uniquely determined systems, such as Stokes' problem, the kernels defining the solution of an overdetermined GBVP depend on the weights given to the observations. By giving a zero weight to an observable, it does not contribute to the solution. This can be used to obtain the solution for T from (3.52) for every combination of dW, dg, $d\Gamma_{zz}$ and dz. E.g. the solution to Stokes' problem comes from $p_\Gamma = p_z = 0$. It can be seen from the expressions above, that a kernel function becomes zero if the combination of observations with which it is multiplied in the integral is not present. If the system of equations is overdetermined, the contribution of one combination of observations to the solution for T, with respect to the uniquely determined situation, is reduced; the potential is built up from several kernels. Their relative importance is governed by the E_n function.

The six kernels are displayed in the figures 3.2–3.4. For every weight, two values were used: one and zero. This means that every observable has a weight equal to the other observables, or is not included in the system of equations. All other choices of weights are also allowed, but these were selected to give a general idea how the kernels look like for different situations. For every kernel of (3.52) this choice yields four functions. For e.g. the kernel K_a the weights p_w and p_g are one. If one of them would be zero, the kernel would be zero too. The two choices for the two other weights yield four possible realizations of the K_a kernel. If p_Γ and p_z are zero, only potential and gravity are available as observations; the K_a kernel reduces to Stokes' function. By adding the vertical gradient, $p_\Gamma = 1$, kernel K_a becomes almost zero. This implies that, if the potential, gravity and vertical gradient are available with identical relative accuracy, such that the weights can be taken equal, the contribution of the combination $(dg - dW)$ to the solution to T is small. If the vertical position is added to Stokes' problem, the kernel is also reduced in magnitude, but not as much as with the addition of the vertical gradient. Finally, the kernel is displayed with both observations added to Stokes' problem.

For the other kernels it works the same way. One remark about the kernel K_c. If $p_g = p_\Gamma = 0$, this kernel becomes a Dirac function. The reason for this is simple: for this combination of weights, the system of equations (3.48) reduces to Bruns' equation, which gives the solution to T from dW and dz point by point.

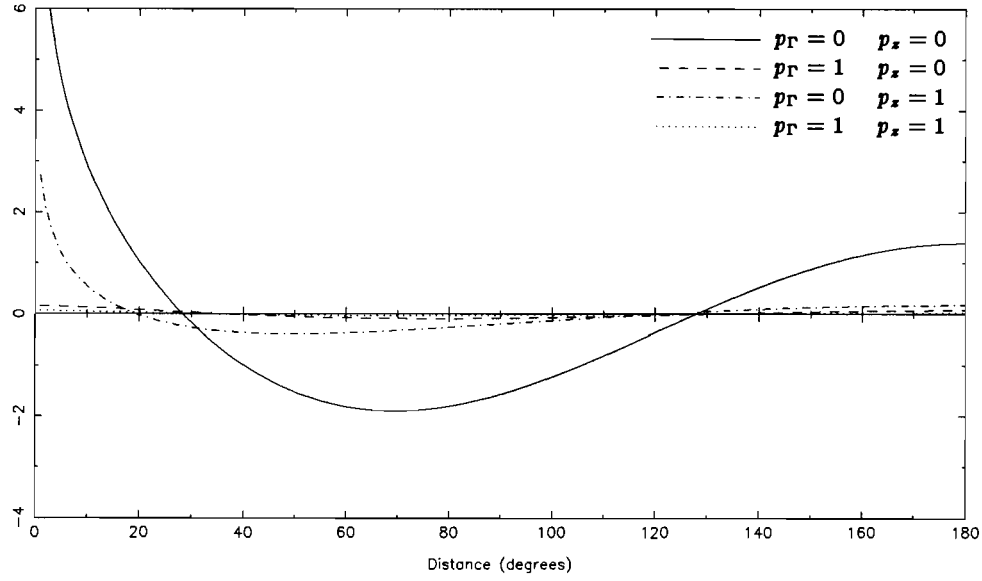

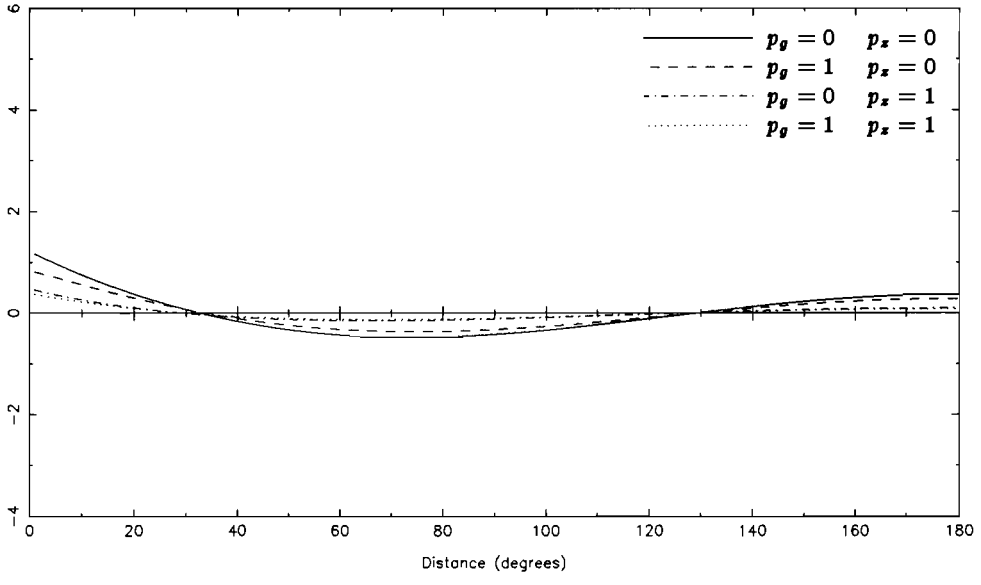

Figure 3.2 *The kernels K_a and K_b.*

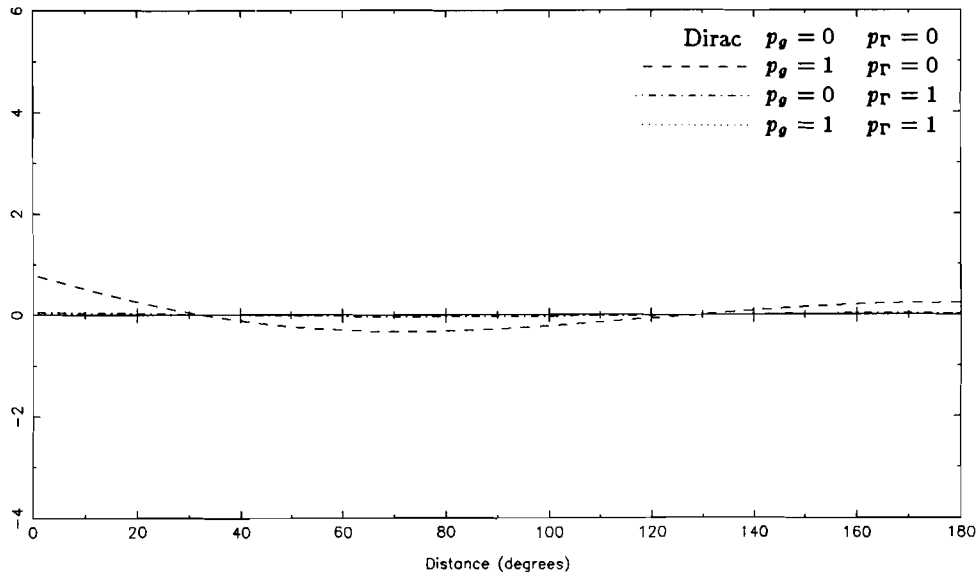

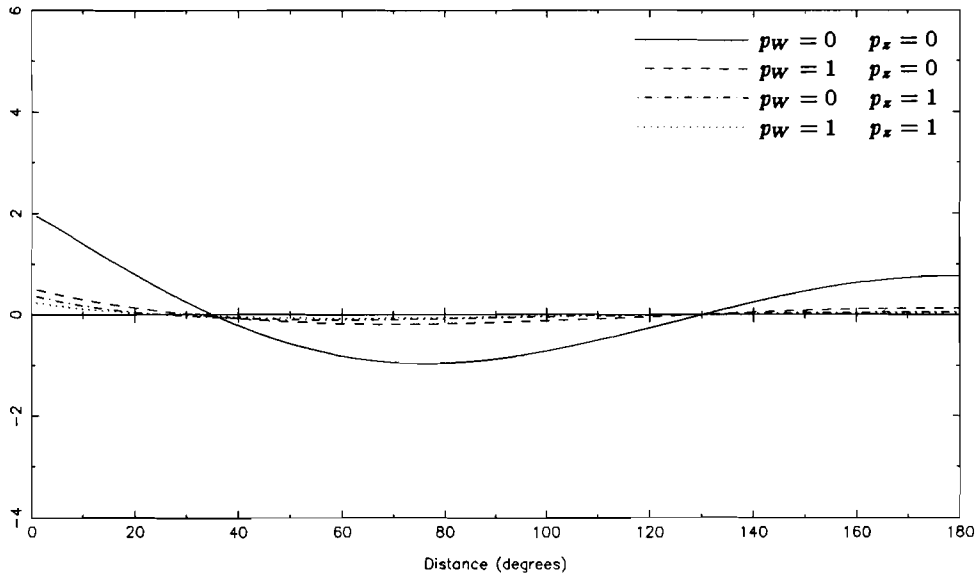

Figure 3.3 *The kernels K_c and K_d .*

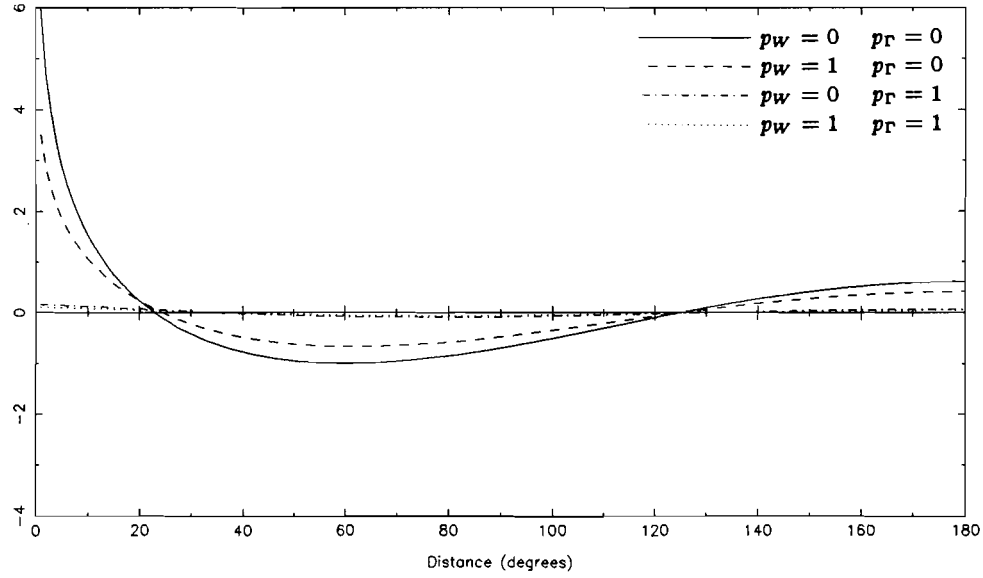

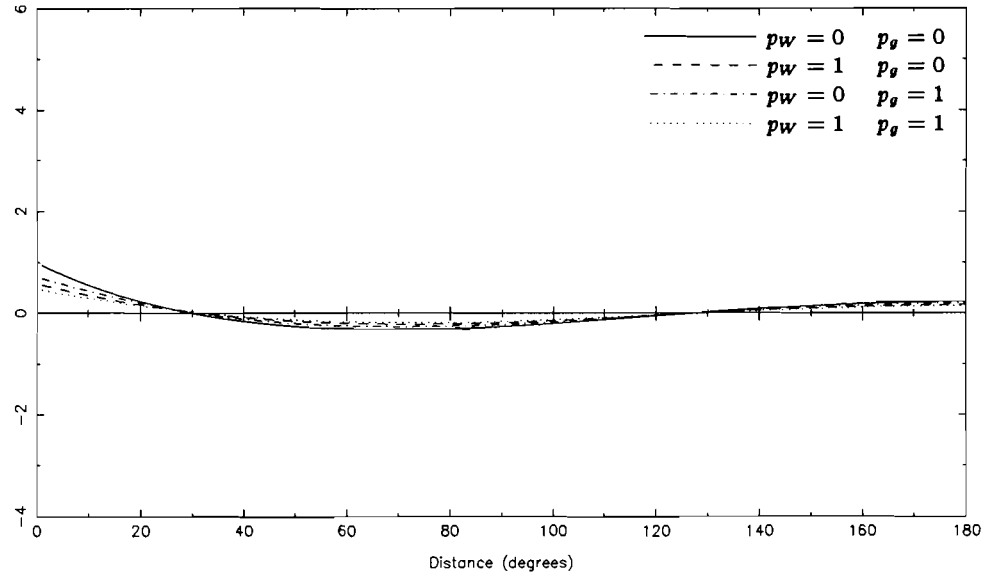

Figure 3.4 *The kernels K_e and K_f .*

3.6 Overdetermined horizontal problem

Now the other three observables, not depending on the vertical displacement dz, are put into one system of equations. In the two dimensional case we only have two observables that depend, in linear circular approximation, on the horizontal shift dx: dx and $d\Phi$. The gradient $d\Gamma_{zz}$ is added too. Using (3.18)-(3.19) we have

$$\begin{pmatrix} dx \\ d\Phi \\ d\Gamma_{zz} \end{pmatrix} = \begin{pmatrix} 1 \\ 1 \\ 0 \end{pmatrix} \Big(dx \Big) + \begin{pmatrix} 0 \\ -\sum_n in\Delta c_n e^{in\phi} \\ -\sum_n in(|n|-1)\Delta c_n e^{in\phi} \end{pmatrix}. \tag{3.53}$$

Applying the least squares solution we find the inverse normal matrix for the potential coefficients

$$Q_{22} = \frac{p_x + p_\Phi}{F_n},$$

with

$$F_n = n^2(p_\Phi p_x + (|n|-1)^2(p_x + p_\Phi)p_\Gamma). \tag{3.54}$$

For Δc_n we derive

$$\Delta c_n = \frac{in}{F_n}(p_\Phi p_x(d\Phi_n - dx_n) + (|n|-1)(p_x + p_\Phi)p_\Gamma d\Gamma_n). \tag{3.55}$$

From this equation the kernel representation for T can be derived. Because the horizontal derivatives are a constant (per degree) times the base functions $e^{in\phi}$, in contrast to the 3D model where the horizontal derivatives have a more complicated relation with the base functions, as the azimuth enters in the integrals, the kernels take a straightforward form. For T we get from (3.55), writing K_g and K_h for the kernels,

$$dT(P) = \Delta c \ln\frac{1}{R} + \frac{1}{2\pi}\int_{-\pi}^{\pi}[K_g(\psi_{PQ})(d\Phi - dx)_Q + K_h(\psi_{PQ})d\Gamma_Q]\, d\phi_Q. \tag{3.56}$$

The two kernels are defined as

$$\begin{Bmatrix} K_g(\psi) \\ K_h(\psi) \end{Bmatrix} = -\sum_n \frac{in}{F_n} e^{in\psi} \begin{Bmatrix} p_x p_\Phi \\ p_\Gamma(p_x + p_\Phi)(|n|-1) \end{Bmatrix}.$$

At first hand, we would expect a combination of three kernels for the three possible combinations of two observables. But because the gradient $d\Gamma_{zz}$ does not depend on the position in circular approximation, the disturbing potential can be completely determined from this gradient; no elimination is required to solve for the potential. The two kernels are displayed in figure 3.5. As with the vertical problem, three

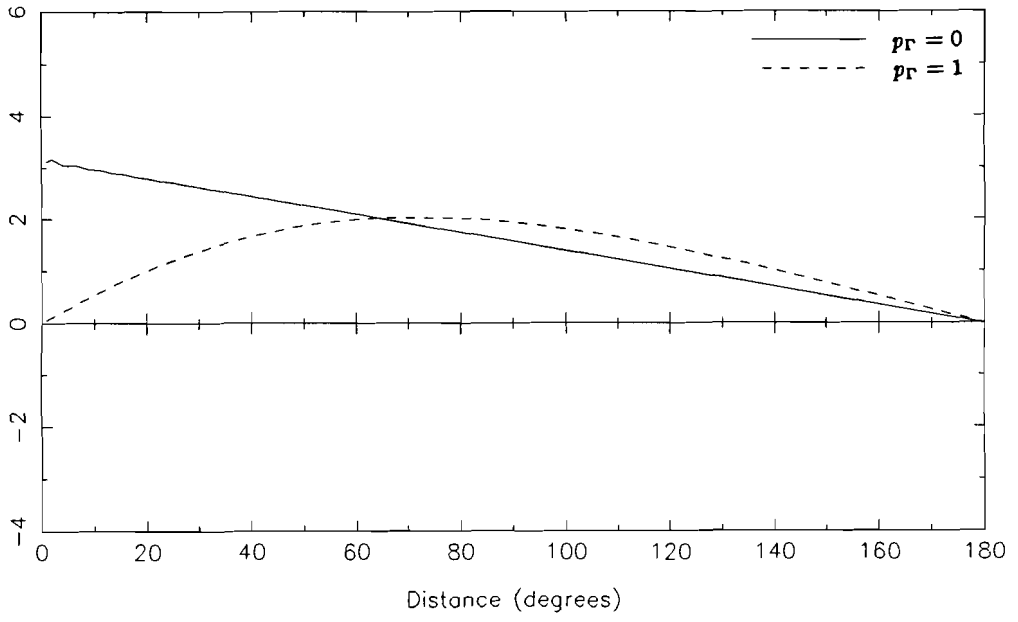

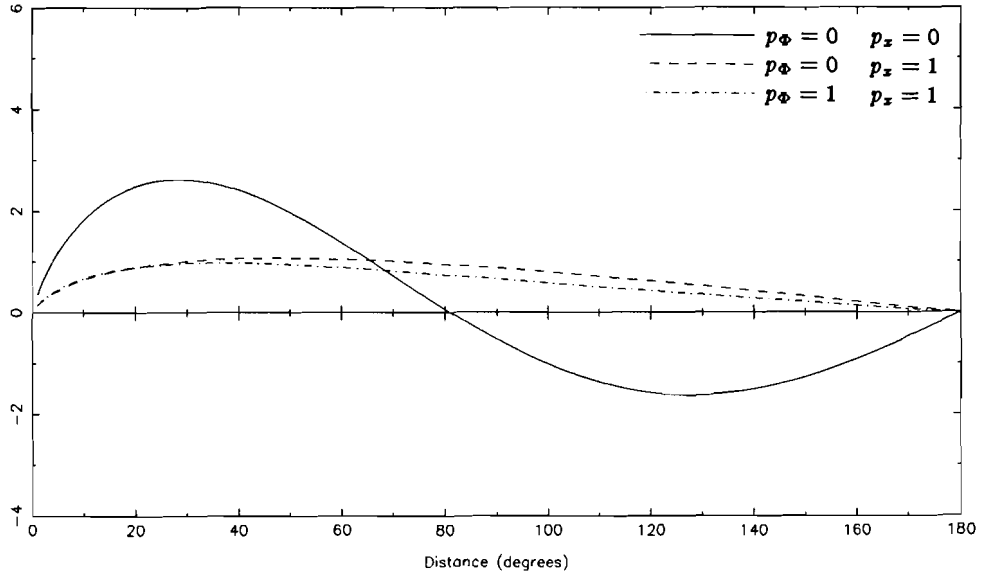

Figure 3.5 *The kernels K_g and K_h .*

unique GBVP's can be derived from this general solution, by taking three possible combinations of two observables. For $p_\Gamma = 0$ we have $K_h = 0$ and

$$K_g = -\sum_n \frac{i}{n} e^{-in\psi} = 2\sum_{n=1}^{\infty} \frac{1}{n} \sin n\psi = \pi - \psi, \qquad 0 < \psi < \pi$$

and for $p_x = 0 \vee p_\Phi = 0$ we find $K_g = 0$ and

$$\begin{aligned} K_h &= \sum_n \frac{-i}{n(|n|-1)} e^{in\psi} = 2\sum_{n=2}^{\infty} \frac{1}{n(n-1)} \sin n\psi \\ &= 2\sin\psi - 2\sin^2\psi/2(\pi - \psi) - 2\sin\psi \ln(2\sin\psi/2) \qquad 0 < \psi < \pi. \end{aligned}$$

The kernel K_h does not change when taking dx instead of $d\Phi$ since T is in both cases completely determined from $d\Gamma_{xz}$, the position dx from the other observable and the solved T. The analytic expressions were computed with (2.32).

3.7 Some remarks on the altimetry-gravimetry problem

For the GBVP's considered up to now, a global homogeneous coverage with the observations was assumed. In reality this condition cannot be met. One reason for this is the subdivision of the earth's surface into continents and oceans, for which different types of data are available. Let us consider the following situation. On land, we have leveling, gravimetry and horizontal position information. This combination supplies us with the potential (up to a constant), scalar gravity and the x–coordinate of the points of observation. At sea, the geometric heights of the sea surface above the reference ellipse are available from satellite altimetry. If it is assumed that, by means of corrections for sea surface topography and sea tides, the height of the geoid can be deduced from it, this gives for ocean areas the combination of height (dz) and potential (the geoid is a equipotential surface), and the horizontal position of the points of observation. The problem is to compute the disturbing potential from this combination of observations. In the literature this problem is known as the *altimetry-gravimetry* GBVP, but other combinations of data, such as gravity anomalies on the continents and gravity disturbances in ocean ares, share the same name. See e.g. (Holota, 1982), (Sacerdote & Sansò, 1983), (Svensson, 1983) or (Mainville, 1986).

This GBVP is formulated and treated in the same way as the other problems. We assume that the horizontal position is known globally, such that $dx = 0$ for all points. Thus dx can be disregarded. The design matrix and the vectors with unknowns and observations become

$$\boldsymbol{y} = \begin{pmatrix} [dW_i] \\ [dg_i] \\ [dz_i] \end{pmatrix} \qquad \boldsymbol{A} = \begin{pmatrix} [-2\pi\delta] & \left[e^{in\phi}\right] \\ [-2\pi\delta] & \left[|n|e^{in\phi}\right] \\ [2\pi\delta] & 0 \end{pmatrix} \qquad \boldsymbol{x} = \begin{pmatrix} [dz_i] \\ [\Delta c_n] \end{pmatrix}.$$

The weight matrix is defined as

$$\boldsymbol{P}_y = \begin{pmatrix} [2\pi p_w \delta_{ij}] & [0] & [0] \\ [0] & [2\pi p_g (1 - I_{sea})\delta_{ij}] & [0] \\ [0] & [0] & [2\pi p_z I_{sea}\delta_{ij}] \end{pmatrix}.$$

The function $I_{sea}(\phi)$ is the indicator function for the ocean areas: it equals unity for the oceans and zero for continental areas. For simplicity all weights are taken equal to unity in the sequel.

The normal matrix becomes

$$\boldsymbol{N} = \begin{pmatrix} [4\pi\delta_{ij}] & -\left[1 + |n|(1 - I_{sea})e^{in\phi_i}\right] \\ -\left[1 + |m|(1 - I_{sea})e^{-im\phi_j}\right] & \left[\frac{1}{2\pi}\int_{-\pi}^{\pi}(1 + |n||m|(1 - I_{sea}))e^{i(n-m)\phi}d\phi\right] \end{pmatrix}.$$

For the inverse of the sub-matrix Q_{22} we find

$$Q_{22}^{-1} = \left[(|n| - 1)(|m| - 1)\frac{1}{2\pi}\int_{-\pi}^{\pi}(1 - I_{sea})e^{-i(m-n)\phi}d\phi\right]_{nm} + \\ + \left[\frac{1}{2\pi}\int_{-\pi}^{\pi} I_{sea}e^{-i(m-n)\phi}d\phi\right]_{nm}.$$

The elements of this matrix are linear combinations of the Fourier coefficients of the indicator function for ocean areas I_{sea} and for land areas $1 - I_{sea}$. Omitting further intermediate results, we find for the potential coefficients

$$\Delta c_n = \frac{1}{2}\sum_m Q_{22,nm}\{(|m| - 1)(dg_m - dW_m) \\ -|m|\frac{1}{2\pi}\int_{-\pi}^{\pi}(dg - dW)I_{sea}e^{-im\phi}d\phi + \frac{1}{2\pi}\int_{-\pi}^{\pi}(dg + dz)I_{sea}e^{-im\phi}d\phi\Big\},$$

where $Q_{22,nm}$ denote the elements of the Q_{22} matrix. For the disturbing potential we get in the space domain

$$dT_P = \frac{1}{2\pi}\int_{-\pi}^{\pi}[K_i(\phi_P,\phi_Q)(dg - dW)_Q + \\ K_j(\phi_P,\phi_Q)(dg - dW)_Q I_{sea}(Q) + \\ K_k(\phi_P,\phi_Q)(dg + dz)_Q I_{sea}(Q)\,]\,d\phi_Q. \qquad (3.57)$$

Although the functions $K_.$ are now functions of *two* variables, as they depend explicitly on the position of both points, the same notation is maintained as before. These functions are:

$$\left.\begin{matrix} K_i(P,Q) \\ K_j(P,Q) \\ K_k(P,Q) \end{matrix}\right\} = \sum_{nm}\frac{1}{2}Q_{22,nm}e^{-im\phi_Q}e^{in\phi_P}\left\{\begin{matrix} (|m| - 1) \\ -|m| \\ 1 \end{matrix}\right. .$$

The elements $Q_{22,nm}$ multiplied by one of the factors of the right hand side, are the (2D) Fourier coefficients of the functions $K_.$. We did not determine so far a *direct* expression for the $K_.$ with respect to the I_{sea} function. Equation (3.57) reduces to *Stokes* for $I_{sea} \equiv 0$. If $I_{sea} \equiv 1$, the combination of integral kernels in (3.57) reduces to the K_c of section 3.5.

The existence of a solution to this problem depends on the function I_{sea}. A solution exists if the matrix Q_{22} can be computed. Hence, it is sufficient to investigate this matrix, to see what condition I_{sea} should fulfil to accomplish invertibility of Q_{22}. This is considered to be beyond the scope of this work.

3.8 Logarithmic, zero and first degree term

Three coefficients of the series of the (disturbing) potential deserve special attention: the logarithmic, zero and first degree term. When solving the GBVP's the logarithmic component of the potential was first omitted from the vector of unknowns and later added to the solution, the potential constant was put to zero and for the first degree coefficients additional constraints were required. In this section a more detailed discussion about the meaning of these coefficients is given and how they should be treated.

As stated before, the logarithmic function is the potential of a point mass. Therefore it has the same role as the zero degree function of the spherical harmonics of the 3D-potential: the most basic approximation of the earth's gravity field. Unfortunately the zero degree term of the Fourier series used for the 2D problem is a constant in the entire plane: it represents the potential constant and has a completely different meaning than the zero degree function for 3D. The zero degree function can be omitted in 2D without loss of generality: the potential constant of every potential function is arbitrary and can be put to zero (just as in 3D, where the constant is usually omitted from the solution to Laplace). The fact that the potential constant is arbitrary is directly related to the fact that only potential differences are observable, by e.g. the combination of leveling and gravimetry, and not the potential itself. In (Rummel et al., 1989) the (unknown) potential of a benchmark is introduced, which is added to the observed potential differences to obtain absolute potential values. In this chapter absolute potential values were created by setting the potential constant to zero. The former method is directly related to practice, but for our theoretical considerations that is not of importance.

In the presented GBVP the Δc was not computed from the data, but simply added to the computed solution. But it is possible, under certain conditions, to compute Δc from the boundary data. As an example this is shown for the vertical

GBVP (3.48). Including the logarithmic term the model yields

$$\begin{pmatrix} dW \\ dg \\ d\Gamma_{zz} \\ dz \end{pmatrix} = \begin{pmatrix} -1 \\ -1 \\ -2 \\ 1 \end{pmatrix} \Big(dz \Big) + \begin{pmatrix} \Delta c \ln \frac{1}{R} + \sum_n \Delta c_n e^{in\phi} \\ \Delta c + \sum_n |n| \Delta c_n e^{in\phi} \\ \Delta c + \sum_n |n|(|n|+1) \Delta c_n e^{in\phi} \\ 0 \end{pmatrix}.$$

Converting to the frequency domain, as was done for scalar Stokes in (3.34), the system becomes for degree zero (for completeness also the Δc_0 is included),

$$\begin{pmatrix} dW_{n=0} \\ dg_{n=0} \\ d\Gamma_{zz,n=0} \\ dz_{n=0} \end{pmatrix} = \begin{pmatrix} -1 & \ln \frac{1}{R} & 1 \\ -1 & 1 & 0 \\ -2 & 1 & 0 \\ 1 & 0 & 0 \end{pmatrix} \begin{pmatrix} dz_{n=0} \\ \Delta c \\ \Delta c_0 \end{pmatrix}. \tag{3.58}$$

Because of the orthogonality of the base functions, the solution can be computed degree by degree: the equations are de-coupled by the transformation to the frequency domain. With the four vertical observations this system is overdetermined. In e.g. the case of scalar Stokes (dW and dg) the system is underdetermined and an additional constraint is required such as the potential of a datum point (determines Δc_0) or the mass of the earth (fixes Δc).

In 3D the same situation is encountered. A system such as (3.58) can be formed with equations found in (Rummel et al., 1989). This will not be repeated here. In (Heiskanen & Moritz, 1967, ch. 2.19) the problem is treated for scalar Stokes. There the situation is discussed for $(\Delta W, \Delta g)$ referring to the geoid with potential W_0. The reference ellipsoid differs in potential from the geoid by δW. The potential constant of the ellipsoid equals the constant of the real field. Taking the same situation for 2D it is from (3.58) with $dW = \delta W/\mu'$, $dz_0 = N_0/R$ and $dg = \Delta g/\gamma_0$,

$$\begin{pmatrix} \delta W \\ \Delta g_0 \end{pmatrix} = \begin{pmatrix} -\gamma_0 & \mu' \ln \frac{1}{R} \\ -\frac{\gamma_0}{R} & \gamma_0 \end{pmatrix} \begin{pmatrix} N_0 \\ \Delta c \end{pmatrix}.$$

Elimination of Δc yields

$$\delta W - R \ln \frac{1}{R} \Delta g_0 = \gamma_0 (\ln \frac{1}{R} - 1) N_0,$$

the analogue of equation 2-187b of (ibid.).

The first degree has a direct physical meaning. Just as for the 3D potential series it is related to the coordinates of the center of mass. From (2.7) it is given

$$c_1 = \tfrac{1}{2} G \int_\Sigma \rho(Q) e^{-i\phi_Q} r_Q \, d\sigma_Q$$

$$\Leftrightarrow \begin{cases} c_1 + c_1^* = G\int_\Sigma \rho(Q) r_Q \cos\phi_Q d\sigma_Q = G\int_\Sigma X_Q \rho(Q) d\sigma_Q \\ ic_1 - ic_1^* = G\int_\Sigma \rho(Q) r_Q \sin\phi_Q d\sigma_Q = G\int_\Sigma Y_Q \rho(Q) d\sigma_Q \end{cases} . \tag{3.59}$$

If Δc_1 of the disturbing potential is zero it means that the center of mass of the normal field (and usually the origin of the coordinate frame) coincides with the center of mass of the earth.

As can be seen directly from (3.34), the first degree can cause singularities in the system of equations. For Stokes this is caused by the dependence of the columns of the matrix $\boldsymbol{A}$: the column for Δc_1 is a linear combination of the columns corresponding to dz. So it is impossible to solve for both dz and Δc_1 from the observables dW and dg. By omitting the first degree term from the observation equations the matrix $\boldsymbol{A}$ becomes regular and the problem can be solved. When all the degrees are included, an additional constraint for the $\Delta c_{n=1}$ has to be given. This is simply a choice of the origin of the coordinate frame with respect to the center of mass of the earth. The question can arise whether the boundary data has to fulfil the condition $(dg - dW)_{n=1} = 0$. As a solution is required in the parameter space this is not necessary. However, it is easy to show that such a constraint on the data can be easily satisfied. If we consider the normal potential function and the observed values of the potential and gravity as being given, then there is still one way to influence the function $(dg - dW)$: by the choice of the telluroid. By moving the telluroid, it will be possible to make the first degree component of $(dg - dW)$ zero, to match the constraint. But as the choice of the telluroid does not affect the final solution to the GBVP, if it is not too far from the real boundary, this translation of the telluroid is useless. The constraint can be matched by simply putting $(dg - dW)_{n=1} = 0$.

For the impossibility of solving the first degree coefficients by Stokes also a less mathematical explanation can be given. When observing the gravity vector and the potential, several definitions have to be made before the measurements can be represented in numbers. For the potential and the length of the gravity vector a gravimetric and geometric scale factor have to be chosen. For the orientation of the gravity vector, the orientation of the axes of the reference frame have to be fixed. But no choice has to be made for the *center* of the reference frame. If this choice is not contained in the data we put into the system of equations, it is impossible to get it out. Since the first degree coefficients are just the coordinates of the center of mass, they give the position of the used reference frame with respect to the real, physical world, it is not surprising that the first degree coefficients can not be solved. When including observations which require the definition of the origin of the reference frame, such as with GPS, which can be represented introducing dx, dz as observations, the singularity vanishes, as can be seen in the kernel for the combination of observations $\{dz, dg\}$. In (Heck, 1991), it is concluded that two of the three first degree harmonics are estimable in case a non-isotropic reference field is used, with the vectorial free GBVP. This is a peculiar statement in the light of the discussion above and the results of (Hörmander, 1976). The latter showed that

for Molodensky's problem, in order to get an unique and existent solution, three suitable functions have to be added to the boundary data, and we have to look for a solution for the potential which is free from first degree terms.

3.9 Astronomical leveling

In section 3.6 it was shown that the disturbing potential can be solved from the combination of 'horizontal' measurements dx and $d\Phi$. Taking into account that $dx = d\phi$, i.e. the difference in direction of the normal local frame between the approximate point P' and the surface point P, we have

$$d\Phi - dx = (\Phi_P - \phi_{P'}) - (\phi_P - \phi_{P'}) = \Phi_P - \phi_P = \xi_P,$$

the deflection of the vertical. Inserting into (3.56) yields for the geoid height $N = R.dT$, omitting the logarithmic term,

$$N_P = \frac{R}{2\pi} \int_{-\pi}^{\pi} K_g(\psi_{PS}) \xi_S d\phi_S, \tag{3.60}$$

with the definition of K_g as in section 3.6. There is a second integral, which supplies a connection between the disturbing potential and the deflection of the vertical. This is the integral of *astronomical leveling*. The deflection of the vertical multiplied by the distance increment equals the change in geoid height:

$$dN = -\xi ds;$$

see (Heiskanen & Moritz, 1967). Integration yields

$$N_P - N_Q = -R \int_{\phi_Q}^{\phi_P} \xi_S d\phi_S. \tag{3.61}$$

So, when computing the geoid height in P, we have two possibilities: integration of deflections over the entire boundary (3.60) or taking the geoid height of another point and integrate the deflection over the connecting line, (3.61). We show that the two solutions are equivalent.

First the analytic expression for K_g is extended to a larger domain (this is easily derived from its series expression):

$$K_g = \begin{cases} \pi - \psi & 0 < \psi < \pi \\ 0 & \psi = 0 \\ -\pi - \psi & -\pi < \psi < 0 \end{cases}.$$

We start with equation (3.60) and show, by splitting up the integral, that (3.61) can be derived from it. Inserting the expression for K_g into (3.60) yields

$$\begin{aligned}
N_P &= \frac{R}{2\pi}\int_{-\pi}^{\phi_P}(-\pi-\psi_{PS})\xi_S d\phi_S + \frac{R}{2\pi}\int_{\phi_P}^{\pi}(\pi-\psi_{PS})\xi_S d\phi_S \\
&= \frac{R}{2\pi}\int_{-\pi}^{\phi_P}(-\pi-\psi_{QS}+\psi_{PQ})\xi_S d\phi_S + \frac{R}{2\pi}\int_{\phi_P}^{\pi}(\pi-\psi_{QS}+\psi_{PQ})\xi_S d\phi_S \\
&= \frac{R}{2\pi}\int_{-\pi}^{\phi_Q}(-\pi-\psi_{QS})\xi_S d\phi_S + \frac{R}{2\pi}\int_{\phi_Q}^{\phi_P}(-\pi-\psi_{QS})\xi_S d\phi_S + \\
&\quad + \frac{R}{2\pi}\psi_{PQ}\int_{-\pi}^{\phi_P}\xi_S d\phi_S + \frac{R}{2\pi}\int_{\phi_Q}^{\pi}(\pi-\psi_{QS})\xi_S d\phi_S + \\
&\quad - \frac{R}{2\pi}\int_{\phi_Q}^{\phi_P}(\pi-\psi_{QS})\xi_S d\phi_S + \frac{R}{2\pi}\psi_{PQ}\int_{\phi_P}^{\pi}\xi_S d\phi_S \\
&= N_Q + \frac{R}{2\pi}\psi_{PQ}\int_{-\pi}^{\pi}\xi_S d\phi_S + \frac{R}{2\pi}\int_{\phi_Q}^{\phi_P}(-\pi-\psi_{QS}-\pi+\psi_{QS})\xi_S d\phi_S \\
&= N_Q - R\int_{\phi_Q}^{\phi_P}\xi_S d\phi_S
\end{aligned}$$

$$\Leftrightarrow N_P - N_Q = -R\int_{\phi_Q}^{\phi_P}\xi_S d\phi_S. \qquad q.e.d.$$

Hence, a consistent connection is established from the GBVP approach to astronomical leveling. In the 3D-GBVP this relation is not so easy to obtain. There the surface integral with ξ and η over the sphere is to be converted to the line integral of astronomical leveling (see (Rummel & Teunissen, 1989b)):

$$\begin{aligned}
N_P &= \frac{R}{4\pi}\int_{\sigma} K(\psi)\,[\xi\cos\alpha + \eta\sin\alpha]\,d\sigma \\
&\stackrel{?}{=} N_Q - \int_Q^P [\xi\cos\alpha + \eta\sin\alpha]\,ds.
\end{aligned}$$

K denotes the integral kernel

$$K(\psi) = -\sum_n \frac{2n+1}{n(n+1)}\frac{\partial}{\partial\psi}P_n(\cos\psi).$$

No answer exists so far, whether a similar connection can be found in this case.

3.10 Reliability

The overdetermined GBVP is not only attractive because of the accuracy improvement with respect to the uniquely determined GBVP, it also gives the opportunity

to test the input data. In case of a uniquely determined system of equations, the observations are exactly represented by insertion of the solved position shifts and potential coefficients back into the model. With an overdetermined system, this will generally not be the case because of the observation noise (and of the approximations introduced into the model, but this aspect is not considered here). If the distribution function of the noise is known, tests can be applied on the difference between the observation and the value computed from solved unknowns by backward substitution, to see whether this difference is acceptable with respect to the adopted stochastic model. As it is beyond the scope of this thesis, we refer to (Baarda, 1968) for the exact formulation. Here only a general outline and some illustrative formulas and figures are given.

For the distribution function of the measurement noise of the *discrete* observations, the Gaussian model will be appropriate. Since the Fourier coefficients of the observations are a linear combination of them, their noise also has a (multi-dimensional) normal distribution. The noise function of *continuous* observations is also a linear combination of its Fourier coefficients. If we assume for the coefficient noise a (infinite) multi-dimensional normal distribution, the noise in one point has also a normal distribution.

Testing of the observations requires the specification of alternative hypotheses. The usual alternative hypotheses is the one which states that one observation has some bias. The magnitude of such a bias that can be detected by the test, is called the minimal detectable bias. Its value depends on the choice of the parameters of the test (the one-dimensional F-test), and of the linear model. The values of these detectable errors show how well the observation is controlled by the other observations. Propagation of the minimal detectable biases into the unknowns, gives an indication how large their maximal bias will be if testing of the data is performed (assuming that the estimation yields unbiased estimates in case the stochastic model of the observations is correct).

The concept of reliability in the GBVP, is worked out for the overdetermined vertical problem (3.48). The formulas are given in the frequency domain, since this gives the most compact and clear formulas. Afterwards, the testing in the space domain is considered.

The minimal detectable bias is defined as

$$\nabla y^i = \boldsymbol{c}^i \sqrt{\frac{\lambda_0}{L}}.$$

The value of λ_0 is related to the parameters α_0 and β_0 of the F-test. With the conventional values

$$\alpha_0 = 0.001, \qquad \beta_0 = 0.8$$

we have $\lambda_0 = 17.07$. The vector $\boldsymbol{c}^i$ indicates the observation. It contains only zero's except the n'th element that equals one. It defines the alternative hypothesis of one

observation having a certain bias. The scalar L is computed as

$$L = (\boldsymbol{c}^i)^*(\boldsymbol{P} - \boldsymbol{P}\boldsymbol{A}\boldsymbol{N}^{-1}\boldsymbol{A}^*\boldsymbol{P})\boldsymbol{c}^i.$$

The capital letters denote the same matrices as in section 3.5. The design matrix for the overdetermined vertical problem is, in the spectral domain, with (3.48),

$$\boldsymbol{A} = \begin{pmatrix} [-\delta_{nm}] & [\delta_{nm}] \\ [-\delta_{nm}] & [|n|\delta_{nm}] \\ [-2\delta_{nm}] & [-|n|(|n|+1)\delta_{nm}] \\ [\delta_{nm}] & [0] \end{pmatrix}.$$

The matrix $\boldsymbol{P}$ now is the inverse variance-covariance matrix of the observations in the *frequency* domain. A diagonal matrix is taken, with variances only depending on the type of observation. The weights p_w, etc., now indicate the weight (inverse variance) for each degree.

$$\boldsymbol{P}_y = \begin{pmatrix} [p_w\delta_{ij}] & [0] & [0] \\ [0] & [p_g\delta_{ij}] & [0] \\ [0] & [0] & [p_\Phi\delta_{ij}] \end{pmatrix},$$

After some manipulations we obtain for the L:

$$\begin{aligned} L_{W_n} &= \frac{p_w p_g p_\Gamma n^2(|n|-1)^2 + p_w p_g p_z n^2 + p_w p_\Gamma p_z n^2(|n|+1)^2}{E_n}, \\ L_{g_n} &= \frac{p_w p_g p_\Gamma (|n|-1)^2(|n|+2)^2 + p_w p_g p_z + p_g p_\Gamma p_z n^2(|n|+1)^2}{E_n}, \\ L_{\Gamma_n} &= \frac{p_w p_g p_\Gamma (|n|-1)^2 + p_w p_\Gamma p_z + p_g p_\Gamma p_z n^2}{E_n}, \\ L_{z_n} &= \frac{p_w p_g p_z (|n|-1)^2 + p_w p_\Gamma p_z (|n|-1)(|n|+2)^2 + p_g p_\Gamma p_z n^2(|n|-1)^2}{E_n}. \end{aligned} \tag{3.62}$$

With (3.49) for E_n. In figure 3.6 the minimal detectable biases are plotted. For the weights we took $p_w : p_z : p_g : p_\Gamma = 100 : 100 : 1 : 0.01$.

The external reliability, the maximal bias in the solved unknowns, is computed by the propagation of the minimal detectable biases of the input data into the unknowns. When taking the alternative hypotheses in the frequency domain, the values for L as given in (3.62) are inserted into (3.50). The result is displayed in figure 3.7. Since a potential coefficient is only computed from the data of the same degree, a bias in one degree of an observation only effects the potential coefficient of the same

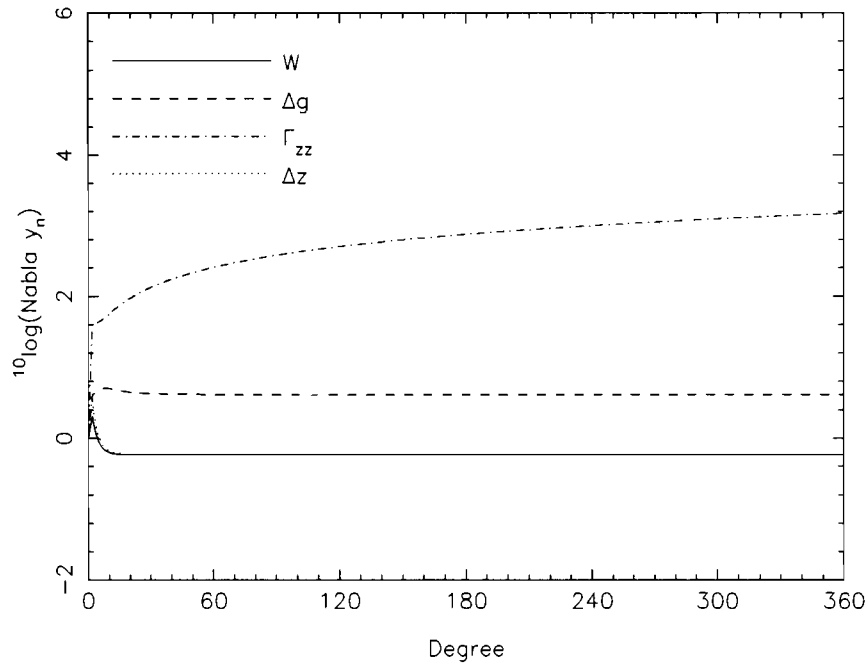

Figure 3.6 *Marginally detectable errors for the frequencies of the boundary data of the overdetermined vertical problem .*

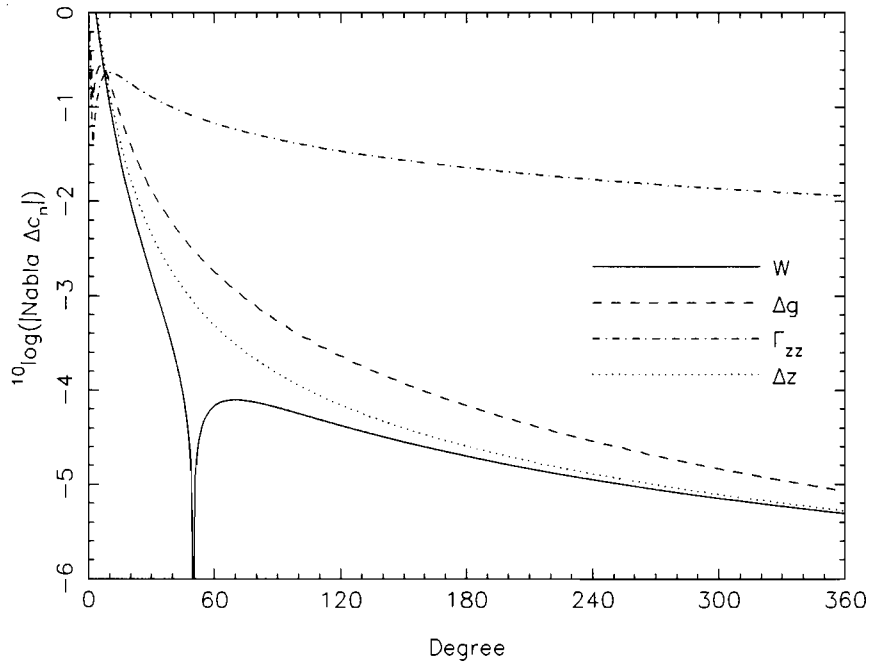

Figure 3.7 *The minimal detectable biases for the potential coefficients computed from the combination $dW, dg, d\Gamma$ and dz.*

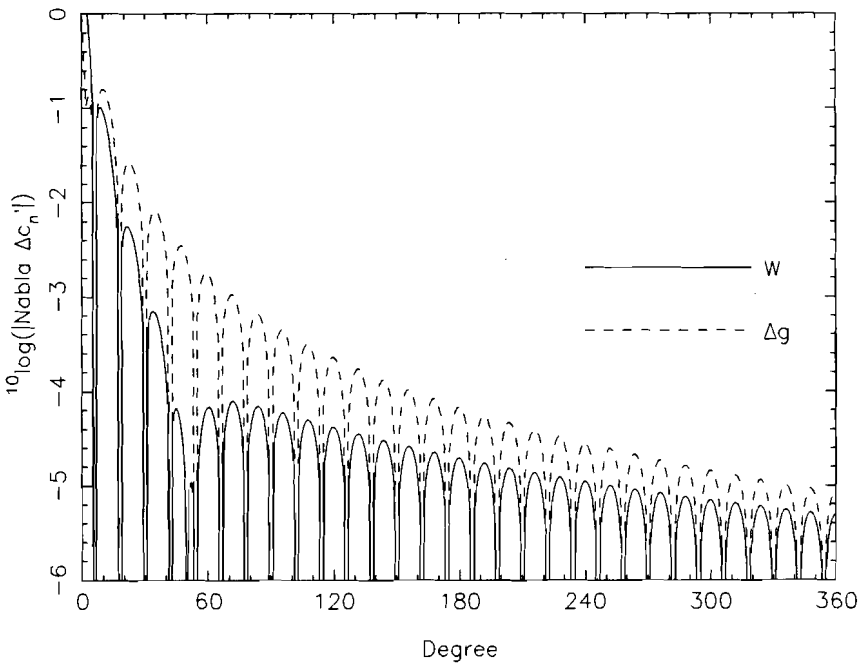

Figure 3.8 *The minimal detectable biases for the cosine potential coefficients computed from the combination $dW, dg, d\Gamma$ and dz. The two lines are related to two alternative hypotheses: a blunder in the observation dW or dg in the point $\phi = 15°$.*

degree. The figure shows the effects of all possible biases in the data for all degrees together. The weights were again taken as $p_w : p_z : p_g : p_\Gamma = 100 : 100 : 1 : 0.01$.

Also for the place domain alternative hypotheses can be derived. By writing the matrix $\boldsymbol{A}$ in the place domain, we find $L_{W_i} = \sum_n L_{W_n}$, etc. Hence, the critical values required for the testing in the place domain are directly computed from (3.62). As could be expected, all points of observation have the same weight in the estimation, the critical values do not depend on the location of the points.

If testing is performed in the place domain, the minimal detectable biases of the potential coefficients are like figure 3.7. There are two differences: a bias in one observation yields a bias in *all* potential coefficients, and the figure is multiplied by the base function $\bar{e}^{in\phi}$, with ϕ the latitude of the point where a bias is present. For clarity, in figure 3.8 the critical values of the *cosine* potential coefficients are shown.

A reasonable testing, and thereby a definition of reliability, is not as simple in reality as presented here. First the testing always takes place under the assumption that the model is perfect. But several approximations were introduced to derive it (linearization, circular approximation and constant radius). Hence, discrepancies between the model and the observations are also generated by these approximations and do not always indicate blunders in the data. Secondly, we always have to assume in our analytical least squares approach that the boundary data is given

either continuous, or in a regular grid. In the 3D-GBVP even the latter case is not possible. But *continuous* data is an assumption far from reality. It also gives problems with the definition of the alternative hypotheses. But since the GBVP can also be solved numerically, this is not a major point. When using discrete data, testing is possible, but not without complications. For instance, the selection of the potential coefficients to be solved, is a critical point. When taking the wrong selection, or if the boundary functions are undersampled, severe aliasing errors can occur in the solution to the potential coefficients. These biases cannot be detected by the proposed tests, and may be much larger in magnitude than biases caused by a blunder in the observation in one single point. In that case the testing procedure on the data does not seem very useful.

4

Higher order approximations of the linear problem

THE LINEAR MODEL, as formulated in section 2, was solved in the foregoing chapter by the introduction of the circular, constant radius approximation. In this chapter the explicit formulation of the linear model without approximation, as well as with only circular approximation is given. The errors introduced by the approximations in the linear GBVP are discussed.

For the solution to the GBVP's in higher approximation an iteration procedure is suggested. First it is shown how such a procedure can be used for matrices. Then we show how it can be implemented in the GBVP. Several GBVP's are presented, different in degree of approximation and in combination of observations. They will be solved ***numerically*** by iteration in chapter 5. In this chapter, different aspects of these models are discussed.

Finally it is shown that one iteration loop with the model in circular approximation, leads to the integrals of the problem of simple Molodensky known from the literature.

First the elliptical normal potential and its derivatives are derived, necessary for the coefficients of the models without circular approximation, and for the computation of the anomalies.

4.1 The normal potential

In section 3.1 it was discussed that for the solution to the GBVP a linearization procedure is applied. This involves linearization with respect to all the unknowns, position and gravity related quantities, and requires approximate values for this purpose. For the approximation of the potential, the normal potential, mainly three

models can be discriminated:

1. point mass potential,
2. elliptical potential,
3. set of potential coefficients.

The first model was already introduced in section 3.2. Model three can be any known set of potential coefficients. Here we will focus on the second model: a potential function with ellipses as equipotential lines.

4.1.1 Series expansion of the normal potential

By solving Laplace's equation in elliptical coordinates, and using the ellipse shape of the equipotential lines, the equation for the elliptical normal potential for the *non-rotating* earth can be derived. The derivation can be found in (Gerontopoulos, 1978):

$$U = U_0 - \mu' \ln(\frac{u}{2} + \frac{1}{2}\sqrt{u^2 + E^2}), \tag{4.1}$$

thereby U_0 denotes the potential constant of the normal field and μ' its GM value. For the coordinates the system $\{u, \beta\}$ is used (see appendix A). From (4.1) a series expression for the normal potential and analytical formulas for the normal values of the other observables, such as γ, are computed.

To find an expansion, (4.1) is modified as

$$U = U_0 + \mu' \ln \frac{1}{u} + \mu' \ln 2 - \mu' \ln(1 + \sqrt{1 + \left(\frac{E}{u}\right)^2}). \tag{4.2}$$

In (Gradshteyn & Ryzhik, 1980) the series

$$\ln(1 + \sqrt{1 + x^2}) = \ln 2 - \sum_{k=1}^{\infty} (-1)^k \frac{(2k-1)!}{2^{2k}(k!)^2} x^{2k} \qquad (x^2 \leq 1)$$

is found. Applying it to (4.2), with $x = E/u$ (outside the ellipse we have $u \leq b$; this guarantees $x \leq 1$), yields

$$U = U_0 + \mu' \ln \frac{1}{u} + \mu' \sum_{k=1}^{\infty} (-1)^k \frac{(2k-1)!}{2^{2k}(k!)^2} \left(\frac{E}{u}\right)^{2k}. \tag{4.3}$$

This series is now compared with the usual expansion of the potential (2.13). Since these two series converge for every point in outer space for every potential, the comparison between the two series along one radial line is sufficient. As test line a vertical profile at the North pole is selected, since it is computationally most convenient. With $\phi = \frac{\pi}{2} \Rightarrow e^{in\phi} = i^n$ (2.13) becomes

$$U = \mu \ln \frac{1}{r} + \sum_{n=-\infty}^{\infty} c_n \left(\frac{R}{r}\right)^{|n|} i^n.$$

This series is now compared term by term with (4.3). First the power of the i has to be rewritten. Since the normal potential U is a real and even function the relation $c_n = c_{-n}$ holds. This yields:

$$\sum_{n=-\infty}^{\infty} c_n \left(\frac{R}{r}\right)^{|n|} i^n = c_0 + \sum_{n=1}^{\infty} c_n \left(\frac{R}{r}\right)^n (i^n + i^{-n}) = c_0 + \sum_{n=1}^{\infty} c_n \left(\frac{R}{r}\right)^n \frac{1+(-1)^n}{i^n}.$$

The nominator of the fraction in the last series equals zero for n odd. This gives, with $r = u$ (because of $\phi = \frac{\pi}{2}$),

$$U = \mu \ln \frac{1}{u} + c_0 + 2 \sum_{n=1}^{\infty} c_{2n} \left(\frac{R}{u}\right)^{2n} (-1)^n.$$

Comparison with (4.3) yields for the coefficients of the normal potential

$$\begin{aligned} \mu &= \mu', \\ c_0 &= U_0, \\ c_{2|n|} &= \tfrac{1}{2}\mu' \frac{(2|n|-1)!}{2^{2|n|}(|n|!)^2} \left(\frac{E}{R}\right)^{2|n|} \quad n \text{ even} \\ c_n &= 0, \quad \text{for } n \text{ odd}. \end{aligned} \tag{4.4}$$

The coefficients rapidly decrease to zero. Usually the first four non-zero terms of the series yield sufficient accuracy.

4.1.2 Derivatives of the normal potential

The first derivatives are computed by the transformation rules explained in appendix A. First the derivatives with respect to the equatorial frame are computed as

$$U_I = \frac{\partial x^A}{\partial x^I} U_A.$$

This connects the covariant derivatives U_A, taken with respect to the coordinates $\{u, \beta\}$, to those for the equatorial frame. The derivatives are computed by (A.2) and (A.13). We have

$$\gamma = \sqrt{U_X^2 + U_Z^2} = \frac{\mu'}{L}$$

and for the orientation $\bar{\beta}$ of the normal gravity vector

$$\sin\bar{\beta} = \frac{v}{L}\sin\beta, \qquad \cos\bar{\beta} = \frac{u}{L}\cos\beta, \tag{4.5}$$

with

$$L = \sqrt{u^2 + E^2\sin^2\beta}, \qquad v = \sqrt{u^2 + E^2}.$$

In the second step the derivatives with respect to the local frame are computed by (A.3):

$$U_i = \frac{\partial x^I}{\partial x^i} U_I.$$

For the partial derivatives (A.10) is used with $\omega = \overline{\beta}$, since the normal local frame is directed with e_z parallel to the normal gravity vector γ. Inserting the partial derivatives, working out the products and applying them on the ellipse potential one finds:

$$\begin{aligned} \frac{\partial U}{\partial z} &= \frac{v}{L}\frac{\partial U}{\partial u} = \frac{-\mu'}{L} = -\gamma, \\ \frac{\partial U}{\partial x} &= \frac{1}{L}\frac{\partial U}{\partial \beta} = 0 \end{aligned} \tag{4.6}$$

The computation of the normal values of the second derivatives of the potential, U_{xz} and U_{zz}, is more laborious. They are related to the partial derivatives U_{AB} by

$$U_{ij} = \frac{\partial x^I}{\partial x^i}\frac{\partial x^J}{\partial x^j}\frac{\partial x^A}{\partial x^I}\frac{\partial x^B}{\partial x^J} U_{AB}.$$

Omitting the intermediate results of this rather lengthy derivation, one finds the gradients

$$U_{xz} = \mu' \frac{E^2 \cos\beta \sin\beta}{L^4}, \qquad U_{zz} = \mu' \frac{uv}{L^4}. \tag{4.7}$$

The third derivatives are computed as

$$U_{ijk} = \frac{\partial x^I}{\partial x^i}\frac{\partial x^J}{\partial x^j}\frac{\partial x^K}{\partial x^k}\frac{\partial x^A}{\partial x^I}\frac{\partial x^B}{\partial x^J}\frac{\partial x^C}{\partial x^K} U_{ABC}.$$

After some manipulations we find

$$\begin{aligned} U_{xxx} = -U_{xzz} = -U_{zxz} = -U_{zzx} &= \mu' \frac{6E^2 uv \sin\beta\cos\beta}{L^7} \\ U_{xzz} = U_{zxz} = U_{zzx} = -U_{zzz} &= \mu' \frac{L^2(2L^2 - 3(u^2+v^2)) + 6u^2v^2}{L^7}. \end{aligned} \tag{4.8}$$

4.2 Errors introduced by the approximations

In the beginning of chapter 3 we started with the general linear GBVP. By means of the introduction of two approximations in this linear model, the use of a circular normal field for the coefficients of the model and the computation of all elements

of the design matrix with the same radius, an analytical solution for the model was found. In this section we will take a closer look at these approximations.

First we repeat the three steps leading to the GBVP that is solved by Stokes' integral. Then the errors are considered introduced by the approximations in the linear model. For that purpose the linear models *without* constant radius approximation or without circular approximation are given explicitly. By means of a Taylor series with respect to the elevation or with respect to the ellipticity parameter, the errors introduced by the two approximations are shown.

4.2.1 The three steps

The first step is the *linearization* of the GBVP. It requires the choice of approximate points (the telluroid) and of a reference (normal) gravity field. The approximate points are usually computed from the observations by a mapping; another method, such as taking approximate coordinates from a map, can also be appropriate. A common choice for the normal field is the elliptical normal potential with elliptical equipotential lines. The normal potential not only defines the functions from which the elements of the design matrix and the anomalies are computed, but also the direction of the normal local frame.

When the *circular approximation* is applied, the elliptical potential used for the computation of the elements of the design matrix is replaced by the point mass potential with circular equipotential lines. The anomalies are left unaffected. The $e_{z'}$ of the normal local frame used for the design matrix is then directed radially, instead of normal to the ellipse. Geometrically this can be interpreted as a mapping of a point with coordinates $\{h, \phi\}$ to a point with the polar coordinates $\{r = R + h, \bar{\phi} = \phi\}$ (see (Moritz, 1980)). It is the level of approximation of the *simple problem of Molodensky*.

The *constant radius approximation*, is the neglect of the different heights of the approximate points in the design matrix. All coefficients are computed with the same geocentric radius $r = R$.

4.2.2 Constant radius approximation

We start again with the linear model (3.5). The elements of the design matrix are computed with the circular reference field, but this time without $r = R$. This yields the system

$$\begin{pmatrix} dW \\ dg \\ d\Phi \end{pmatrix} = \begin{pmatrix} 0 & -\frac{R}{r} & \left(\frac{R}{r}\right)^{|n|} e^{in\phi} \\ 0 & -\left(\frac{R}{r}\right)^2 & |n| \left(\frac{R}{r}\right)^{|n|+1} e^{in\phi} \\ \frac{R}{r} & 0 & -in \left(\frac{R}{r}\right)^{|n|} e^{in\phi} \end{pmatrix} \begin{pmatrix} dx \\ dz \\ \Delta c_n \end{pmatrix}. \tag{4.9}$$

Now for each point of observation, the elements of the matrix depend on the elevation in that point; $r = R + h$. Since the deviation h of r from R is small, (4.9) can be

written by a linearization with respect to r in $r = R$ without much loss of accuracy as:

$$\begin{pmatrix} dW \\ dg \\ d\Phi \end{pmatrix} = \left\{ \begin{pmatrix} 0 & -1 & e^{in\phi} \\ 0 & -1 & |n|e^{in\phi} \\ 1 & 0 & -ine^{in\phi} \end{pmatrix} + \frac{h}{R} \begin{pmatrix} 0 & 1 & -|n|e^{in\phi} \\ 0 & 2 & -|n|(|n|+1)e^{in\phi} \\ -1 & 0 & in|n|e^{in\phi} \end{pmatrix} \right\} \begin{pmatrix} dx \\ dz \\ \Delta c_n \end{pmatrix}. \tag{4.10}$$

The design matrix $\boldsymbol{A}$ is now split into two: the matrix in constant radius approximation, as (3.18), and an additional matrix that takes into account the elevation of the surface points. This latter matrix makes the difference between the model in constant radius approximation and only circular approximation. The coefficients of the position unknowns are affected by a relative error of $h/R(\leq 10^{-3})$. The error made in the coefficients for the potential strongly depends on the degree. They are affected by a relative error of $|n|h/R$ or n^2h/R. Consequently the effect can be strong. E.g. for $n = 360$, with $h/R = 10^{-3}$, this yields an error of maximum 36% (for dW) or 1296% (for dg and $d\Phi$). Thus high degree coefficients are severely affected by the constant radius approximation. But the situation is not as bad as it looks. As the potential coefficients represent the overall effect over all observations, a few points with a high elevation will not necessarily result in large errors of the potential coefficients. How large the error really is, is not easy to be concluded from (4.10). In chapter 5 numerical estimates will be made.

4.2.3 Circular approximation

Now we take a further step and investigate the effect of the circular approximation. Instead of computing the coefficients in the linear model (3.5) from the point mass potential, the elliptic potential (4.1) is used. For the coordinates the elliptical system $\{u, \beta\}$ is applied since it yields compact formulae with the elliptical normal field. Also the series of the disturbing potential is written with respect to these coordinates. Inserting the derivatives of the normal potential into (3.5), the series (B.4) for the potential and using (4.6) for the differentiation of T, the model becomes

$$\begin{pmatrix} \Delta W \\ \Delta g \\ \Delta \Phi \end{pmatrix} = \begin{pmatrix} 0 & -\frac{\mu'}{L} & \mu' \left(\frac{a+b}{u+v}\right)^{|n|} e^{in\beta} \\ -\mu' \frac{E^2 \cos\beta \sin\beta}{L^4} & -\mu' \frac{uv}{L^4} & \mu' \frac{|n|}{a+b} \frac{u+v}{L} \left(\frac{a+b}{u+v}\right)^{|n|+1} e^{in\beta} \\ \mu' \frac{uv}{L^3} & -\mu' \frac{E^2 \cos\beta \sin\beta}{L^3} & -\mu' in \left(\frac{a+b}{u+v}\right)^{|n|} e^{in\beta} \end{pmatrix} \begin{pmatrix} \Delta x \\ \Delta z \\ \Delta c_n^{ell} \end{pmatrix}.$$

Introducing the dimensionless quantities (the prime denotes that the values are taken on the reference ellipse)

$$dW = \frac{\Delta W}{\mu'}, \qquad dg = \frac{\Delta g}{\gamma'} = \Delta g \frac{L'}{\mu'}, \qquad d\Phi = \Delta\Phi, \qquad dx = \frac{\Delta x}{b}, \qquad dz = \frac{\Delta z}{b},$$

gives

$$\begin{pmatrix} dW \\ dg \\ d\Phi \end{pmatrix} = \begin{pmatrix} 0 & -\frac{b}{L} & \left(\frac{a+b}{u+v}\right)^{|n|} e^{in\beta} \\ -\frac{bL'E^2\cos\beta\sin\beta}{L^4} & -\frac{bL'uv}{L^4} & |n|\frac{L'}{L}\left(\frac{a+b}{u+v}\right)^{|n|} e^{in\beta} \\ \frac{buv}{L^3} & -\frac{bE^2\cos\beta\sin\beta}{L^3} & -in\left(\frac{a+b}{u+v}\right)^{|n|} e^{in\beta} \end{pmatrix} \begin{pmatrix} dx \\ dz \\ \Delta c_n^{ell} \end{pmatrix}. \tag{4.11}$$

The system (4.11) is the linear model in elliptical approximation without any further approximation. To investigate the influence of the circular approximation, (4.11) is linearized with respect to e'^2. This yields, with $e'^2 = E^2/b^2$, on the ellipse $u = b$,

$$\begin{pmatrix} dW \\ dg \\ d\Phi \end{pmatrix} = \left\{ \begin{pmatrix} 0 & -1 & e^{in\beta} \\ 0 & -1 & |n|e^{in\beta} \\ 1 & 0 & -ine^{in\beta} \end{pmatrix} + e'^2 \begin{pmatrix} 0 & -\frac{1}{2}\sin^2\beta & -\frac{|n|}{4}e^{in\beta} \\ \cos\beta\sin\beta & \frac{4\sin^2\beta-1}{2} & -\frac{|n|}{4}(|n|+2\sin^2\beta)e^{in\beta} \\ \frac{1-3\sin^2\beta}{2} & -\cos\beta\sin\beta & \frac{in|n|}{4}e^{in\beta} \end{pmatrix} \right\} \begin{pmatrix} dx \\ dz \\ \Delta c_n^{ell} \end{pmatrix}. \tag{4.12}$$

The first matrix of this system is almost the design matrix of (3.18). This is not surprising since we took $e' = 0$ and $u = b$. The only difference is the argument of the base functions: β instead of ϕ. But both angles coincide since the ellipse degenerates to a circle for $e' = 0$.

Like with constant radius approximation, the largest error is introduced into the potential coefficients; the coefficients for the position unknowns are less influenced by the circular approximation. The total error in T is about $\frac{1}{2}e'^2 \approx 0.3\%$; see e.g. (Moritz, 1980).

It should be emphasized that in this application the use of elliptical coordinates and potential series is a only matter of convenience. Although the potential coefficients of a series with respect to an elliptical coordinate frame are different from the circular coefficients, the conclusion of this paragraph, the accuracy of the matrix in circular approximation, will not be different for coefficients with respect to the circular coordinates as the general trend, loss of accuracy with increasing degree, is the same.

From the systems (4.9) and (4.11) can be seen why a direct analytical solution to these higher order problems is not straightforward: the columns of the design matrix $\boldsymbol{A}$ are no longer orthogonal. This yields generally a full normal matrix which cannot be inverted analytically.

4.3 Iteration and matrices

In this section an iteration procedure for the solution of the GBVP is proposed. It is derived from a series expression for the computation of the inverse of a matrix. Since the GBVP was written as $\boldsymbol{y} = \boldsymbol{A}\boldsymbol{x}$, these series can be applied to the GBVP by using it for the computation of the inverse matrix $\boldsymbol{A}^{-1}$ (for uniquely determined problems), or for the inversion of the normal matrix in case least squares are used to obtain the solution to the GBVP. The iteration procedure is set up such that only the inversion of a simple operator is required, which can be done analytically.

4.3.1 Series for a matrix inverse

The inverse of a matrix, if it is sufficiently close to the unit matrix, can be computed by a kind of Taylor series. Writing this matrix as $(\boldsymbol{I}-\boldsymbol{M})$, where $\boldsymbol{I}$ is the unit matrix and $\boldsymbol{M}$ the matrix containing the small deviations, its inverse is

$$(\boldsymbol{I}-\boldsymbol{M})^{-1} = \sum_{i=0}^{\infty} \boldsymbol{M}^i = \boldsymbol{I} + \boldsymbol{M} + \boldsymbol{M}^2 + \boldsymbol{M}^3 + \cdots. \tag{4.13}$$

Occasionally this series is referred to as a *Neumann series*. It can be found in many text books such as (Courant & Hilbert, 1957) or (Varga, 1962). It can also be applied for the inversion of *every* regular square matrix $\boldsymbol{A}$ if an *approximate inverse* is available. The matrix $\boldsymbol{A}$ is decomposed into

$$\boldsymbol{A} = \boldsymbol{A}_0 + \boldsymbol{\Delta A},$$

where $\boldsymbol{\Delta A}$ is small. Taking $\boldsymbol{M} = -\boldsymbol{A}_0^{-1}\boldsymbol{\Delta A}$ yields

$$\boldsymbol{A} = \boldsymbol{A}_0(\boldsymbol{I}-\boldsymbol{M}) \quad \Leftrightarrow \quad \boldsymbol{A}^{-1} = \left(\sum_{i=0}^{\infty} \boldsymbol{M}^i\right) \boldsymbol{A}_0^{-1}, \tag{4.14}$$

by using (4.13). So an approximation of $\boldsymbol{A}$ is required which is close to $\boldsymbol{A}$ and preferably easily invertible.

The series (4.13) converges if its *spectral radius* $\rho(\boldsymbol{M})$, the maximum eigenvalue of $\boldsymbol{M}$, is smaller than one (Varga, 1962). This condition is easy understandable if the diagonalization explained in section 2.3 is applied to $\boldsymbol{M}$:

$$\boldsymbol{M} = \boldsymbol{S}\boldsymbol{\Lambda}\boldsymbol{S}^* \quad \Leftrightarrow \quad (\boldsymbol{I}-\boldsymbol{M})^{-1} = \boldsymbol{I}+\boldsymbol{S}\boldsymbol{\Lambda}\boldsymbol{S}^*+\boldsymbol{S}\boldsymbol{\Lambda}\boldsymbol{S}^*\boldsymbol{S}\boldsymbol{\Lambda}\boldsymbol{S}^*+\cdots = \boldsymbol{S}(\boldsymbol{I}+\boldsymbol{\Lambda}+\boldsymbol{\Lambda}^2+\cdots)\boldsymbol{S}^*.$$

This series converges if

$$\lim_{n\to\infty} \boldsymbol{\Lambda}^n = 0 \quad \Leftrightarrow \quad \lim_{n\to\infty} \lambda_j^n = 0 \quad \forall j \quad \Rightarrow \quad |\lambda_j| < 1 \quad \forall j$$

(the matrix $\boldsymbol{\Lambda}$ is a diagonal matrix with the elements λ_j). For the full proof see (ibid.). The *spectral norm* of the matrix $\boldsymbol{M}$ is defined as

$$\|\mathbf{M}\| = \sup_{\mathbf{x}\neq\mathbf{0}} \frac{\|\boldsymbol{M}\boldsymbol{x}\|}{\|\boldsymbol{x}\|}.$$

In (ibid.) it is found $\|M\| \geq \rho(M)$. Such that

$$\frac{\|(I - A_0^{-1}A)x\|}{\|x\|} < 1 \quad \forall x \tag{4.15}$$

guarantees convergence of the series (4.14). Or, with $y = Ax$,

$$\frac{\|x - A_0^{-1}y\|}{\|x\|} < 1 \quad \forall x.$$

This means that the *maximum possible* relative error of the first estimation of the solution, must be less than one. This is not the same as the relative error of the first estimate, with one specific x. Only if the condition above is satisfied for *all possible* x, convergence is guaranteed (for instance in an application to the GBVP a relative error of 30% of the first estimate, already led to divergence).

4.3.2 Iteration for a uniquely determined system of equations

As usual, the linear system is written as $y = Ax$. In case of a determined problem, i.e., with a full rank square matrix A, the solution to x can be determined by inverting the matrix A. Then series (4.14) can be applied. It is shown that this series leads to an easy iteration scheme.

First the matrix A is approximated by a simpler version, which can be easily inverted. This approximate matrix is called A_0. The first estimate of the solution is

$$x_0 = A_0^{-1}y.$$

Backward substitution of x_0 in the original model does not reproduce the original input data y exactly. The difference is used to improve the estimate for x:

$$\begin{aligned} y_0 &= Ax_0 \neq y \\ x_1 &= x_0 + A_0^{-1}(y - y_0), \end{aligned}$$

and so on. Generally it is

$$\begin{aligned} x_n &= x_{n-1} + A_0^{-1}(y - y_{n-1}) \\ y_n &= Ax_n. \end{aligned} \tag{4.16}$$

Combination of the two equations yields

$$x_n = A_0^{-1}y - A_0^{-1}Ax_{n-1} + x_{n-1} = A_0^{-1}y + Mx_{n-1}, \tag{4.17}$$

with $M = I - A_0^{-1}A$. This definition is the same as used in (4.14).

Now the equality of (4.14) and (4.17), with a finite number of terms, shall be proven by induction: if a Neumann series up to degree n is used for the inversion of A, the solution becomes

$$x_n = \sum_{i=0}^{n} M^i A_0^{-1}y. \tag{4.18}$$

Suppose iteration (4.17) also yields this estimate for $\boldsymbol{x}_n$. Then for $n+1$ one finds with (4.17)

$$\boldsymbol{x}_{n+1} = \boldsymbol{A}_0^{-1}\boldsymbol{y} + \boldsymbol{M}\boldsymbol{x}_n = \boldsymbol{A}_0^{-1}\boldsymbol{y} + \boldsymbol{M}\sum_{i=0}^{n}\boldsymbol{M}^i\boldsymbol{A}_0^{-1}\boldsymbol{y} = \sum_{i=0}^{n+1}\boldsymbol{M}^i\boldsymbol{A}_0^{-1}\boldsymbol{y}.$$

For $n = 0$, (4.18) yields $\boldsymbol{x}_0 = \boldsymbol{A}_0^{-1}\boldsymbol{y}$, which completes the proof. Hence, performing n iterations in the scheme above, yields exactly the same result as the approximation of $\boldsymbol{A}^{-1}$ by the first $n+1$ terms of the Neumann series. Consequently, the iteration will converge if the Neumann series converges. See e.g. (Strang, 1986, ch. 5.3) for a similar discussion about iterative solutions.

4.3.3 Application to the determined problem

The iteration procedure (4.16) is now applied to the GBVP. In the foregoing section, the iteration was derived for a discrete system of observations. But since matrices can be seen as finite dimensional operators, as shown in section 2.3, no discrimination will be made between the discrete GBVP, and the GBVP with continuous data.

For the uniquely determined problem, the least-squares operator as used in chapter 3, is equal to the inverse of $\boldsymbol{A}$ ($\boldsymbol{A}^{-1} = (\boldsymbol{A}^*\boldsymbol{A})^{-1}\boldsymbol{A}^*$). Hence, the solution can be obtained by the inversion of $\boldsymbol{A}$. This inverse is computed by the series (4.14). Since the approximate matrix $\boldsymbol{A}_0$ has to be inverted, the linear model in circular constant radius approximation is taken for $\boldsymbol{A}_0$, to be able to derive its inverse analytically.

Let us now consider the meaning of the steps in (4.16) when applied to the linear GBVP. The solution steps can be written as

$$\boldsymbol{A}_0(\boldsymbol{x}_n - \boldsymbol{x}_{n-1}) = (\boldsymbol{y} - \boldsymbol{y}_{n-1});$$

the residuals of the unknowns $(\boldsymbol{x}_n - \boldsymbol{x}_{n-1})$ are computed from the residuals $(\boldsymbol{y} - \boldsymbol{y}_{n-1})$ by Stokes' formula (in case $\boldsymbol{y}$ contains W and g). For $n = 0$ this is the ordinary Stokes solution to the GBVP from chapter 3. Backward substitution $\boldsymbol{y}_n = \boldsymbol{A}\boldsymbol{x}_n$, can be seen as the recomputation of the anomalies with the most recent position and disturbing potential contained in $\boldsymbol{x}_n$. In case of convergence, the new anomalies will be much smaller than the old ones and will give a small correction to the unknowns in the next solution step.

Up to now, the disturbances and the anomalies were considered as unknowns and observations, respectively. The anomalies were computed before applying the iteration procedure. This is not strictly necessary. If the vector $\boldsymbol{y}$ is defined as the vector of the observations themselves, and $\boldsymbol{x}$ contains the coefficients of the *total* potential and the position, then the first step, $\boldsymbol{x}_0 = \boldsymbol{A}_0^{-1}\boldsymbol{y}$, can be seen as the computation of approximate values of potential and position. The step of backward substitution yields approximate values of the observations. Then the second solution is comparable to the Stokes solution with anomalies. With this application, it will be very clear that the iteration boils down to taking new approximate values in each step.

The matrix $\boldsymbol{A}$ is not necessarily the linear model (3.5). The iteration can be applied for any $\boldsymbol{A}$ better than $\boldsymbol{A}_0$, e.g. $\boldsymbol{A}$ in circular approximation. Then the solution obtained by iteration, equals the solution to the GBVP in circular approximation. On the other hand, also a *non-linear* model for $\boldsymbol{A}$ can be considered. In that case the backward substitution is not anymore a linear matrix operation, but requires a non-linear operator applied to the vector of unknowns, or unknown functions, in case of the continuous problem. It leads to the solution of the non-linear GBVP.

4.3.4 Application to the overdetermined problem

For the overdetermined GBVP the least squares operator (3.22) was used. In this case the inverse of the normal matrix is required, for which the iteration method presented can be applied.

Denoting the approximate normal matrix by $\boldsymbol{N}_0 = \boldsymbol{A}_0^*\boldsymbol{A}_0$, the series (4.14) for the inversion of the normal matrix yields:

$$\boldsymbol{N}^{-1} = \sum_{i=0}^{\infty} \boldsymbol{M}^i \boldsymbol{N}_0^{-1},$$

with $\boldsymbol{M} = \boldsymbol{I} - \boldsymbol{N}_0^{-1}\boldsymbol{N}$. This gives the solution

$$\boldsymbol{x} = \sum_{i=0}^{\infty} \boldsymbol{M}^i \boldsymbol{N}_0^{-1} \boldsymbol{A}^* \boldsymbol{y}.$$

The *iteration*

$$\begin{aligned} \boldsymbol{x}_n &= \boldsymbol{x}_{n-1} + \boldsymbol{N}_0^{-1}\boldsymbol{A}^*(\boldsymbol{y} - \boldsymbol{y}_{n-1}) \\ \boldsymbol{y}_n &= \boldsymbol{A}\boldsymbol{x}_n \end{aligned} \tag{4.19}$$

gives the same solution. This is derived by taking the combination of the two equations:

$$\boldsymbol{x}_n = \boldsymbol{N}_0^{-1}\boldsymbol{A}^*\boldsymbol{y} + \boldsymbol{M}\boldsymbol{x}_{n-1},$$

with the matrix $\boldsymbol{M}$ as defined above. Except for the matrix in front of $\boldsymbol{y}$, this equation is identical to (4.17), and gives the solution

$$\boldsymbol{x} = \lim_{n\to\infty} \boldsymbol{x}_n = \sum_{i=0}^{\infty} \boldsymbol{M}^i \boldsymbol{N}_0^{-1} \boldsymbol{A}^* \boldsymbol{y} = \boldsymbol{N}^{-1}\boldsymbol{A}^*\boldsymbol{y},$$

as obtained with the series for the matrix inversion.

When *all* matrices $\boldsymbol{A}$ are approximated in the solution step of the iteration, as was done in chapter 3 to derive the solution of the overdetermined problems, the scheme becomes

$$\begin{aligned} \boldsymbol{x}_n &= \boldsymbol{x}_{n-1} + \boldsymbol{N}_0^{-1}\boldsymbol{A}_0^*(\boldsymbol{y} - \boldsymbol{y}_{n-1}) \\ \boldsymbol{y}_n &= \boldsymbol{A}\boldsymbol{x}_n, \end{aligned}$$

which gives the solution

$$\boldsymbol{x} = \sum_{i=0}^{\infty} \boldsymbol{M}'^{i} \boldsymbol{N}_0^{-1} \boldsymbol{A}_0^* \boldsymbol{y},$$

with $\boldsymbol{M}' = \boldsymbol{I} - \boldsymbol{N}_0^{-1}\boldsymbol{A}_0^*\boldsymbol{A}$. With (4.13) this is

$$\boldsymbol{x} = (\boldsymbol{I} - \boldsymbol{M}')^{-1}\boldsymbol{N}_0^{-1}\boldsymbol{A}_0^*\boldsymbol{y} = (\boldsymbol{N}_0^{-1}\boldsymbol{A}_0^*\boldsymbol{A})^{-1}\boldsymbol{N}_0^{-1}\boldsymbol{A}_0^*\boldsymbol{y} = (\boldsymbol{A}_0^*\boldsymbol{A})^{-1}\boldsymbol{A}_0^*\boldsymbol{y} \neq \boldsymbol{N}^{-1}\boldsymbol{A}^*\boldsymbol{y}.$$

We see that this iteration will *not* converge to the right solution although the difference is small. This can be seen from the solution after one iteration. Writing $\boldsymbol{A} = \boldsymbol{A}_0 + \boldsymbol{\Delta A}$, and omitting all terms quadratic in $\boldsymbol{\Delta A}$, the difference between the two methods becomes, after some manipulations,

$$\Delta \boldsymbol{x}_1 = \boldsymbol{N}_0^{-1}\boldsymbol{\Delta A}^*(\boldsymbol{I} - \boldsymbol{A}_0\boldsymbol{N}_0^{-1}\boldsymbol{A}_0^*)\boldsymbol{y}.$$

$(\boldsymbol{I} - \boldsymbol{A}_0\boldsymbol{N}_0^{-1}\boldsymbol{A}_0^*)\boldsymbol{y}$ is the projection of $\boldsymbol{y}$ onto the column space of $\boldsymbol{A}_0$. Generally, this will be a small vector (it is that part of the observation vector that cannot be represented by the model in circular constant radius approximation) and it is multiplied by the small matrix $\boldsymbol{\Delta A}$, so the deviation of the solution cannot be large. However, it has to be emphasized that this iteration is not suited to reach an exact solution of an overdetermined problem. Instead, iteration (4.19) should be used.

This second iteration method is somewhat easier to use, since the closed expressions of chapter 3 can be applied directly in the solution step of the iteration. With the first iteration, the computation of the right hand side of the normal equations is more complicated ($\boldsymbol{A}^*\boldsymbol{y}$ instead of $\boldsymbol{A}_0^*\boldsymbol{y}$), but not insurmountable.

The solution to uniquely determined systems can not only be found by directly inverting the design matrix, but also by least squares. As the results of both methods coincide, the application of iteration (4.19) to the uniquely determined problem leads to the same solution as (4.16).

4.3.5 Some remarks on the iteration

For the approximate operator $\boldsymbol{A}_0$, always the linear model in circular constant radius approximation is taken (Stokes' solution for W, g). That is required to be able to compute its inverse analytically. Since this matrix cannot be changed in the subsequent steps, other iterative methods, which require an adaptation of the approximate matrix in each step, such as conjugate gradient or successive over-relaxation, cannot be applied. If numerical techniques are used to determine $\boldsymbol{A}_0^{-1}$, they can be applied, obviously.

Geometrically, the iteration can be interpreted as follows. The least squares operator, or the inverse of $\boldsymbol{A}$ in case of the uniquely determined problem, is the projection of the observations onto the column space of $\boldsymbol{A}$. By making an approximation in the estimator, the projection direction and the projection space are changed; it is now the orthogonal projection onto the column space of $\boldsymbol{A}_0$. It gives an approximate representation of the observed $\boldsymbol{y}$ by a linear combination of the columns of $\boldsymbol{A}_0$. In

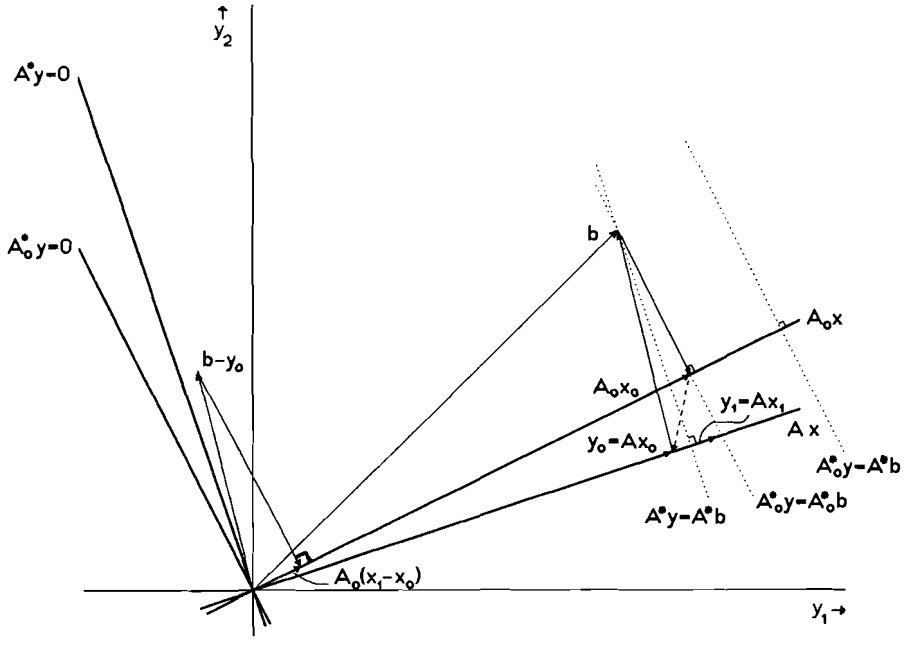

Figure 4.1 *One step of the iterative solution of $Ax = b$ by least squares.*

the step of backward substitution, the same linear combination is taken, but now with the columns of A. This yields a vector that is subtracted from the original vector y, which is projected onto A_0, and so on. This is schematically depicted in figure 4.1. In this figure the initial solution and the solution after one iteration of the system $Ax = b$ is depicted. The initial solution is obtained by the intersection of the space $A_0^* y = A_0^* b$ with the approximated model space $A_0 x$. The insertion of the solved vector of unknowns x into the real model A, indicated by a dashed line in the figure, yields y_0, which is subtracted from b. The projection of this vector of differences onto A_0 yields a correction to the initial solution: $x_1 - x_0$. The difference between the two methods of iteration for the overdetermined problem, discussed in this chapter, appears as a parallel shift of the line of projection.

The iteration procedure is comparable to the well-known Newton-Raphson iteration. There exist two differences: here the approximate A_0 is not necessarily the linearization of A, it is somewhat adapted (circular and constant radius approximation). Secondly, in each step the same A_0 is used. With Newton-Raphson, for each step a new linearization is taken. In figure 4.2 the iteration proposed here, is shown for the one-dimensional non-linear equation $Ax = b$. As can be seen in the figure, the linear approximation A_0 is not a tangent of the function and is not changed during the iteration. E.g. in (Strang, 1986, ch. 5) a comprehensive discussion about iteration techniques can be found.

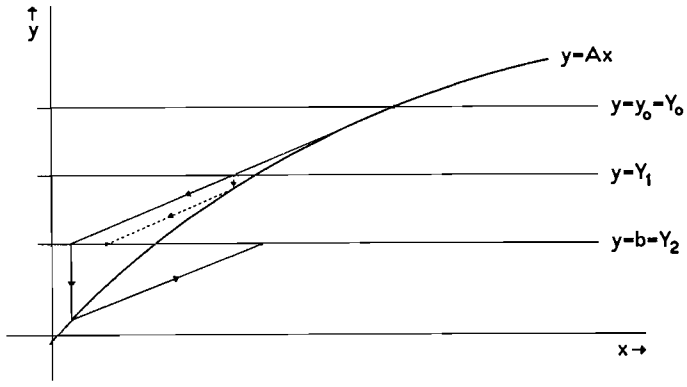

Figure 4.2 *One step of the Newton-Raphson iteration (solid line), and of the Hörmander iteration (dashed line).*

In case the iteration does not converge, the iteration as proposed by Hörmander can be applied. Here a sketch will be given (see e.g. (Moritz, 1980) for a detailed description). The difference with a Newton-like method is in the solution step of the iteration. Before starting the iteration, the interval between the value computed with the first estimate of the unknowns, $\boldsymbol{y}_0$, and the target point $\boldsymbol{y}$ is subdivided into a number of intervals. For instance define

$$\boldsymbol{Y}_n = \boldsymbol{y}_0 + \frac{n}{N}(\boldsymbol{y} - \boldsymbol{y}_0),$$

(N denotes the number of iterations). Then the solution step is changed as

$$\boldsymbol{x}_n = \boldsymbol{x}_{n-1} + \boldsymbol{A}_0^{-1}(\boldsymbol{Y}_n - \boldsymbol{y}_{n-1}).$$

This adaptation provides smaller values on the right hand side than with the original procedure which may turn divergence into convergence. For an one-dimensional problem it is shown in figure 4.2. It can be seen that the intermediate results of the iteration are close to the original function, such that the linearization error is small.

4.4 The problems to be solved by iteration

The iteration procedure explained in the previous section is numerically tested for several GBVP's. The results are given in chapter 5; here the chosen models are discussed.

The GBVP's considered are uniquely determined problems for the observables potential, gravity and astronomical latitude. Three types of models are taken, each in five degrees of approximation. These problems are solved by the procedure (4.16). The three types are:

- **Fixed:** The disturbing potential is solved from either potential, gravity or astronomical latitude observations. The position of the measurement points is known (fixed boundary).
- **Scalar:** The disturbing potential and the vertical position (elevation) are computed from the combination of potential and gravity observations. The horizontal position (latitude) is known (geodetic version according to Molodensky).
- **Vectorial:** Position and potential are unknown. All three observables are used in the solution.

This classification is made to see how much the unknown position affects the determination of the potential; it is well-known from the 3D GBVP that especially the horizontal position determination with vectorial Stokes, is quite weak. It also resembles situations common in practice. The *fixed* GBVP is encountered if the position of the points can be determined without the requirement of knowing the potential, for instance by precise space positioning. If the horizontal position is known from land surveying, the *scalar* problem can be formulated to solve for the vertical position and the gravity field from e.g. potential (leveling) and gravity observations. The last one, the *vectorial* problem, is more theoretically of importance since the accuracy of the horizontal position determined by astronomical latitude is much worse than with other data available nowadays.

The three GBVP's are solved in five degrees of approximation. For each of them a solution will be sought by means of iteration. In terms of the previous section, the choice of the unknowns and the approximations in the model, establish the $\boldsymbol{A}$ matrix. The matrix $\boldsymbol{A}_0$ will always be the model in circular, constant radius approximation, whose inverse is *Stokes' solution* of the GBVP, in case W and g are given on the boundary. If the iteration converges, the solution obtained will be equal to the solution for the considered problems. How close this solution is to the *real* one, the actual potential of the earth and its shape, is another issue. The five levels of approximation are:

I. **Simple Molodensky:** The anomalies, computed from the observations and the *elliptical* normal potential, are projected, with the use of some mapping, on a point above the reference circle, with an elevation equal to the elevation of the anomaly above the reference ellipse. It is the model in circular approximation (4.9). If we imagine that the earth is built up of the reference ellipse with the gravity field and the topography and everything else firmly attached to it, then this model can be seen as a deformation of this ellipse, with everything that goes on with it, to a circle. The equipotential lines change from ellipse-like to circle-like lines, the isozenithals (lines of parallel gravity) become almost radial and the topography is an elevation h above the reference circle. The GBVP is then solved for the circular earth created in this way. The model of *Simple Molodensky* would be exact (except for the linearization), if this adopted earth was the real one.

Another possibility is to take a reference circle from the beginning, instead of the reference ellipse, with a circular (point mass) normal potential for the approximate values. Then no mapping is required to use the formulas of *simple Molodensky*. But since the earth's surface and the equipotential lines of the gravity field have an elliptical shape, the anomalies created this way would be very large, and the iteration is likely to diverge.

II. **Linear on ellipse:** In case of this model the reference ellipse is not changed. The anomalies are only projected onto the reference ellipse. The topography, the elevation of the points, is neglected. So in this model, the other approximation in *Stokes' solution* has been dropped (with respect to *simple Molodensky*). With *Stokes* the flattening and the topography are neglected, with *simple Molodensky* only the flattening and with this model only the topography.

III. **Quadratic:** It is identical to the former approximation but now also the quadratic terms of the Taylor series expansion of the observables with respect to the position are included (Heck, 1988). The anomalies are, as with the former model, projected onto the ellipse.

IV. **Moving linear:** With this linear model, no other approximation is used than the linearization of the observation equations. Elevation and flattening are taken into account. We call this model *moving* since another feature is added to improve it. Initially, the linearization is taken in the approximate points (telluroid), obtained by a mapping (or from a map or just by guess). With the first solution by *Stokes*, better estimates of the position become available. By the backward substitution of *Stokes'* solution in the linear model, better approximate values are computed of the observations. With these two, a new linearization can be established: the approximate points $\boldsymbol{x}'$ in the equations (3.5) are replaced by the position computed by *Stokes*. This new equation is solved by *Stokes*, and so on. In the foregoing models, the backward substitution step of the iteration yields new approximate values of the observations, as discussed before. But that is only one part of the linear formula (although the most important one). The other elements of it are taken in the same point $\boldsymbol{x}'$ in each step of the iteration, which is not the case in our mobile model. The normal potential used in the linear term, is not changed during the iteration because it is multiplied by a small value, the position correction, which is approximately as large as the disturbance term.

V. **Non-linear:** This sounds difficult, but since we only apply the non-linear model in the backward substitution of the iteration, it is not that complicated. Instead of linearized observation equations, the exact relations between the unknowns and the observables are used. To make the formulas straight, not the anomalies are used for the backward substitution, but the full solution. This means that the position shifts are converted into corrections for the coordinates we work with, e.g. $\{h, \phi\}$, and the normal potential is added to the solved

disturbing potential. This gives new approximate values of the observations, which are used in turn to produce new anomalies.

Before continuing the discussion about the models and their solution, one remark. For some people it may be obvious, but for others the following point may be confusing, I believe (at least it was for me). For each model considered here, including *Stokes*, the anomalies are computed in exactly the same way: choice of an approximate point, computation of the values of the observables from the *elliptical* normal potential and subtraction from the observations. Then, these anomalies are taken as observations, located on the telluroid (established by the approximate points). The approximations taken when solving the GBVP, are in the *model*, connecting the anomalies with the unknowns, without changing the anomalies themselves. So the introduction of e.g. circular approximation, does not yield larger anomalies, but only an inferior coefficient matrix.

The presentation of the five models was given implicitly for the *vectorial* GBVP. But also for the other two GBVP's, the *fixed* and the *scalar* problem, their characteristics still hold true. In case of the scalar problem, the linearization is only carried out with respect to z. For establishing the telluroid, only an elevation for the approximate points has to be taken. With the *fixed* GBVP, no linearization takes place. The telluroid coincides with the earth's surface; all anomalies become disturbances and are situated on the real boundary of the earth.

At this point, we have defined the GBVP in six levels of approximation: the problem in circular, constant radius approximation and the five models presented above. In the sequel they are denoted by roman numbers:

0 : Stokes	III : quadratic on ellipse
I : simple Molodensky	IV : moving linear
II : linear on ellipse	V : non-linear

In order to get an overview of the differences between the models, the observation equations for potential and gravity are written for all models in one system of equations

$$
\begin{array}{l|l|l|l|l|l}
 & \text{non-linear} & & & & \\
 & \text{quadratic} & & & & \\
 & \text{linear} & & & & \\
\Delta W = & U_{i'}(\boldsymbol{x}')\Delta x^{i'} + & T(\boldsymbol{x}') & + \tfrac{1}{2}U_{i'j'}(\boldsymbol{x}')\Delta x^{i'}\Delta x^{j'} + T_{i'}\Delta x^{i'} & + \cdots & \\
-\Delta g = & U_{z'i'}(\boldsymbol{x}')\Delta x^{i'} + & T_{z'}(\boldsymbol{x}') & + \tfrac{1}{2}U_{z'i'j'}(\boldsymbol{x}')\Delta x^{i'}\Delta x^{j'} + T_{z'i'}(\boldsymbol{x}')\Delta x^{i'} & + \cdots & + W_z - W_{z'} \\
 & & \textit{fixed} & & & \textit{fixed}
\end{array}
$$

The boxes indicate the parts of the equation used for the *linear* models 0–II and IV, the *quadratic* model III and the *non-linear* model V. With the dashed box the components of the *fixed* GBVP are indicated. As before, the components and coordinates

Table 4.1 *The elements of the observation equation depending on the approximation.*

Model	U	e_z	x'
0	$-\ln r$	radial	circle
I	$-\ln r$	radial	circle + topography
II	$-\ln(u+v)$	$-\gamma_0$	ellipse
III	$-\ln(u+v)$	$-\gamma_0$	ellipse
IV	$-\ln(u+v)$	$-\gamma$	ellipse + topography
V	$-\ln(u+v)$	$-\gamma$	ellipse + topography

with respect to the *normal* local frame (the direction of its z-axis depended on the approximation of the model) are discriminated from those with respect to the *actual* local frame (direction of the z-axis defined by the direction of the gravity vector) by primes. In the vectorial problem the indices i', j' attain the values $\{1,2\}$, denoting $\{x,z\}$ respectively. For the scalar problem we only have $i' = j' = 2$. The observation equation for the astronomical latitude is omitted. It is similar to the equation for gravity, only the non-linear part is more complicated.

The choice of the normal potential for the coefficients of the model, the orientation of the normal local frame and the location of the approximate points, depend on the model (table 4.1). For the normal potential function, from which the coefficients of the models are computed, either the circular normal potential $-\ln r$ or the elliptical potential $-\ln(u+v)$ is taken . The orientation of the normal local frame $\{x', z'\}$ is derived from the applied normal potential function. With models II and III the direction of the normal gravity on the ellipse is used (γ_0). In some models the topography is considered for the approximate points $\boldsymbol{x}'$. In case the topography is unknown (vectorial problem) or partially unknown (scalar problem), the best approximate value available (from the last iteration) is used.

So far about the formulation of the models. It was not our intention to give operational formulae at this point. They can be found in section 5.2. The only purpose was an elucidation of the presented models. Finally, we mention some aspects of the *convergence* of the models. For all approximations of the *fixed* GBVP and with the models II and III for the other problems, the criterion (4.15) can directly be applied. But for the other models this is less straightforward. In the backward substitution with e.g. *moving linear*, the model is updated in each step. So the iteration procedure as discussed in section 4.3, is slightly modified: instead of the backward substitution with one fixed model, $\boldsymbol{A}$ is changed during the iteration. This brings up the question of to *which* solution the iteration converges. It is not easy to give a conclusive answer to this question. We will only give some tentative remarks, and see how the model performs with the numerical tests presented in chapter 5. The method of solution with *moving linear* can be interpreted as follows. After each solution step with *Stokes*, a new linear model is set up. This is again solved by *Stokes* and so on. So it is a succession of linear models solved in circular constant

radius approximation. These solutions are of course not the exact solutions to the linear models, but if they head into the right direction, the row of solutions, which is the same as the row of approximate points established by this procedure, runs from the initial approximate point to the real point on the earth's surface, in case of convergence. In that case the linearization error with respect to the position is lifted by this model; the neglect of the difference $\partial W/\partial z - \partial W/\partial z'$ is not compensated for. That is all we say about it here. One final remark. If the approximate point used for the linearization, is somewhere between telluroid and earth surface, then the model cannot become worse than the original model set up at the telluroid. If convergence of the latter can be proved by the criterion given in section 4.3, the moving model will converge to a solution at least as good as the one obtained by a fixed linear model.

For the *non-linear* model we do not hazard a prophecy. The convergence condition for the iteration with matrices can not be applied easily (since the $\boldsymbol{M}$ operator becomes quite complicated). The only thing we are confident about, is that the results should be at least as good or better than the *moving linear* model. See e.g. (Hörmander, 1976), (Moritz, 1980) or (Sansò, 1977) for some considerations about the convergence of the non-linear problem.

4.5 Analytical solution of simple Molodensky

For the iteration in the circular approximated model, *simple Molodensky*, a solution in the form of a series of integrals is available both for the 3D and for the 2D problem. It will be shown here that one step of iteration, as described in the last section, leads to the same result as the first two integrals of the solution to *simple Molodensky*. For 3D this is equation (8–50) of (Heiskanen & Moritz, 1967); a sketch of this similarity was given in (Rummel, 1988) and (Rummel et al., 1989). In 2D also for the linear problem solutions are available, see (Gerontopoulos, 1978). But as the solution in that case is much more complicated, and derived by a complete different approach than used here, it does not allow an easy comparison with the iterative solution.

First it is shown that one iteration step yields a solution in the form of an integral formula like (8–68) of (Heiskanen & Moritz, 1967). Then the 2D counterpart of this integral formula is derived from the solution to simple Molodensky given in (Gerontopoulos, 1978). The astronomical latitude is omitted from the problem. The logarithmic term is not included.

As already shown in section 4.1.2, the model for simple Molodensky can be written as

$$\boldsymbol{y} = \boldsymbol{A}\boldsymbol{x} \approx \left\{ \boldsymbol{A}_0 + \frac{h}{R}\frac{\partial}{\partial r}\boldsymbol{A} \right\} \boldsymbol{x}. \tag{4.20}$$

Thereby $\boldsymbol{A}$ denotes the model in circular approximation, (4.10), and $\boldsymbol{A}_0$ the model in circular, constant radius approximation, (3.18). The solution with one iteration

is, with (4.20),

$$\begin{aligned} \boldsymbol{x}_0 &= \boldsymbol{A}_0^{-1}\boldsymbol{y} \\ \boldsymbol{y}_0 &= \boldsymbol{A}\boldsymbol{x}_0 \approx \left\{\boldsymbol{A}_0 + \frac{h}{R}\frac{\partial}{\partial r}\boldsymbol{A}\right\}\boldsymbol{x}_0 \\ \boldsymbol{x}_1 &= \boldsymbol{x}_0 + \boldsymbol{A}_0^{-1}(\boldsymbol{y} - \boldsymbol{y}_0) \approx \boldsymbol{x}_0 - \boldsymbol{A}_0^{-1}\frac{h}{R}\frac{\partial}{\partial r}\boldsymbol{A}\boldsymbol{x}_0. \end{aligned} \tag{4.21}$$

Insertion of Stokes' solution (3.44) for the first iteration $\boldsymbol{x}_0$, yields for the new observations $\boldsymbol{y} - \boldsymbol{y}_0$ by backward substitution:

$$\boldsymbol{y} - \boldsymbol{y}_0 \approx -\frac{h}{R}\frac{\partial}{\partial r}\begin{pmatrix} \frac{R}{r}(-dW + dT) + \sum_n \left(\frac{R}{r}\right)^n \frac{1}{|n|-1}(dg_n - dW_n)e^{in\phi} \\ -\left(\frac{R}{r}\right)^2(-dW + dT) + \sum_n \left(\frac{R}{r}\right)^{n+1} \frac{|n|}{|n|-1}(dg_n - dW_n)e^{in\phi} \end{pmatrix}.$$

This vector is now used as observation vector for the second solution step with Stokes integral. The solution of T becomes

$$\begin{aligned} T = \frac{1}{2\pi}\int_{-\pi}^{\pi} St(\psi)\Bigg[(dg - dW) - \frac{h}{R}\frac{\partial}{\partial r}\Bigg\{\left(-\left(\frac{R}{r}\right)^2 + \left(\frac{R}{r}\right)\right)(-dW + dT) \\ + \sum_n \left(n\left(\frac{R}{r}\right) - 1\right)\left(\frac{R}{r}\right)^n \frac{1}{|n| - 1}(dg_n - dW_n)e^{in\phi}\Bigg\}\Bigg]\, d\phi. \end{aligned}$$

Taking the radial derivatives in this equation at zero elevation $r = R$, the solution reduces to

$$T_P = \frac{1}{2\pi}\int_{-\pi}^{\pi} St(\psi_{PQ})\left[(dg - dW)_Q - \frac{h_Q}{R}\left\{\frac{\partial}{\partial r}(dg - dW)_Q - \frac{1}{R}dW_Q\right\}\right] d\phi_Q.$$

This can also be written as

$$T_P = \frac{1}{2\pi}\int_{-\pi}^{\pi} St(\psi_{PQ})\left[(dg - dW)_Q - \frac{h_Q}{R}\frac{\partial}{\partial r}(dg - \frac{R}{r}dW)_Q\right] d\phi_Q. \tag{4.22}$$

The derivatives can safely be taken at zero level, since they are multiplied by h. The error introduced is therefore of second order.

Now the same equation is derived from the solution for the Molodensky problem given in (Gerontopoulos, 1978). The first two terms of his equation (1–74) on page 36 are

$$T = T_0 + T_1 \qquad \text{with} \qquad T_0 = \frac{R}{\pi}\int_{-\pi}^{\pi} \Delta g \frac{R + h}{R + h_P} St(\psi)\, d\phi$$

In T_0 the ratio can be replaced by 1 in circular approximation. T_1 is

$$T_1 = \frac{1}{\pi}\int_{-\pi}^{\pi} \frac{(R + h)^2}{R + h_P} St(\psi) G_1\, d\phi \approx \frac{R}{\pi}\int_{-\pi}^{\pi} G_1 St(\psi)\, d\phi \tag{4.23}$$

with

$$G_1 = \frac{R}{\pi}\int_{-\pi}^{\pi} \frac{h-h_P}{\ell^2}\frac{R+h_P}{R+h}\Delta g\, d\phi \approx \frac{R}{\pi}\int_{-\pi}^{\pi} \frac{h-h_P}{\ell^2}\Delta g\, d\phi$$

For comparison with (4.22), (4.23) has to be rewritten. The same procedure is followed as in (Heiskanen & Moritz, 1967, chapter 8–8). First some auxiliary formulas are deduced.

The integral of Poisson is (Rikitake et al., 1987)

$$V(r,\phi) = \frac{r^2-R^2}{2\pi}\int_{-\pi}^{\pi} V(R,\phi')\frac{1}{\ell^2}d\phi',$$

where ℓ denotes the distance between the points $\{r,\phi\}$ and $\{R,\phi'\}$. With

$$\frac{\partial}{\partial r}\frac{r^2-R^2}{\ell^2} = \frac{2r}{\ell^2} - (r^2-R^2)\frac{2}{\ell^4}(2r-2R\cos\psi) \stackrel{\text{def}}{=} M$$

the radial derivative becomes

$$\frac{\partial}{\partial r}V(r,\phi) = \frac{1}{2\pi}\int_{-\pi}^{\pi} MV(R,\phi)d\phi. \tag{4.24}$$

With the auxiliary potential V_1 one finds

$$V_1 = \frac{R}{r} \Rightarrow V_1(R) = 1 \quad \text{and} \quad \frac{\partial V_1}{\partial r} = -\frac{R}{r^2} = \frac{1}{2\pi}\int_{-\pi}^{\pi} M d\phi.$$

Multiplying with V and subtracting from (4.24) yields for $r = R$

$$\left.\frac{\partial V}{\partial r}\right|_P = -\frac{1}{R}V(P) + \frac{R}{\pi}\int_{-\pi}^{\pi}\frac{V-V_P}{\ell^2}d\phi.$$

With (2.10) and (3.17) it is

$$\frac{R}{\pi}\int_{-\pi}^{\pi}\frac{V-V_P}{\ell^2}d\phi = \frac{\partial V}{\partial r} + \frac{1}{R}V_P = \sum_n(-\frac{|n|}{R}+\frac{1}{R})c_n e^{in\phi} = -\frac{1}{R}\sum_n(|n|-1)c_n e^{in\phi}. \tag{4.25}$$

After these derivations, the G_1 function of (4.23) can be rewritten. First the substitution

$$(h-h_P)\Delta g = -h_P(\Delta g - \Delta g_P) + (h\Delta g - h_P\Delta g_P)$$

is used for the denominator of (4.23). This gives for G_1:

$$\begin{aligned} G_1 =& \frac{R}{\pi}\int_{-\pi}^{\pi}\frac{h-h_P}{\ell^2}\Delta g d\phi \\ =& -h_P\frac{R}{\pi}\int_{-\pi}^{\pi}\frac{\Delta g-\Delta g_P}{\ell^2}d\phi + \frac{R}{\pi}\int_{-\pi}^{\pi}\frac{h\Delta g - h_P\Delta g_P}{\ell^2}d\phi. \end{aligned}$$

Now the two parts are written as a series with the use of (4.25):

$$G_1 = \frac{h_P}{R}\sum_n (|n|-1)\Delta g_n e^{in\phi} - \frac{1}{R}\sum_n (|n|-1)(h\Delta g)_n e^{in\phi}$$
$$\stackrel{\text{def}}{=} G_{11} + G_{12}.$$

The expression Δg_n indicates the Fourier coefficients of Δg. The first function becomes

$$G_{11} = \frac{h_P}{R}\sum_n (|n|+1)\Delta g_n e^{in\phi} - 2\frac{h_P}{R}\Delta g \approx \frac{h_P}{R}\sum_n (|n|+1)\Delta g_n e^{in\phi}$$
$$= -h_P\frac{\partial \Delta g}{\partial h} = -h_P\frac{\partial \Delta g}{\partial r}$$

(because of the circular approximation, h is taken parallel to r). And the second function is

$$G_{12} = -\frac{1}{R}\sum_n (|n|-1)(h\Delta g)_n e^{in\phi}.$$

Inserting $G_1 = G_{11} + G_{12}$ into (4.23) yields

$$T = \frac{R}{\pi}\int_{-\pi}^{\pi} St(\psi)(\Delta g - \frac{\partial \Delta g}{\partial r}h)d\phi - h_P \Delta g_P.$$

Introducing dimensionless quantities, and using the definition of Stokes' kernel St as derived in chapter 3 (the difference in the definition is introduced by the use of complex series used here, and the use of sine/cosine series by Gerontopoulos; the factor 2 in (2.21) is not included in the latter definition), and $h_P = 0$, since (4.22) is computed on the circle $r_P = R$, this yields

$$T_P = \frac{1}{2\pi}\int_{-\pi}^{\pi} St(\psi_{PQ})(dg - \frac{h}{R}\frac{\partial dg}{\partial r})_Q d\phi. \tag{4.26}$$

If, as for (4.22), the mapping $\Delta W = 0$ was used, the equations would be identical. Thus it is shown that one step iteration gives the same solution of T as one step of the Molodensky series, derived along a completely different line. Very likely the next iterations will supply the other terms of the Molodensky series. This is not investigated here.

5

Numerical experiments

AT LAST THE COMPUTATIONS can be commenced. We will find out how the iteration procedure proposed in chapter 4 works in 'practice'.

First an earth, with topography and gravity field, is generated. The aim is to get a synthetical earth, with features close to the real one, as far as a 2D world can be compared to a 3D world at all. Then observations are computed.

The models of GBVP's to be solved by iteration are now formulated explicitly. After the discussion of a few additional aspects of the iterative solution, the first results are presented. Since the number of parameters in the problem, such as measurement interval, types of observation, number of coefficients a.s.o., is large, only a few situations are presented, which seem to be characteristic. For the selection we will emphasize on theoretical relevance. No attention will be paid to practical aspects, such as actual implementation or computation time.

5.1 Generation of an imaginary world

The numerical experiments described in this chapter, take place on a generated, imaginary earth. They are selected because of their relevance for the 3D case, but can be applied here under simpler conditions. For this purpose a 2D world has to be designed that resembles the features of our real world. For the constants appearing in the formulas, such as the size of the earth, the values of the geodetic reference system 1967 (GRS67) are applied.

A world in the context of physical geodesy, has only two major elements: topography, which determines the boundary of the earth, and a gravity field. Both have to be generated for our experiments, bearing in mind their relation. For this relation the concept of isostatic compensated topography is used. Since for the 3D earth it turns out that the isostatic model yields potential coefficients, computed from the topography, that have a correlation of typically 60% with the real coefficients

(Rummel et al., 1988), some approximations in this relation are allowed. A topography is generated with characteristic structures derived from the earth, from which potential coefficients are computed for the short wavelength part of the spectrum. These are combined with potential coefficients generated according to the power of a 3D earth model. This finally gives a set of 7200 potential coefficients, and topographic heights of 7200 points, equidistant in geographic latitude. These two data sets are used for the computation of four types of observations (W, g, Φ, W_{zz}) in each grid point on the earth's surface. These three sets are the basis for the numerical experiments.

5.1.1 Relation topography and potential

To be able to generate a potential that is compatible with the topography, we start with the derivation of the coefficients of the potential generated by the topographic masses. As guideline (Rummel et al., 1988) is used. There a relation is worked out between potential coefficients and isostatically compensated topography according to the model of local compensation by Airy.

In chapter 2, the relation between mass density and potential coefficients was already established, (2.7). What has to be added here, is the relation between the topography and the mass distribution according to Airy's model.

For the potential series (2.13) is used. The coefficients are computed with (2.7) and (2.12) as

$$c_n = \frac{1}{2|n|M} \int_\Sigma \rho e^{-in\phi_Q} \left(\frac{r_Q}{R}\right)^{|n|} d\phi_Q \qquad (n \neq 0). \tag{5.1}$$

The coefficients are divided by GM to make them dimensionless. As before, the c_0 is put to zero. Since the logarithmic function of the series (2.13) only depends on the total mass of the earth, it does not play any role here, and is left out.

The integration over the total mass Σ is split up into two: the contribution of the topography and of its compensation. The integral for the potential coefficients of the isostatic compensated topography becomes

$$c_n^I = \frac{R}{2|n|M} \int_{-\pi}^{\pi} [A^T(Q) - A^C(Q)] e^{-in\phi_Q} d\sigma_Q, \tag{5.2}$$

with the topographic contribution

$$A^T(Q) = \int_{r=R}^{R+h} \left(\frac{r_Q}{R}\right)^{|n|+1} \rho_{cr}(Q) dr_Q, \tag{5.3}$$

and the compensation

$$A^C(Q) = \int_{r=R-D-t}^{R-D} \left(\frac{r_Q}{R}\right)^{|n|+1} \Delta\rho(Q) dr_Q, \tag{5.4}$$

with

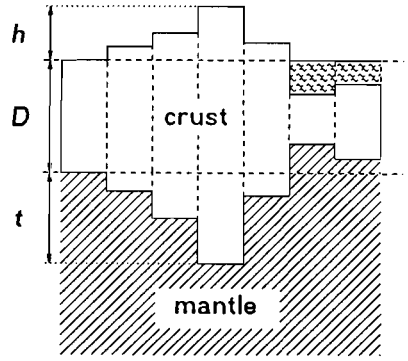

Figure 5.1 *The isostatic compensation according to Airy. The ocean area on the right gives negative compensation depths.*

h	: topographic height	t	: root thickness
ρ_{cr}	: density of the crust	ρ_m	: mantle density.
D	: depth of compensation	$\Delta\rho = \rho_m - \rho_{cr}$	

See also figure 5.1. For ocean areas, with negative elevation, the density ρ_{cr} should be replaced by $\rho_{cr} - \rho_w$ (ρ_w is the density of ocean water). Since $\rho_w < \rho_{cr}$, ocean areas have a negative compensation depth.

The contributions A^T and A^C are computed in circular approximation. Since an approximate relation between the topography and the potential is sufficient, as explained in the introduction, it is accurate enough for our purposes. We underline that the h, t and D are taken with respect to the ellipse.

Assuming that ρ_{cr} and $\Delta\rho$ do not depend on the radial position, (5.3) and (5.4) are written as

$$A^T = \rho_{cr}\frac{R}{|n|+2}\left[\left(\frac{R+h}{R}\right)^{|n|+2} - 1\right]$$
$$A^C = \Delta\rho\frac{R}{|n|+2}\left[\left(\frac{R-D}{R}\right)^{|n|+2} - \left(\frac{R-D-t}{R}\right)^{|n|+2}\right]. \qquad (5.5)$$

The root thickness t depends on the topographic height of the corresponding surface point. The relation between t and h is derived from the equilibrium of mass condition between the topographic and the compensating mass:

$$\int_{r=R}^{r=R+h} \rho_{cr} r\, dr d\phi = \int_{r=R-D-t}^{R-D} \Delta\rho\, r\, dr d\phi.$$

Or, with the integrations carried out,

$$\frac{\rho_{cr}}{2}[(R+h)^2 - R^2] = \frac{\Delta\rho}{2}[(R-D)^2 - (R-D-t)^2],$$

or

$$\frac{\rho_{cr}}{\Delta\rho}\left(2\frac{h}{R}+\frac{h^2}{R^2}\right)\frac{R^2}{(R-D)^2}=\frac{2t}{R-D}-\frac{t^2}{(R-D)^2}.$$

This equation is rewritten as

$$t=\tfrac{1}{2}\frac{\rho_{cr}}{\Delta\rho}\frac{R^2}{R-D}\left(2\frac{h}{R}+\frac{h^2}{R^2}\right)+\frac{\frac{1}{2}t^2}{R-D}.$$

As it is tedious to solve this equation exactly, an approximate solution is taken. Neglecting the terms of order h/R ($< 10^{-3}$), the solution is

$$t=\frac{\rho_{cr}}{\Delta\rho}\left(\frac{R}{R-D}\right)h. \tag{5.6}$$

The computation of A^T and A^C directly by (5.5) is time consuming since the ratios with h_Q and t_Q have to be evaluated for every point and every degree. To reduce this computational effort, a binomial expansion is used up to the third order in h/R (an alternative method can be found in (Moritz, 1990)). This gives for (5.5):

$$\begin{aligned}A^T &\approx \rho_{cr}\frac{R}{|n|+2}\left[1+(|n|+2)\frac{h}{R}+\frac{(|n|+2)(|n|+1)}{2}\left(\frac{h}{R}\right)^2+\right.\\ &\left.+\frac{(|n|+2)(|n|+1)|n|}{6}\left(\frac{h}{R}\right)^3-1\right]\\ &=\rho_{cr}h\left[1+\frac{|n|+1}{2}\frac{h}{R}+\frac{(|n|+1)|n|}{6}\left(\frac{h}{R}\right)^2\right]\end{aligned}$$

$$\begin{aligned}A^C &\approx \Delta\rho\frac{R}{|n|+2}\left[\left(\frac{R-D}{R}\right)^{|n|+2}-\left(\frac{R-D}{R}\right)^{|n|+2}\left(1-(|n|+2)\frac{t}{R-D}+\right.\right.\\ &\left.\left.+\frac{(|n|+2)(|n|+1)|n|}{2}\left(\frac{t}{R-D}\right)^2-\frac{(|n|+2)(|n|+1)|n|}{6}\left(\frac{t}{R-D}\right)^3\right)\right]\\ &=\Delta\rho\, t\left(\frac{R-D}{R}\right)^{|n|+1}\left[1-\frac{|n|+1}{2}\frac{t}{R-D}+\frac{(|n|+1)|n|}{6}\left(\frac{t}{R-D}\right)^2\right].\end{aligned}$$

Insertion in (5.2) yields after replacing t by (5.6), with $\bar{\rho}=M/(\pi R^2)$, the mean density of the earth,

$$\begin{aligned}c_n^I=\frac{\rho_{cr}}{\bar{\rho}}\frac{1}{|n|}&\left[\left(1-\left(\frac{R-D}{R}\right)^{|n|}\right)\frac{1}{2\pi}\int_{-\pi}^{\pi}\frac{h}{R}e^{-in\phi}d\phi\right.\\ &+\frac{|n|+1}{2}\left(1+\frac{\rho_{cr}}{\Delta\rho}\left(\frac{R-D}{R}\right)^{|n|-2}\right)\frac{1}{2\pi}\int_{-\pi}^{\pi}\left(\frac{h}{R}\right)^2e^{-in\phi}d\phi\\ &\left.+\frac{|n|(|n|+1)}{6}\left(1-\frac{\rho_{cr}^2}{\Delta\rho^2}\left(\frac{R-D}{R}\right)^{|n|-4}\right)\frac{1}{2\pi}\int_{-\pi}^{\pi}\left(\frac{h}{R}\right)^3e^{-in\phi}d\phi\right].\end{aligned} \tag{5.7}$$

Now the computation of c_n^I is easy since the position dependent quantity h only appears in Fourier integrals, which can be computed by a Fast Fourier Transform (FFT). Multiplication by the preceding ratios gives the potential coefficients of the topographic mass. In (Rummel et al., 1988) it is shown that the approximate solution to c_n^I by the binomial series has an accuracy of better than 3% up to degree 200. Since the topography is not very rough, see next section, it is assumed that (5.7) is accurate enough for all degrees.

For ocean areas the heights in (5.7) have to be replaced by the *equivalent rock topography*

$$h = \frac{\rho_{cr} - \rho_w}{\rho_{cr}} d,$$

where d is the (negative) ocean depth. This is required to compensate for the density difference between water and crust.

For the Airy model it is used:

$$\rho_{cr} = 2.67 \times 10^3\,\mathrm{kg/m^3} \qquad \rho_m = 3.27 \times 10^3\,\mathrm{kg/m^3}$$
$$\rho_w = 1.03 \times 10^3\,\mathrm{kg/m^3} \qquad D = 30\,\mathrm{km}$$

5.1.2 Generation of topography

For the construction of the earth, we start with the topography. The topography will be represented by elevations h above the reference ellipse for the 7200 points (5.5 km interspace). For the relation between potential and topography it was assumed in (5.7) that the heights h are *mean* elevations of blocks. Since 7200 points are generated, there will be only one point per block. Although this gives not a very good representation, it is assumed that the representation error will be negligible since the blocks are small.

Because it is desirable that there is some resemblance between the topography on the 3D earth and the generated topography that will be used for the simulations, a height data set of average elevations of one degree by one degree blocks, collected by the university of Graz, is used. Our aim is to compute a one dimensional power spectrum from this set, that is representative for the earth and which can be used as model for the topography generation. From the block averages the spherical harmonic coefficients are computed up to degree 180. From these coefficients various one-dimensional power spectra are computed: degree variances and the Fourier power spectra for three profiles along a parallel. One could start a theoretical discussion whether degree variances or a Fourier power spectrum has to be used as model for the generation. But test computations showed that there is almost no difference between the two. Hence, we just take the Fourier spectrum of the height profile along the equator as model without further discussion (actually we should take a profile containing the poles, see chapter 1). The Fourier coefficients of the 2D topographic heights up to degree 180 are now generated such that their amplitude is in correspondence with the model but with an arbitrary phase derived from a computer random number generator.

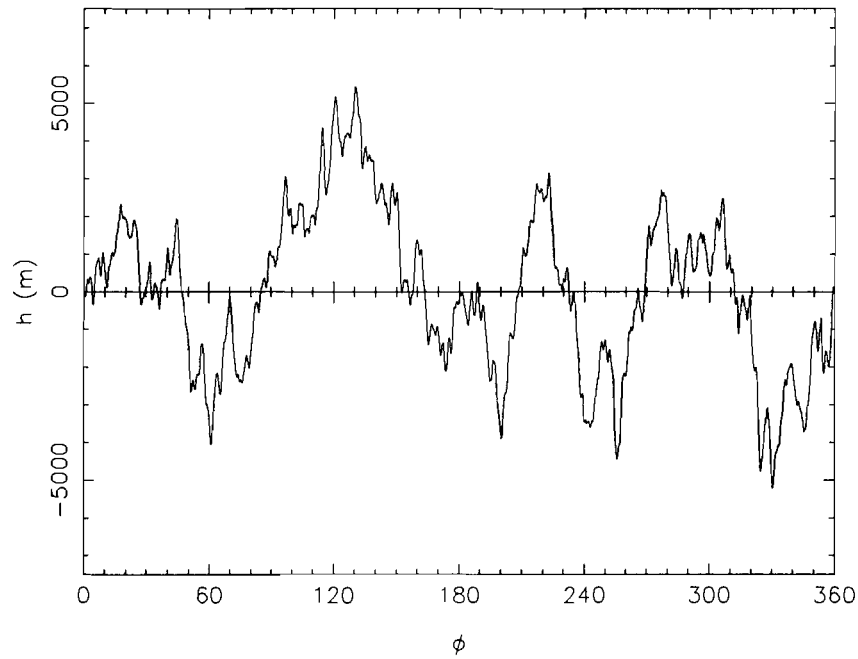

Figure 5.2 *The topography above the reference ellipse.*

For the degrees 181–3600 an analytical model has to be used. This model has to satisfy two demands: continuation of the trend in the power spectrum of the Graz set and a rapid decrease in power for the high degrees to limit the roughness of the topography. On the face of it, the model $1.6 \times 10^{13}/n^5$ m^2 was selected. The Fourier coefficients of the topography are computed as follows. As for the lower degrees, the phase is taken random. The amplitude of the coefficients equals the model value multiplied by 10^x ($-\frac{1}{2} < x < \frac{1}{2}, x$: random number, uniformly distributed) to get a variation of the power in a bandwidth as was found from the Graz set for the low degrees. After some runs, the final topography was selected. It contains four oceans and a mountain of approximately 5 kilometer altitude (see figure 5.2). The complete power spectrum of the generated heights is displayed in figure 5.3.

5.1.3 Generation of the potential

For the generation of the potential of the imaginary world, two sources are used: a set of spherical harmonic coefficients (OSU89A), see (Rapp & Pavlis, 1990), and the topography. The OSU model will be used for the low degrees of the potential, which are largely generated by the mass distributions of core and mantle. The high degree coefficients are mainly determined by the mass distribution of the topography.

First a one dimensional power spectrum is computed from OSU89A, which can serve as power model for the coefficients to be generated. Since the normal potential for the 3D earth has values quite different from the normal potential applied here, not the full OSU model is used, but only its deviation from the normal field GRS67.

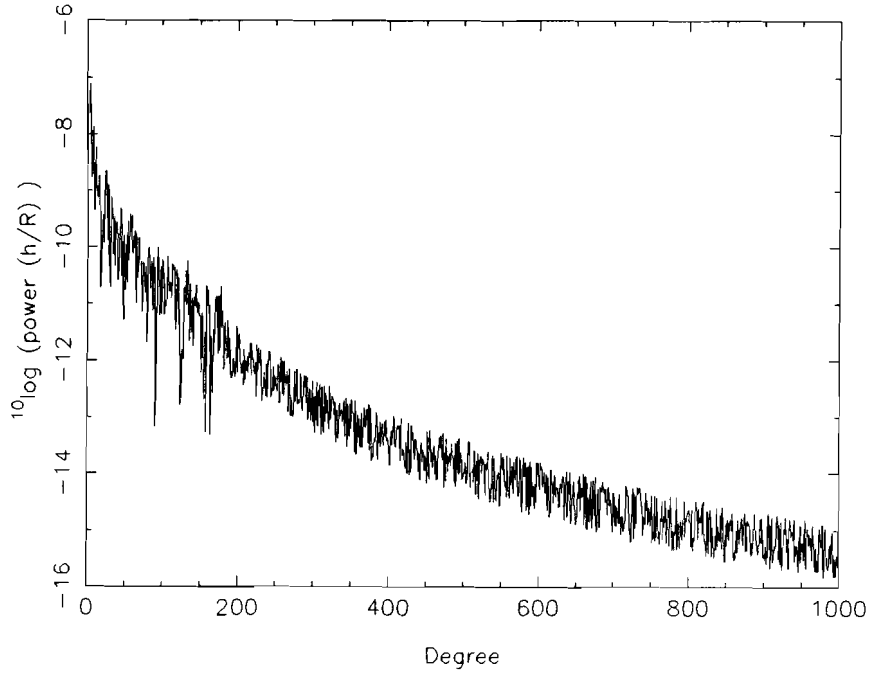

Figure 5.3 *The power spectrum of the* 2D *topography.*

As was done for the topography, the power spectrum of the potential along the equator is used as power model. Degree variances of profiles parallel to the equator are not very different from their Fourier power spectra, as can be seen from figure 5.4 for the equator. With this power model a set of potential coefficients is generated with an arbitrary phase and an amplitude in accordance with the model. The 2D normal field coefficients are added. This gives a set up to degree 360, the maximum degree of OSU89. Another set of potential coefficients is related to the topography, computed with (5.7). This set we denote the EQRT (= equivalent rock topography) set. As final step these two sets are combined.

The combination is made by giving a weight of $1-n^2/(400+n^2)$ to the coefficient from the low degree set and $n^2/(400+n^2)$ to the coefficient of the EQRT set. It is difficult to give a justification for such a choice, as our situation is hypothetical. The reason we took such weights is the large power in the low degree set with respect to the EQRT set in the low frequencies, and the fact that the EQRT coefficients are *computed* from the given topography and the other coefficients are *generated.*

The geoid computed from the total potential is depicted in figure 5.5. It shows a geoid that is quite similar to geoid profiles of the 3D earth. The power spectrum of the total potential model is given figure 5.6. The power spectrum is computed by taking the square of the Fourier coefficients.

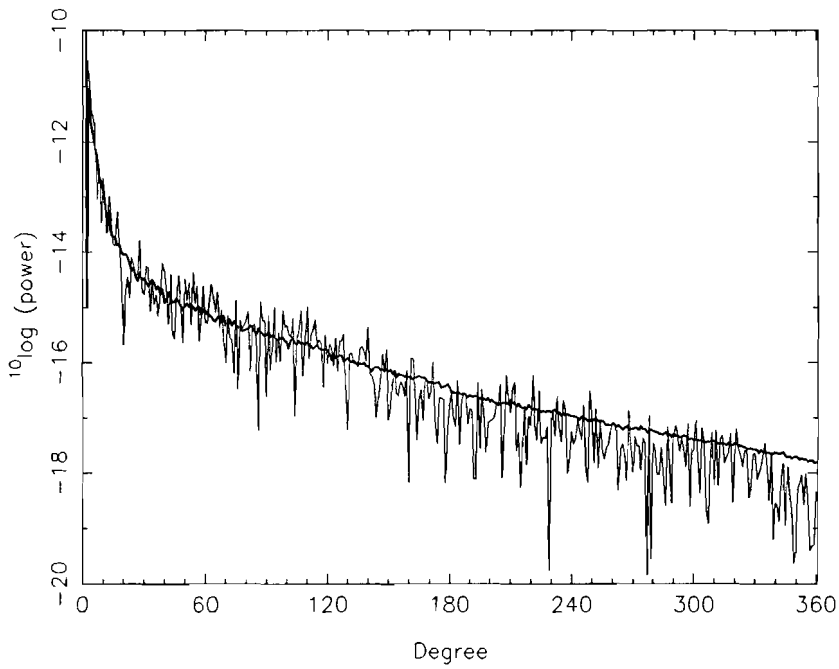

Figure 5.4 *Power of OSU89A. Thin line is the Fourier power spectrum for a potential profile along the equator. The thick line denotes the degree variances.*

5.1.4 Synthesis of the observations

The synthesis of the observations can be divided into three steps: transformation of coordinates, computation of derivatives of the potential and the combination of them to observations. These steps are described below. All quantities are taken dimensionless, as explained in chapter 3.

1. **Transformation of the coordinates:** This is an easy task to start with. For the position location of the observations their elliptic coordinates $\{h, \phi\}$ are available: the ϕ is taken at regular intervals and h is the generated topography. The potential is given by coefficients with respect to a series expressed in the polar coordinates $\{r, \bar{\phi}\}$. Therefore we start with the transformation from geographic to polar coordinates by (A.4) and (A.7).
2. **Computation of the derivatives of the potential:** From the series of the potential W, the derivatives can be computed. As the series for W is identical to the expansion for T, formulas (3.17) can be applied for the derivatives of W with respect to $\{r, \bar{\phi}\}$.
3. **Combination to observations:** All the observations can be expressed as a combination of W and its derivatives with respect to the polar coordinates. The series found in the previous step lead to the observation values.

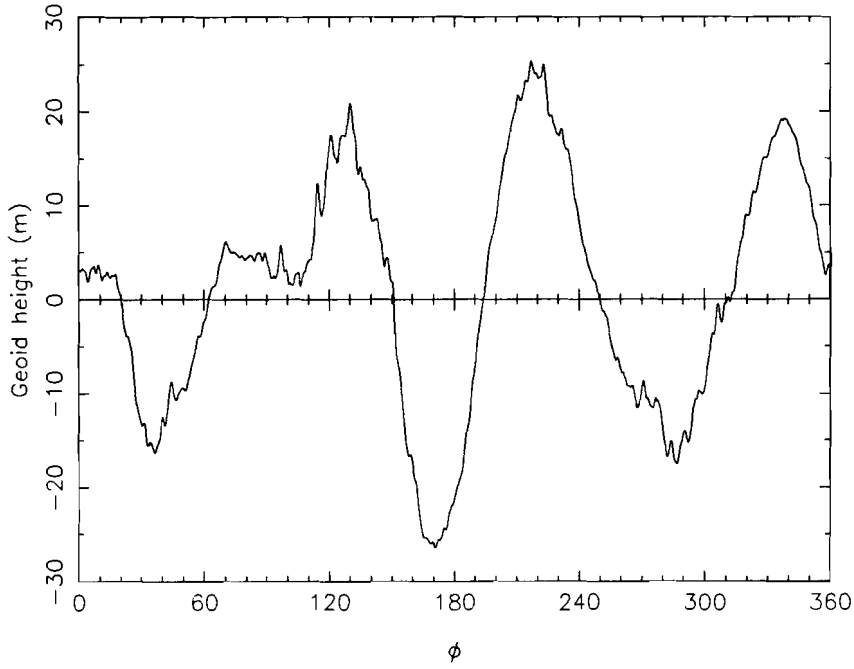

Figure 5.5 *The geoid computed from the total potential with respect to the reference ellipse.*

The gravity scalar g is defined as

$$g = \|\nabla W\|. \tag{5.8}$$

Writing (5.8) in index notation we find, using the coordinates $\{r, \bar{\phi}\}$,

$$g = \|W_\alpha\| = \sqrt{g^{\alpha\beta} W_\alpha W_\beta} = \sqrt{W_r^2 + \frac{1}{r^2} W_{\bar{\phi}}^2}. \tag{5.9}$$

For Φ, the direction of the gravity vector with respect to the $e_{I=1}$, we have

$$\tan \Phi = \frac{W_Z}{W_X} \tag{5.10}$$

with

$$W_I = \frac{\partial x^\alpha}{\partial x^I} W_\alpha.$$

Inserting the partial derivatives found in appendix A, yields

$$W_X = W_r \cos\phi - \frac{1}{r} W_{\bar{\phi}} \sin\bar{\phi}$$
$$W_Z = W_r \sin\phi + \frac{1}{r} W_{\bar{\phi}} \cos\bar{\phi}.$$

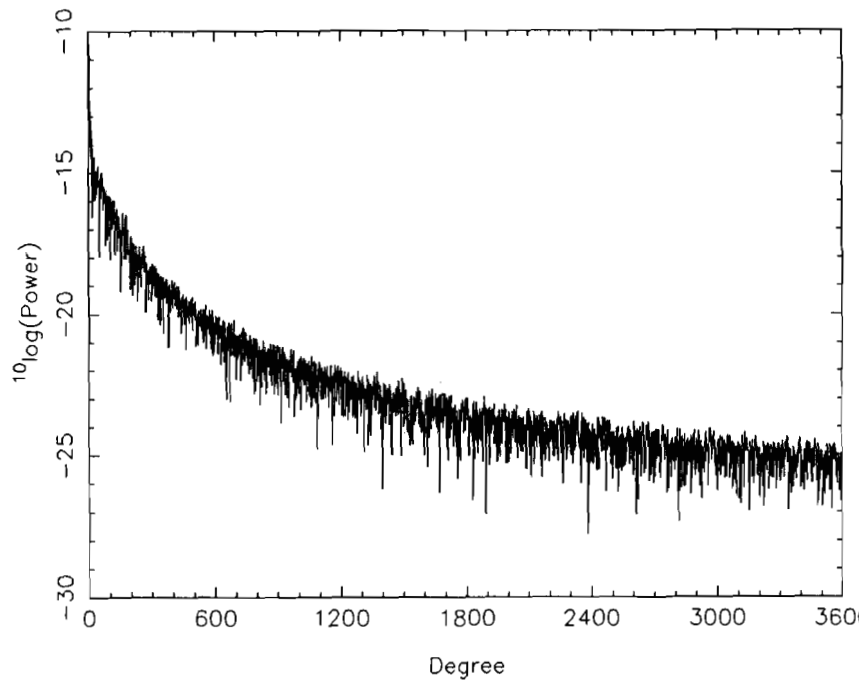

Figure 5.6 *The power of the total potential.*

With $\tan\Phi$ we have to be careful since it is periodic with π. It has always to be taken such that the vector g points inwards. For e.g. $W_X < 0$ and $W_Z < 0$ we find $0 < \Phi < \pi/2$.

The gradients are computed in the same way as the gradients of the normal potential, compare section 4.1. First the second derivatives with respect to the equatorial frame e_I are computed from the polar coordinates as

$$W_{IJ} = \frac{\partial x^A}{\partial x^I}\frac{\partial x^B}{\partial x^J}W_{AB}.$$

These gradients are rotated to the actual local frame by

$$W^{ij} = \frac{\partial x^i}{\partial x^I}\frac{\partial x^j}{\partial x^J}W^{IJ}.$$

For the partial derivatives, which represent a rotation, the angle $\omega = \Phi$ is substituted into (A.10). This finally gives after a few manipulations

$$\begin{aligned} W_{xz} &= W_{XZ}\cos 2\Phi + W_{ZZ}\sin 2\Phi \\ W_{zz} &= W_{XZ}\sin 2\Phi - W_{ZZ}\cos 2\Phi. \end{aligned} \tag{5.11}$$

5.2 The five models for backward substitution

The five approximations, in which the GBVP will be solved numerically, were discussed in chapter 4. Here the explicit formulae are given for these models. Since

all are solved by iteration, they are only used for the backward substitution step. After the formulae are presented, we will discuss how the total procedure of solution works.

5.2.1 Explicit formulation of the models

The explicit formulas for the five models are given below for the vectorial Stokes problem. For the fixed and the scalar problem, the columns for dx and dz and for dx, respectively, are omitted. All linear models are derived from (3.5). Quantities are made dimensionless by the normal values on the circle (3.13).

As usual, the polar coordinates $\{r, \bar{\phi}\}$ are used in the series expression of the disturbing potential

$$T = \Delta c \ln \frac{1}{r} + \sum_n \Delta c_n \left(\frac{R}{r}\right)^{|n|} e^{in\bar{\phi}}.$$

For later use, also the series with the elliptical coordinates $\{u, \beta\}$ are applied:

$$T = \Delta c^{ell} \ln \frac{2}{u+v} + \sum_n \Delta c_n^{ell} \left(\frac{a+b}{u+v}\right)^{|n|} e^{in\beta}.$$

The use of a series requires the expression of derivatives of T with respect to the same coordinates. As much as possible the same coordinates are used for the other parts of the model to avoid coordinate transformations. The notation T_a is used for the dimensionless partial derivatives of T with respect to a. Derivations are omitted.

- **Simple Molodensky:** The equations are (4.9):

$$\begin{pmatrix} dW \\ dg \\ d\Phi \end{pmatrix} = \begin{pmatrix} 0 & -\left(\frac{R}{r}\right) \\ 0 & -\left(\frac{R}{r}\right)^2 \\ \left(\frac{R}{r}\right) & 0 \end{pmatrix} \begin{pmatrix} dx \\ dz \end{pmatrix} + \begin{pmatrix} T \\ -T_r \\ -T_{\bar{\phi}} \end{pmatrix}. \qquad (5.12)$$

  The r is computed by $r = R + h$ and the latitude by $\bar{\phi} = \phi$. No expression with the elliptical potential series is given.

- **Linear on ellipse:** The derivatives of the normal potential, which are the coefficients for the position corrections, are given in section 4.1. For the derivatives of the disturbing potential the relation

$$T_i = \frac{\partial x^I}{\partial x^i} \frac{\partial x^\alpha}{\partial x^I} T_\alpha$$

  is applied for the formulation with polar coordinates. For the rotation from the equatorial frame to the local frame, (A.10) is used with $\omega = \phi$; on the ellipse ϕ coincides with the direction $\bar{\beta}$ of the normal gravity vector. The relations

(4.5) can be used to express the sines and cosines of β, which appear in the derivatives of U, in those of ϕ. This gives the model

$$\begin{pmatrix} dW \\ dg \\ d\Phi \end{pmatrix} = \begin{pmatrix} 0 & -\frac{R}{L'} \\ -\frac{R^2E^2\cos\phi\sin\phi}{abL'^2} & -\frac{R^2ab}{L'^4} \\ \frac{Rab}{L'^3} & -\frac{RE^2\cos\phi\sin\phi}{abL'} \end{pmatrix} \begin{pmatrix} dx \\ dz \end{pmatrix} + \tag{5.13}$$

$$+ \begin{pmatrix} T \\ -(\cos\bar{\phi}\cos\phi + \sin\bar{\phi}\sin\phi)T_r - (\cos\bar{\phi}\sin\phi - \sin\bar{\phi}\cos\phi)\left(\frac{R}{r}\right)T_{\bar{\phi}} \\ (\sin\phi\cos\bar{\phi} - \cos\phi\sin\bar{\phi})\left(\frac{L'}{R}\right)T_r - (\sin\phi\sin\bar{\phi} + \cos\phi\cos\bar{\phi})\left(\frac{L'}{r}\right)T_{\bar{\phi}} \end{pmatrix}.$$

L' can be written with (4.5) as

$$L' = \sqrt{u^2 + E^2\sin^2\beta} \overset{u=b}{=} \sqrt{b^2 + \frac{E^2L'^2}{v^2}\sin^2\phi}$$

because on the ellipse $u = b$, $v = a$ and $\overline{\beta} = \phi$. Solving L' from this equation yields

$$L' = \frac{b}{\sqrt{1 - e^2\sin^2\phi}}.$$

Hence, it is not required to know the coordinates $\{u, \beta\}$; $\{r, \bar{\phi}\}$ and $\{h, \phi\}$ are sufficient.

If elliptical coordinates are used, the transformation

$$T_i = \frac{\partial x^I}{\partial x^I}\frac{\partial x^A}{\partial x^I}T_A$$

can be applied for the local derivatives. For the rotation to the local frame the angle $\omega = \overline{\beta}$ is used. This yields with (4.5)

$$\begin{pmatrix} dW \\ dg \\ d\Phi \end{pmatrix} = \begin{pmatrix} 0 & -\frac{R}{L'} \\ -\frac{R^2E^2\cos\beta\sin\beta}{L'^4} & -\frac{R^2ab}{L'^4} \\ \frac{Rab}{L'^3} & -\frac{RE^2\cos\beta\sin\beta}{L'^3} \end{pmatrix} \begin{pmatrix} dx \\ dz \end{pmatrix} + \begin{pmatrix} T \\ -\frac{a}{L'}T_u \\ -T_\beta \end{pmatrix}. \tag{5.14}$$

All components of this equation are expressed with respect to $\{u, \beta\}$.

- **Quadratic:** This model is an extension of the preceding one with the quadratic terms included. See page 76 for the general model. On the ellipse

it is:

$$\begin{pmatrix} dW \\ dg \\ d\Phi \end{pmatrix} = \begin{pmatrix} 0 & -\frac{R}{L'} \\ -\frac{R^2E^2\cos\phi\sin\phi}{abL'^2} & -\frac{R^2ab}{L'^4} \\ \frac{Rab}{L'^3} & -\frac{RE^2\cos\phi\sin\phi}{abL'} \end{pmatrix} \begin{pmatrix} dx \\ dz \end{pmatrix} +$$

$$+ \begin{pmatrix} T \\ -(\cos\bar{\phi}\cos\phi + \sin\bar{\phi}\sin\phi)T_r - (\cos\bar{\phi}\sin\phi - \sin\bar{\phi}\cos\phi)\left(\frac{R}{r}\right)T_{\bar{\phi}} \\ (\sin\phi\cos\bar{\phi} - \cos\phi\sin\bar{\phi})\left(\frac{L'}{R}\right)T_r - (\sin\phi\sin\bar{\phi} + \cos\phi\cos\bar{\phi})\left(\frac{L'}{r}\right)T_{\bar{\phi}} \end{pmatrix} +$$

$$+ \begin{pmatrix} \left(\frac{R}{r}\right)T_{\bar{\phi}} & T_r \\ \left(\frac{R}{r}\right)^2 T_{\bar{\phi}} - \left(\frac{R}{r}\right)T_{r\bar{\phi}} & -T_{rr} \\ \left(\frac{L'}{R}\right)T_{rr} & \left(\frac{L'}{R}\right)\left(\left(\frac{R}{r}\right)^2 T_{\bar{\phi}} - \left(\frac{R}{r}\right)T_{r\bar{\phi}}\right) \end{pmatrix} \begin{pmatrix} dx \\ dz \end{pmatrix} +$$

$$+\frac{1}{2}\begin{pmatrix} U_{xx} & 2U_{xz} & U_{zz} \\ -U_{xxx} & -2U_{xzz} & -U_{zzz} \\ -U_{xxx} & -2U_{xzz} & -U_{xzz} \end{pmatrix} \begin{pmatrix} (dx)^2 \\ dx\,dz \\ (dz)^2 \end{pmatrix}. \qquad (5.15)$$

The dimensionless derivatives of U are computed from those given in section 4.1. They are

$$U_{xz} = \frac{R^2E^2\cos\phi\sin\phi}{abL'^2}, \qquad -U_{xx} = U_{zz} = \frac{R^2ab}{L'^4},$$

$$U_{xxx} = -U_{xzz} = -U_{xxz} = -U_{zzz} = \frac{6R^3E^2\sin\beta\cos\beta}{L'^5},$$

$$U_{xxz} = U_{xzx} = U_{zxx} = -U_{zzz} = \frac{R^3L'^2(2L'^2 - 3(a^2+b^2)) + 6R^3a^2b^2}{L'^7}.$$

The model is not presented in elliptical coordinates.

- **Moving linear.** It is like *linear on ellipse*, naturally without the restriction to the ellipse. For the model expressed in elliptical coordinates it does not make much difference since by (4.5) the orientation of the normal vector can be computed directly from the coordinate β for all values of u. For the model with the series in polar coordinates, a similar relation is not available. Thus a transformation has to be performed to find $\sin\beta$ and $\cos\beta$.

For the model with the polar series it is

$$\begin{pmatrix} dW \\ dg \\ d\Phi \end{pmatrix} = \begin{pmatrix} 0 & -\frac{R}{L} \\ -\frac{R^2E^2\cos\beta\sin\beta}{L^4} & -\frac{R^2uv}{L^4} \\ \frac{Ruv}{L^3} & -\frac{RE^2\cos\beta\sin\beta}{uvL^3} \end{pmatrix} \begin{pmatrix} dx \\ dz \end{pmatrix} + \tag{5.16}$$

$$+ \begin{pmatrix} T \\ -(u\cos\bar{\phi}\cos\beta + v\sin\bar{\phi}\sin\beta)\frac{1}{L}T_r - (v\cos\bar{\phi}\sin\beta - u\sin\beta\cos\bar{\phi})\frac{1}{L}\left(\frac{R}{r}\right)T_{\bar{\phi}} \\ (v\sin\beta\cos\bar{\phi} - u\cos\beta\sin\bar{\phi})\frac{1}{R}T_r - (v\sin\beta\sin\bar{\phi} + u\cos\beta\cos\bar{\phi})\frac{1}{R}\left(\frac{R}{r}\right)T_{\bar{\phi}} \end{pmatrix}$$

For the elliptical series it is

$$\begin{pmatrix} dW \\ dg \\ d\Phi \end{pmatrix} = \begin{pmatrix} 0 & -\frac{R}{L} \\ -\frac{R^2E^2\cos\beta\sin\beta}{L^4} & -\frac{R^2uv}{L^4} \\ \frac{Ruv}{L^3} & -\frac{RE^2\cos\beta\sin\beta}{L^3} \end{pmatrix} \begin{pmatrix} dx \\ dz \end{pmatrix} + \begin{pmatrix} T \\ -\frac{v}{L}T_u \\ -T_\beta \end{pmatrix}. \tag{5.17}$$

- **Non-linear.** For the non-linear model, the same formulas are used as for the synthesis of the observations in section 5.1.4. Instead of using the solved disturbing potential and the coordinate corrections, the full potential and the actual position are used, since this yields briefer formulas. If this total potential is called W' the model for backward substitution becomes

$$\begin{aligned} W &= W' \\ g &= \sqrt{g^{\alpha\beta}W'_\alpha W'_\beta} = \sqrt{W'^2_r + \left(\frac{R}{r}\right)^2 W'^2_{\bar{\phi}}} \\ \Phi &= \arctan\frac{-W'_Z}{-W'_X} = \frac{-W'_r\sin\bar{\phi} - \frac{R}{r}W'_{\bar{\phi}}\cos\bar{\phi}}{-W'_r\cos\bar{\phi} + \frac{R}{r}W'_{\bar{\phi}}\sin\bar{\phi}} \end{aligned} . \tag{5.18}$$

And expressed in derivatives with respect to the elliptical coordinates

$$\begin{aligned} W &= W' \\ g &= \sqrt{g^{AB}W'_A W'_B} = \sqrt{\left(\frac{v}{L}\right)^2 W'^2_u + \left(\frac{R}{L}\right)^2 W'^2_\beta} \\ \Phi &= \arctan\frac{-W'_Z}{-W'_X} = \frac{-vW'_u\sin\beta - R\frac{u}{v}W'_\beta\cos\beta}{-uW'_u\cos\beta + RW'_\beta\sin\beta}. \end{aligned} \tag{5.19}$$

The W' is computed by adding the normal potential U to the last solution for T. For the computation of g and Φ, it is impossible to apply these formulas to T and U separately and add the results as the relations are non-linear. In

that case we would compute the sum of the normal derivative of T and of the normal derivative of U, with the normal directions given by T and U, respectively. While the real value of g is the sum of the derivatives of T and U with respect to the normal of the total potential W.

5.2.2 The implementation of the iteration procedure

Now let us see how the solution is actually computed from the boundary data. Only the *vectorial* problem is discussed here. It should be obvious that for the *scalar* GBVP and for the *fixed* problem some simplifications apply. Where necessary the differences with the vectorial problem are indicated. Although Stokes' integral gives only the solution of the disturbing potential from potential and gravity anomalies, the solution step will often be denoted by *Stokes* for simplicity. As the core of the solution is Stokes' formula, we start there.

Because of computational simplicity, Stokes is applied in the frequency domain. The coefficients of the disturbing potential Δc_n are computed from the spectral components of the anomaly difference $dg - dW$ by a simple multiplication (3.44). To be able to compute these spectral components by Fast Fourier Transform (FFT), dg and dW would have to be given equidistantly on the reference circle. This demand of maximum data regularity, gives a simple, unambiguous one-to-one relation of the space domain functions and their Fourier coefficients.

The anomalies are obtained by subtracting the normal values in the approximate points from the observations. Then they are projected onto the reference circle by $\{r = R, \bar{\phi} = \phi\}$. Hence, to accomplish data on the circle equidistantly spaced in $\bar{\phi}$, the anomalies have to be located in the points of a regular ϕ-grid. For the elevations h no condition is required since r is kept fixed. They are computed by the condition of equal normal potential and observed potential value. These choices for the approximate coordinates define a mapping which is an adapted version of the *Marussi*-mapping. The difference is in the selection of the latitude of the approximate point. Instead of using the observed astronomical latitude, a grid is used. In case of regularly distributed observations, as is the case in our simulations, this difference is only small. If the data are given irregularly, an interpolation has to be applied to avoid too large anomalies.

With Stokes' solution, coordinate shifts and disturbing potential coefficients are obtained. Before they are used for the backward substitution, the position of the observation points is computed in $\{h, \phi\}$ to check the accuracy of the solution and also for the models which require updated positions for the backward substitution: the *moving linear* model and the *non-linear* model. The elliptical coordinates are computed by the linear relations

$$\begin{pmatrix} h \\ \phi \end{pmatrix} = \begin{pmatrix} h_0 \\ \phi_0 \end{pmatrix} + \begin{pmatrix} \frac{\partial h}{\partial x} & \frac{\partial h}{\partial z} \\ \frac{\partial \phi}{\partial x} & \frac{\partial \phi}{\partial z} \end{pmatrix} \begin{pmatrix} \Delta x \\ \Delta z \end{pmatrix}.$$

Where $\{h_0, \phi_0\}$ denote the coordinates of the telluroid point. The partial derivatives are computed as

$$\frac{\partial x^a}{\partial x^i} = \frac{\partial x^a}{\partial x^I} \frac{\partial x^I}{\partial x^i},$$

which are given in (A.9) and (A.10). For the latter the angle ω has to be defined; it is the direction of the normal gravity vector. On the ellipse the partial derivatives are easily obtained since the direction of the normal gravity vector is equal to the latitude ϕ. As it changes only slightly with increasing elevation, the required relation is computed in linear approximation with respect to the ellipse. Without further derivation we give

$$\begin{aligned} h &= h_0 + \Delta z \\ \phi &= \phi_0 + \left(\frac{1}{M} - \frac{h}{M^2}\right) \Delta x + \frac{he^2 \sin\phi \cos\phi \sqrt{1 + e^2 \cos^2\phi}}{bM} \Delta z \end{aligned} \tag{5.20}$$

Thereby

$$M = \frac{a(1 - e^2)}{(1 - e^2 \sin^2\phi)^{\frac{3}{2}}},$$

the curvature of the ellipse.

In (5.20), the coordinates are computed from the position shifts obtained from the iterations made so far. In chapter 4 it was shown that the iteration can be seen as taking new approximate values in each step, and solving with them a new problem by Stokes. With this perception it is natural to compute the position incrementally, by applying (5.20) to the $(\Delta x, \Delta z)$ of the last iteration step, with $\{h_0, \phi_0\}$ from the former solution, instead of using the total solution. Then the question arises, which of the methods, total or incremental computation of the position, is best. For the *linear* approximations of the GBVP, there is no difference. For the non-linear model, we can only work with the total potential and shifts, as explained in section 5.2.1. Only for the quadratic model, a difference may occur. It turns out to be very small. If a large number of iterations is required, the incremental method may be less accurate due to computer rounding-off errors.

The solved Δc_n, dx and dz are now substituted in one of the models of (5.2.1). This yields new anomalies, which are subtracted from the original ones, taken from the observation data. These anomaly differences yield a small disturbing potential and position shifts in the next solution step. They are added to the solutions from the previous step, as described in section 4.3.2.

One point in the total process requires more attention. It is the effect of the neglect of ellipticity in the solution step (Stokes) of the iteration. The step of backward substitution requires the computation of the disturbing potential, or its derivatives, in the approximate point. Usually, the solved disturbing potential is represented by coefficients and base functions. This representation makes it easy to compute the potential and its derivatives in every point required. But there is

a snake in the grass: the solved coefficients are not unambiguous. To see this, we consider the procedure again.

After the subtraction of the normal values, the first step was the *mapping* onto the circle by $\bar{\phi} = \phi$. In this circular world, the exact relation between potential and observation is given. The computation step (Stokes) yields the disturbing potential, usually expressed by Fourier coefficients, as the relation between potential and observations is straightforward in the spectrum. The obtained disturbing potential can now be interpreted in basically two ways: either as the solution of the disturbing potential function on the reference circle, or as the solution on another boundary. The first seems to be the most logical interpretation, but we have to keep in mind that the input data was not originally situated on the circle. It was put there by a mapping. To annul, partly, the effect of this mapping, the inverse mapping can be applied to T such that the solved function is placed on the earth's surface.

As the surface of the earth is irregular, the application of the exact inverse mapping is not practical. Instead, the topography is omitted from the inverse mapping, such that the boundary turns into an ellipse. Let us assume that the solution of T is given by Fourier coefficients. For both cases, with and without the inverse mapping to the ellipse, the coefficients refer to a sine/cosine series with respect to a graduation along the boundary obtained by the inverse mapping. Hence, without the mapping, the Fourier coefficients found in the solution step, are the coefficients with respect to the series (2.13). In the other case, they are coefficients with respect to the geographic coordinates. As no series is available with respect to $\{h, \phi\}$, series (B.4) have to be used. Details of this aspect will be discussed in section 5.5.2.

Summarizing we can say that the Fourier coefficients found in the solution step, can be interpreted both as solution of the potential coefficients with respect of the polar coordinates, and as solution of the coefficients with respect to the elliptical coordinates. Only the latter will be more accurate than the former. Hence, the iteration will work better if the elliptical series are applied. This will be discussed in section 5.4.

Using the elliptical series means that the final result of the iteration is a set of elliptical coefficients. Since usually the coefficients with respect to the polar coordinates are required, a transformation has to be applied. If the coefficients are interpreted as polar coefficients in each backward substitution step, the final result will be polar coefficients. Hence, no transformation is required, which can balance the slower convergence.

With the model in circular approximation, the anomalies are mapped onto the circle only once. In the backward substitution step, only the topography is added. Although in the computation the solved Fourier coefficients are considered to be with respect to the polar coordinates, an inverse mapping applied back to the boundary was never applied, where the anomalies were located originally. We saw before, that the solved potential is closer to the disturbing potential on the ellipse than the potential along the circle. Hence, after the iteration in the circular model, this inverse mapping is applied. For the coefficients this simply means that they are

interpreted as elliptical coefficients. The final step becomes the conversion of them to the polar coefficients.

5.3 First results

Now the total scheme is complete, first calculations can be made. To avoid the mixing of all kinds of effects, we take here a rather idealized situation with respect to the data. Later, other data conditions are considered.

Two sets of observation points are taken, one at 72 locations, with a constant separation of five degrees in ϕ, and the other with 720 points. If the observations are taken as samples of the total potential or gravity function, as would be realistic, aliasing occurs since the potential function generated, has a maximum degree of 3600. Instead, for the observation synthesis the potential coefficients are only used up to half the sample frequency, this means to a maximum degree of 36 and 360, respectively. This does not exclude all possible aliasing effects, as the points of observation are not situated on a circle, but on the earth's surface. But aliasing should remain small.

As observations W, g or Φ are used for the *fixed* problem, the combination (W, g) for the *scalar* problem and (W, g, Φ) for the *vectorial* problem. The unknowns are the coordinates of the observation points and the first 36 or 360 Fourier coefficients, respectively, of the disturbing potential.

The solution is judged by comparison with the real potential and position. To reduce the amount of numbers, the relative error

$$\frac{\|\boldsymbol{x}_n - \boldsymbol{x}\|}{\|\boldsymbol{x}\|} = \sqrt{\frac{\sum_i (x_{n,i} - x_i)^2}{\sum_i x_i^2}} \tag{5.21}$$

is computed for each kind of unknown: dx, dz and for Δc_n. Thereby $\boldsymbol{x}$ denotes the real value of the unknown, and $\boldsymbol{x}_n$ the estimate after n iterations. In the tables, the model used for the backward substitution is indicated by roman numbers:

I : simple Molodensky	IV : moving linear
II : linear on ellipse	V : non-linear
III : quadratic on ellipse	

Summarizing, the observations satisfy the following conditions:

- maximum frequency in the data is half the sampling rate
- regularly distributed
- no observation noise.

In section 5.6 more realistic data will be used.

We start with the *fixed* GBVP with gravity observations in 72 points. The result

is given in table 5.1. The columns are the relative errors of the disturbing potential, computed by (5.21), after zero (Stokes' solution) up to four iterations. The rows contain the results for the four employed models; the quadratic approximation does not exist in the fixed GBVP since no linearization with respect to the coordinates occurs. For models II, IV and V, the first result is identical because all are computed by Stokes without iteration. Stokes' solution with model I is different since the transformation from elliptical potential series to polar series is applied, to compensate for the circular approximation, as discussed above. If this would be left out, the first result for I without iteration would be the same as for the other methods; the transformation reduces the error approximately by a factor of two. The transformation is only applied for testing the results, it is *not* used in the iteration. We observe that iteration in the model in circular approximation, does not have much effect. With model II, one iteration is useful. With linear model IV, an almost exact solution is reached after 3 iterations. The non-linear model, finally, converges to the 'exact' solution.

Table 5.1 *Relative errors of the potential for the fixed problem with 72 gravity observations.*

	Number of iterations				
Model	0	1	2	3	4
I	0.003223	0.003213	0.003214	0.003214	0.003214
II	0.006437	0.000798	0.000835	0.000834	0.000834
IV	0.006437	0.000170	0.000013	0.000004	0.000004
V	0.006437	0.000170	0.000012	0.000001	0.000000

It can be concluded from this table, that for the given situation, the fixed problem with 72 gravity observations, the neglect of the ellipticity is more serious than a neglect of the topography (compare the results with models I, no ellipticity, and II, without topography).

The linear model IV converges to almost the exact solution. The small remaining difference is caused by the neglect of the difference in direction between the normal induced by the total potential and that from the elliptical potential; see section 4.4.

With the non-linear model, the convergence seems good. But as only a limited number of figures is presented in the table, we take a closer look. With the FORTRAN REAL*8 data type, used in all computations, the mean error for the disturbing potential reduces to 10^{-12} after 18 iterations. Increasing the word length by using REAL*16 data representation, the error decreases to 10^{-28} after 28 iterations. For *both* data types this means a loss of accuracy of about six figures in the total computation (including the observation synthesis), which seems acceptable. As the improved data representation fully contributes to the reduction of the error, we may conclude that the iteration with the non-linear model really converges to the *exact* solution of the GBVP.

In table 5.2 the results after seven iterations for all three observables of the fixed problem with 72 points are given. Two points deserve attention. First we observe for the potential that model IV gives the same accuracy as model V. This is caused by the *linearity* of the fixed GBVP in the potential. Secondly, the astronomical latitude observations yield accuracies comparable with those of models I and II. Models IV and V give hardly better results, in contrast with the other observation types. We do, so far, not have a satisfactory explanation for this result.

Table 5.2 *Relative errors of the potential for the fixed problem with 72 observations after 7 iterations.*

	Observation		
Model	W	g	Φ
I	0.002575	0.003214	0.003959
II	0.000579	0.000834	0.000641
IV	0.000000	0.000004	0.000428
V	0.000000	0.000000	0.000428

As was discussed in chapter 3, the first degree harmonics are not estimable from the vectorial problem. Hence, this harmonic has to be determined externally. As it was taken zero in the observation synthesis, the first degree coefficient is put to zero. To get comparable results for the various problems, it is taken zero for all considered problems. Also the logarithmic component is put to zero, as it is not estimable from 'horizontal' observations, such as astronomical latitude and because of the uniqueness problem in case the potential constant is unknown. In the observation synthesis the mass of the earth was put equal to the mass of the ellipse.

With the horizontal observations, the highest degree cannot be estimated either. If we denote the number of points N_{obs}, then the frequencies for the observation synthesis run from zero to $N_{obs}/2$, to achieve a one-to-one relation between coefficients and observations. The zero and $N_{obs}/2$ degree only contribute to the cosine part of the observation, the sine functions yield zero for these frequencies in all grid points. Differentiating the potential in the horizontal (ϕ) direction, turns the sines into cosines and vice versa. When recovering the potential from astronomical latitude, these two frequencies are lost, and have to be determined from external information. They are excluded in the computation of the error of the disturbing potential of table 5.2.

We see that, except for the astronomical latitude observations, all outcomes are reasonable. But only for the non-linear model we are able to judge the result precisely, since that model should yield the exact solution. The other models all contain approximations with respect to the exact model. To see whether the deviations from the real solution are caused by these approximations or by the iteration procedure, the solutions of the models I, II and IV with gravity observations were also computed by the inversion of the design matrix. It turned out that these solutions give exactly the same result as obtained by iteration. Hence, it can be concluded that the iteration procedure works correctly.

Next, the *scalar* GBVP is considered. The points of departure are the same as with the fixed problem. As observations the combination of potential and gravity is used. The accuracy of the solution is again represented by the total relative error.

Table 5.3 *Relative errors of the potential and average errors in vertical position for the scalar problem with 72 points.*

		Number of iterations				
Unknown	Model	0	1	2	3	4
T	I	0.003874	0.003645	0.003645	0.003645	0.003645
	II	0.007089	0.001118	0.001139	0.001139	0.001139
	III	0.007089	0.001120	0.001142	0.001142	0.001142
	IV	0.007089	0.000176	0.000015	0.000007	0.000007
	V	0.007089	0.000177	0.000012	0.000001	0.000000
h	I	0.096186	0.093054	0.093079	0.093080	0.093080
meter	II	0.096186	0.021729	0.021565	0.021566	0.021566
	III	0.096186	0.021675	0.021517	0.021518	0.021518
	IV	0.096186	0.000836	0.000183	0.000177	0.000175
	V	0.096186	0.000962	0.000045	0.000004	0.000000

Since also the vertical position is determined, the relative total error of the elevation is given too. The results are presented in table 5.3.

Generally speaking, the outcome is the same as with the fixed problem; only slightly worse. The model in quadratic approximation (III) performs poorly. The elevation is only marginally improved and the disturbing potential even deteriorated. In (Heck, 1988) it was shown, that the quadratic terms can be of considerable magnitude in some areas of the world. But results presented here are *global* errors, such that regional effects do not show up. Secondly, the use of the quadratic model requires much more computations than the linear one, such that rounding-off errors play a larger role.

The results of the *vectorial* GBVP, finally, are presented in table 5.4. The accuracy of the solved potential and elevation is almost unaffected by the introduction of the horizontal position as unknown. This can be attributed to the good approximate values available for the latitude. We make use of the fact that the observations are located on a regular grid by using the same grid for the telluroid points. The error in horizontal position is represented by the solved latitude, multiplied by the mean radius of the earth to get a quantity comparable to the vertical position. The reason for the slow convergence of the latitude is unclear so far. But we have to keep in mind that the horizontal coordinate is completely differently incorporated into the problem than the vertical unknown. It is in first approximation not related to the potential and we had to force the approximate values for x to be located in a regular grid.

For all GBVP's with 72 observations, as presented above, the iteration works according to our expectation. Now three GBVP's, *fixed* with gravity observations, *scalar* and *vectorial*, are considered with *720 points* of observation; the maximum frequency in the data is 360. The results are given in table 5.5. As the results with the quadratic model are not satisfactory, they are left out here. It is certain that

Table 5.4 *Relative errors of the potential and average errors in position for the vectorial problem with 72 points.*

		Number of iterations						
Unknown	Model	0	1	2	3	4	5	6
T	I	0.003874	0.003645	0.003645	0.003645	0.003645	0.003645	0.003645
	II	0.007089	0.001112	0.001138	0.001138	0.001138	0.001138	0.001138
	III	0.007089	0.001114	0.001142	0.001141	0.001141	0.001141	0.001141
	IV	0.007089	0.000175	0.000015	0.000007	0.000007	0.000007	0.000007
	V	0.007089	0.000177	0.000012	0.000001	0.000000	0.000000	0.000000
h	I	0.096186	0.093054	0.093079	0.093080	0.093080	0.093080	0.093080
meter	II	0.096186	0.021559	0.021555	0.021556	0.021556	0.021556	0.021556
	III	0.096186	0.021500	0.021505	0.021506	0.021506	0.021506	0.021506
	IV	0.096186	0.000804	0.000182	0.000177	0.000175	0.000175	0.000175
	V	0.096186	0.000934	0.000044	0.000004	0.000000	0.000000	0.000000
$R\phi$	I	0.996572	1.038099	1.038602	1.038611	1.038611	1.038611	1.038611
meter	II	0.996572	0.168598	0.139360	0.140535	0.140599	0.140580	0.140580
	III	0.996572	0.168164	0.138753	0.139935	0.140000	0.139980	0.139980
	IV	0.996572	0.072099	0.003370	0.000592	0.000471	0.000470	0.000470
	V	0.996572	0.072155	0.003273	0.000321	0.000045	0.000005	0.000000

the iteration does not work very well for this case. The better models yield about the same accuracy as the model in circular approximation (I). The iterations do not converge to the solution. After a series of tests it became clear that the relatively disappointing performance is caused by the use of polar potential coefficients. This aspect will be clarified in the next section.

5.4 Divergence and ellipticity

In section 5.2.2 the difference in convergence between the polar and elliptical series was discussed. In the previous section we saw that the GBVP's with 720 points (maximum degree 360) do not converge if the polar series for the potential are used. Here we will investigate under what circumstances this divergence can be expected.

As example, a simple GBVP is taken: potential observations on a fixed boundary with the polar potential coefficients as unknowns. This problem is especially simple since it is *linear*.

First some more results with this GBVP are presented in table 5.6. It shows that up to about 600 points the non-linear model still converges, although the convergence slows down with an increasing number of points. With 720 points there is no real convergence or divergence. The results go up and down. With 900 points the system collapses.

Table 5.5 *The three types of problems with 720 points. For the fixed problem gravity data was used.*

Fixed		Number of iterations						
Unknown	Model	0	1	2	3	4	5	6
	I	0.004154	0.004109	0.004151	0.004153	0.004154	0.004154	0.004154
	II	0.008837	0.003395	0.003233	0.003184	0.003193	0.003262	0.003373
	IV	0.008837	0.002208	0.001329	0.001091	0.001073	0.001137	0.001202
	V	0.008837	0.002208	0.001329	0.001091	0.001073	0.001137	0.001202
Scalar								
T	I	0.005163	0.004417	0.004492	0.004496	0.004497	0.004497	0.004497
	II	0.009553	0.005045	0.004944	0.004912	0.004917	0.004962	0.005036
	IV	0.009553	0.002306	0.001366	0.001098	0.001078	0.001138	0.001203
	V	0.009553	0.002305	0.001365	0.001098	0.001078	0.001138	0.001202
h	I	0.103608	0.091271	0.093197	0.093314	0.093323	0.093323	0.093323
meter	II	0.103608	0.102539	0.102671	0.102666	0.102665	0.102665	0.102666
	IV	0.103608	0.018444	0.008808	0.003850	0.002760	0.001547	0.001501
	V	0.103608	0.018443	0.008752	0.003810	0.002793	0.001512	0.001435
Vectorial								
T	I	0.005163	0.004417	0.004492	0.004496	0.004497	0.004497	0.004497
	II	0.009553	0.005043	0.004944	0.004912	0.004917	0.004962	0.005036
	IV	0.009553	0.002305	0.001366	0.001099	0.001078	0.001139	0.001204
	V	0.009553	0.002305	0.001365	0.001098	0.001078	0.001139	0.001204
h	I	0.103608	0.091271	0.093197	0.093314	0.093323	0.093323	0.093323
meter	II	0.103608	0.102466	0.102670	0.102665	0.102665	0.102665	0.102665
	IV	0.103608	0.018425	0.008856	0.003957	0.002746	0.001705	0.001856
	V	0.103608	0.018424	0.008801	0.003914	0.002780	0.001665	0.001894
$R\phi$	I	1.351246	1.195529	1.189309	1.188614	1.188521	1.188508	1.188505
meter	II	1.351246	1.974044	1.780721	3.225725	5.749357	9.772169	13.328539
	IV	1.351246	1.747251	1.408844	2.995327	4.705208	7.037035	8.940772
	V	1.351246	1.747186	1.408682	2.995214	4.705158	7.036900	8.940552

The model is written as the linear system

$$\begin{pmatrix} T(\phi_1) \\ T(\phi_2) \\ \vdots \\ T(\phi_N) \end{pmatrix} = \begin{pmatrix} \cdots & \left(\frac{R}{r_1}\right)^{|n|} e^{in\bar{\phi}_1} & \cdots \\ \cdots & \left(\frac{R}{r_2}\right)^{|n|} e^{in\bar{\phi}_2} & \cdots \\ & \vdots & \\ \cdots & \left(\frac{R}{r_N}\right)^{|n|} e^{in\bar{\phi}_N} & \cdots \end{pmatrix} \begin{pmatrix} \vdots \\ \Delta c_n \\ \vdots \end{pmatrix}.$$

Here N denotes the number of observations. The coordinates $\{r, \bar{\phi}\}$ are the *real*

Table 5.6 *The relative errors of the disturbing potential for the fixed problem with potential observations solved by the non-linear model.*

Number of points	Number of iterations						
	0	1	2	3	4	5	6
72	0.006648	0.000175	0.000012	0.000001	0.000000	0.000000	0.000000
360	0.008761	0.001703	0.000685	0.000308	0.000145	0.000071	0.000038
480	0.008879	0.001935	0.000916	0.000537	0.000341	0.000231	0.000165
600	0.008927	0.002084	0.001146	0.000830	0.000684	0.000585	0.000526
720	0.008945	0:002167	0.001319	0.001100	0.001091	0.001161	0.001226
900	2.227764	6.565019	23.131648	87.985038	360.182283	> 1000	> 1000

Table 5.7 *The spectral radii of the M-matrix of the fixed problem with potential observations.*

Number of points	Circle + topography	Ellipse	Ellipse + topography	Ellipse with optimal R
72	0.02	0.08	0.08	0.06
360	0.12	0.49	0.46	0.35
480	0.16	0.71	0.66	0.49
600	0.20	0.95	0.88	0.65
720	0.24	*1.23*	*1.14*	0.83
900	0.29	*1.73*	*1.59*	*1.18*

polar coordinates of the points of observation. As usual, the number of coefficients is taken equal to the number of observation points.

When solving this BVP by iteration, it means that the matrix $\boldsymbol{A}$, so desired in an approximation, is inverted by the Neumann series. The approximate matrix $\boldsymbol{A}_0$ is $\boldsymbol{A}$ in circular constant radius approximation:

$$\boldsymbol{A}_0 = \begin{pmatrix} \dots & e^{in\phi_1} & \dots \\ \dots & e^{in\phi_2} & \dots \\ & \vdots & \\ \dots & e^{in\phi_N} & \dots \end{pmatrix}.$$

It was produced by the mapping $\{r = R, \bar{\phi} = \phi\}$. The series for the inverse of $\boldsymbol{A}$ converges if the spectral radius of $\boldsymbol{M} = \boldsymbol{I} - \boldsymbol{A}_0^{-1}\boldsymbol{A}$ is smaller than unity (see section 4.3). In table 5.7 these spectral radii are computed for several numbers of points, and for three possible choices of $\boldsymbol{A}$: the exact matrix (model IV and V), without topography (model II) and in circular approximation (model I). The right hand column will be explained later. As expected, the spectral radii for the elliptical models are larger than unity for 720 points. Only the model in circular approximation converges.

From the table we conclude that the ellipticity of the earth gives more convergence problems than the topography (consider also that circular approximation without topography yields zero eigenvalues for all numbers of points). Strangely enough, the inclusion of the topography in the elliptical model decreases the spectral radius.

The matrix $\boldsymbol{M}$ is closer examined. Its elements, denoted by M_{mn}, are according to $\boldsymbol{M} = \boldsymbol{I} - \boldsymbol{A}_0^{-1}\boldsymbol{A}$:

$$M_{mn} = -\frac{1}{N}\sum_{j=1}^{N}\left(\frac{R}{r_j}\right)^{|n|} e^{in\bar{\phi}_j} e^{-im\phi_j} + \delta_{mn}. \tag{5.22}$$

The fraction R/r is linearized as

$$\left(\frac{R}{r_j}\right)^{|n|} \approx 1 - |n|\frac{r_j - R}{R}.$$

The radius vector is

$$r \approx h + \sqrt{b^2 + E^2\cos^2\beta} \approx h + b + \frac{E^2}{2b}\cos^2\beta = h + b + \frac{E^2}{4b} + \frac{E^2}{4b}\cos 2\beta.$$

Inserting these approximations, and $\beta \approx \phi \approx \bar{\phi}$, $e^2 \approx E^2/Rb$, into (5.22), yields

$$M_{mn} \approx \frac{|n|}{N}\sum_{j=1}^{N}\left\{\frac{h+b-R}{R} + \frac{e^2}{4} + \frac{e^2}{4}\cos 2\phi\right\} e^{i(n-m)\bar{\phi}_j}.$$

The summation is nothing but the Fourier expansion of the expression in braces. So we compute

$$M_{mn} \approx |n|\left(\frac{b-R}{R} + \frac{e^2}{4}\right)\delta_{mn} + |n|\frac{e^2}{8}\delta_{|m-n|,2} + |n|\left(\frac{h}{R}\right)_{m-n}.$$

The term with h/R denotes the dimensionless Fourier coefficients of the topography. Some approximations were introduced to arrive at this formula, but the structure of this matrix will be clear: The ellipticity yields a diagonal and two off-diagonals. The topography fills the entire matrix, with increasing magnitude towards the diagonal (the power of the topography increases with decreasing degree). We refer to a similar consideration in (Knickmeyer, 1984). From the eigenvalues of $\boldsymbol{M}$ in table 5.7 we concluded that the ellipticity of the earth has a major influence compared to the topography. Since both effects fill the matrix in quite a different way, their relative effect on the largest eigenvalue cannot be easily determined. The most important property of the elements of the matrix is their proportionality with $|n|$, causing an increase of the eigenvalues of $\boldsymbol{M}$ for increasing maximum degree. The maximum degree was in all cases related to the number of points. Therefore it was not yet clear which of the two caused the divergence. From the expression for M_{mn}, we may conclude that the maximum degree is crucial.

If the topography does not contain a zero degree component, the diagonal elements of $\boldsymbol{M}$ can be made zero by taking for the reference circle:

$$R = \frac{b}{1 - \frac{1}{4}e^2}.$$

With this 'optimized' R (it is not optimized in the sense of minimization of the largest eigenvalue, which would be more relevant), the spectral radius of $\boldsymbol{M}$ is slightly reduced (last column of table 5.7). To improve these results a little, the optimal R used in this table was not computed by this approximate formula, but estimated by running numerical test on the $\boldsymbol{M}$ matrix. However, the improvement was marginal.

5.5 Use of the elliptical series

As discussed, the use of potential series with respect to elliptical coordinates, instead of polar coordinates, could improve the convergence of the iteration. In the first part of this section, tests are presented to show this. For these tests, conditions are selected that allow a fair comparison between both types of series. In the second part we will focus on the use of the elliptical series in other situations.

5.5.1 The problem in elliptical coordinates

For the solution of the GBVP with the use of the series in polar coordinates, the observations were synthesized from the generated potential, expressed in these series, up to half the sampling frequency. This is done to avoid aliasing. As shown in appendix B, a signal bandlimited with respect to the polar series, is *not* bandlimited with respect to an elliptical series. Hence, the use of the polar series for the observation synthesis up to half the sampling degree, yields aliasing effects if the GBVP is solved using the elliptical series. To get a fair comparison with the series in polar coordinates, a potential with respect to elliptical coordinates is generated, from which the observations are synthesized.

This generation is done in a straightforward manner. First the normal potential is subtracted from the potential in polar coordinates. The coefficients of the *disturbing* potential with respect to the *polar* series are now used as coefficients for the disturbing potential with respect to the *elliptical* series. By addition of the normal potential, which has only one non-zero component: the logarithm, the required expansion is obtained. Although these potential coefficients are not strictly related with the isostatically compensated topography, it will do for this test purpose.

From the series, again two sets of observations are synthesized, one with 72 points and a second one with 720 points. As the Fourier series used now are with respect to the argument β, the observations are computed in a regular β–grid. The respective coordinates u are obtained by an interpolation and coordinate transformation of the original topography data set in $\{h, \phi\}$.

The iteration works in the same way as with polar coordinates. The models with the $\{u, \beta\}$ coordinates are already provided. The part lacking is the computation of the new position in elliptical coordinates from the position corrections with respect to the local frame. Fortunately the relations are simple. We have

$$\begin{pmatrix} u \\ \beta \end{pmatrix} = \begin{pmatrix} u_0 \\ \beta_0 \end{pmatrix} + \begin{pmatrix} \frac{\partial u}{\partial x} & \frac{\partial u}{\partial z} \\ \frac{\partial \beta}{\partial x} & \frac{\partial \beta}{\partial z} \end{pmatrix} \begin{pmatrix} \Delta x \\ \Delta z \end{pmatrix}.$$

Thereby $\{u, \beta\}$ denote the coordinates of the approximate point. The partial derivatives are computed by

$$\frac{\partial x^A}{\partial x^i} = \frac{\partial x^A}{\partial x^I} \frac{\partial x^I}{\partial x^i},$$

which are given in appendix A. This yields

$$\begin{aligned} \Delta u &= \frac{v}{L} \Delta z \\ \Delta \beta &= \frac{R}{L} \Delta x. \end{aligned} \tag{5.23}$$

The iterative solutions are computed for the models II, IV and V. The Molodensky problem is left out since it does not make sense to apply elliptical series in a model in circular approximation. Also the quadratic model is omitted because of its small difference with the linear model on the ellipse.

The problems with 72 points all give about the same accuracy as with the polar series. The only difference is a small increase in convergence. The results are not presented here. We concentrate on the GBVP's with 720 points, which did not work properly with the polar series. In table 5.8 the errors are given. The accuracies of the models are now comparable to the situation with 72 points and polar series. The aspect of most interest is the convergence. We observe that all models converge nicely, and reach an accuracy not worse than that obtained with 72 points. Hence, it can be concluded that the application of the elliptical series works very well and does overcome the convergence problem caused by ellipticity.

5.5.2 Elliptical series and geographic coordinates

In the last section we showed that the potential series with respect to the elliptical coordinates $\{u, \beta\}$ performed well. But an idealized case was considered there: the observations were distributed equidistantly in β and the solved potential coefficients were compared with 'true' coefficients also given with respect to $\{u, \beta\}$. Here we return to the points of departure of section 5.3: the observation data are distributed equidistantly in geographic latitude (ϕ) and potential coefficients with respect to the polar coordinates have to be solved, a situation closer to reality.

The regular distribution of the anomalies with respect to β on the circle, required for the computation of the elliptic Fourier coefficients by FFT, is established by

Table 5.8 *The relative total errors for the* GBVP*'s with 720 points using the elliptical series for the potential. Gravity was used for the fixed problem.*

Fixed		Number of iterations						
Unknown	Model	0	1	2	3	4	5	6
T	II	0.001745	0.001890	0.001890	0.001890	0.001890	0.001890	0.001890
	IV	0.001745	0.000062	0.000006	0.000004	0.000004	0.000004	0.000004
	V	0.001745	0.000061	0.000005	0.000001	0.000000	0.000000	0.000000
Scalar								
T	II	0.002838	0.002894	0.002896	0.002896	0.002896	0.002896	0.002896
	IV	0.002838	0.000084	0.000008	0.000006	0.000006	0.000006	0.000006
	V	0.002838	0.000083	0.000005	0.000001	0.000000	0.000000	0.000000
h	II	0.064130	0.060160	0.060179	0.060179	0.060179	0.060179	0.060179
meter	IV	0.064130	0.001598	0.000168	0.000148	0.000148	0.000148	0.000148
	V	0.064130	0.001551	0.000051	0.000003	0.000001	0.000000	0.000000
Vectorial								
T	II	0.002838	0.002883	0.002886	0.002886	0.002886	0.002886	0.002886
	IV	0.002838	0.000073	0.000008	0.000006	0.000006	0.000006	0.000006
	V	0.002838	0.000072	0.000005	0.000001	0.000000	0.000000	0.000000
h	II	0.064130	0.059878	0.059918	0.059918	0.059918	0.059918	0.059918
meter	IV	0.064130	0.001284	0.000164	0.000149	0.000148	0.000148	0.000148
	V	0.064130	0.001232	0.000041	0.000004	0.000001	0.000000	0.000000
$R\Phi$	II	0.327938	0.309321	0.309336	0.309335	0.309335	0.309335	0.309335
meter	IV	0.327938	0.017066	0.002263	0.000756	0.000677	0.000675	0.000675
	V	0.327938	0.017100	0.002180	0.000351	0.000064	0.000012	0.000003

mapping the anomalies, which are equidistant in ϕ, to the circle by $\beta = \phi$. For the vectorial problem we are free to choose an approximate latitude, in that case an equidistant β-grid is taken, which deviates only a little from a geographical ϕ-grid. So far not much difference with the polar series.

A difference enters in the step of backward substitution. As explained before, the potential coefficients computed by Stokes (or one of the other appropriate formulas) are now used as coefficients for the series in *elliptical* coordinates. Hence, the models formulated with these coordinates are used. Since the original 'true' coefficients are given with respect to *polar* coordinates, the final solution for the coefficients is transformed to polar coordinates, see appendix B. The results for the models II, IV and V are presented in table 5.9. For the fixed problem gravity observations are used.

Comparison with table 5.8 shows that the results are slightly worse. This is caused by *aliasing*. The signal in the data is *bandlimited* with respect to the polar

Table 5.9 *The relative total errors for the problems with 720 points regularly distributed in geographic latitude, using the elliptical series for the potential.*

Fixed		Number of iterations						
Unknown	Model	0	1	2	3	4	5	6
T	II	0.004153	0.002802	0.002848	0.002853	0.002851	0.002850	0.002850
	IV	0.004153	0.000508	0.000128	0.000062	0.000048	0.000046	0.000046
	V	0.004153	0.000509	0.000128	0.000062	0.000048	0.000046	0.000046
Scalar								
T	II	0.005163	0.004670	0.004701	0.004704	0.004703	0.004702	0.004702
	IV	0.005163	0.000586	0.000129	0.000064	0.000049	0.000046	0.000046
	V	0.005163	0.000586	0.000129	0.000064	0.000049	0.000046	0.000046
h	II	0.103608	0.102634	0.102667	0.102665	0.102665	0.102665	0.102665
meter	IV	0.103608	0.008162	0.000549	0.000412	0.000178	0.000140	0.000125
	V	0.103608	0.008181	0.000504	0.000369	0.000106	0.000039	0.000018
Vectorial								
T	II	0.181587	0.005215	0.005174	0.005174	0.005174	0.005174	0.005174
	IV	0.181587	0.002565	0.000480	0.000468	0.000470	0.000471	0.000471
	V	0.181587	0.002106	0.000129	0.000063	0.000048	0.000046	0.000046
h	II	4.263366	0.104232	0.104055	0.104057	0.104057	0.104057	0.104057
meter	IV	4.263366	0.048120	0.010755	0.010807	0.010885	0.010901	0.010898
	V	4.263366	0.038312	0.000550	0.000364	0.000107	0.000045	0.000035
$R\Phi$	II	4.348873	2.558599	2.548758	2.548758	2.548758	2.548758	2.548758
meter	IV	4.348873	1.104638	1.031215	1.015436	1.019246	1.023208	1.024302
	V	4.348873	1.105167	1.030297	1.011436	1.018178	1.022155	1.023253

series, which does not imply bandlimitation with respect to the elliptical series, as was the case in table 5.8. But since the real potential has no real bandlimitation, this difference is not a point of importance. Only for the vectorial problem the results are noticeably worse, especially the horizontal position is determined quite bad, as with the non-linear model. A reasonable explanation is not found yet. But it can be concluded from these results that the application of elliptical series generally works very well with observations on a regular ϕ-grid.

In figure 5.7 the error power spectra of the potential, computed from the *scalar* problem, for the three models are plotted. They are computed as the quadratic sum per degree of the difference 'solved' minus 'true' potential coefficient. The increasing error, due to aliasing, with increasing degree is clearly visible of the curve for the non-linear model (V). Also rounding-off errors play a role. The linear model IV deviates from model V only for the low degrees. For the higher degrees the aliasing errors dominate the non-linear effects. The linear model on the ellipse (II) yields

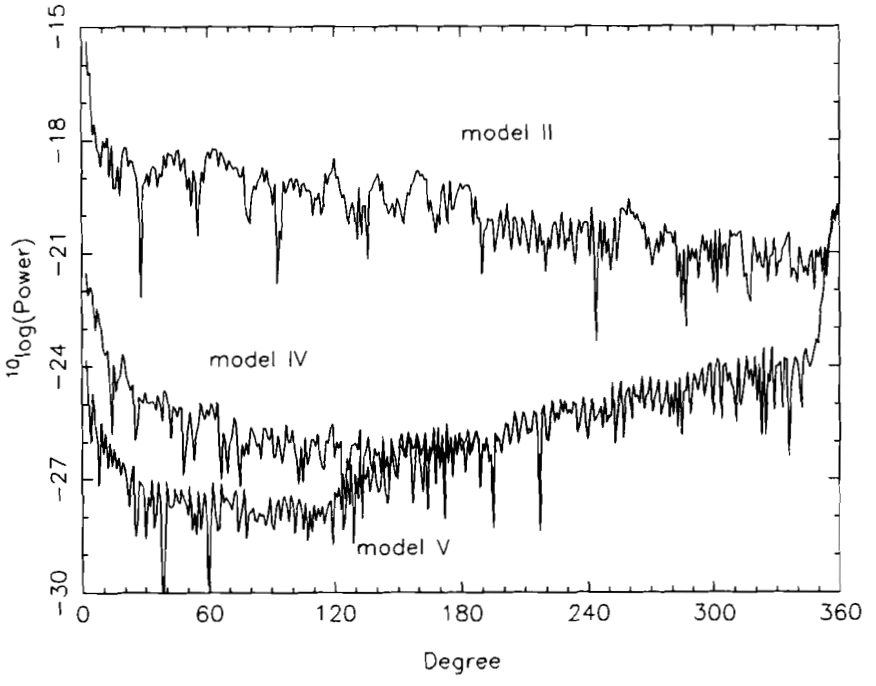

Figure 5.7 *The error power spectra of the solved potential coefficients from 720 potential and gravity observations. Elliptical potential series are applied.*

the largest errors in the *lower* degrees. This is caused by the high power in the low degree coefficients.

In figure 5.8 we clearly see the gain in accuracy by the application of elliptical potential series. Form the data set of 720 potential and gravity measurements, the potential is recovered by the application of a series in polar coordinates and in elliptical coordinates (with conversion afterwards). The accuracy improvement reaches a few orders of magnitude, especially for the higher frequencies. It should be emphasized that we always have to keep in mind that a bandlimited potential is assumed and errorless observations are used. If taking these two error sources into account, the difference between the two series is smaller.

5.6 Other data conditions

On the data used for the tests so far, assumptions and restrictions have been imposed usually not fulfilled in practice. We mention the three most important ones:

1. Band limitation in data. The full spectrum of the potential should be used for the observation synthesis.

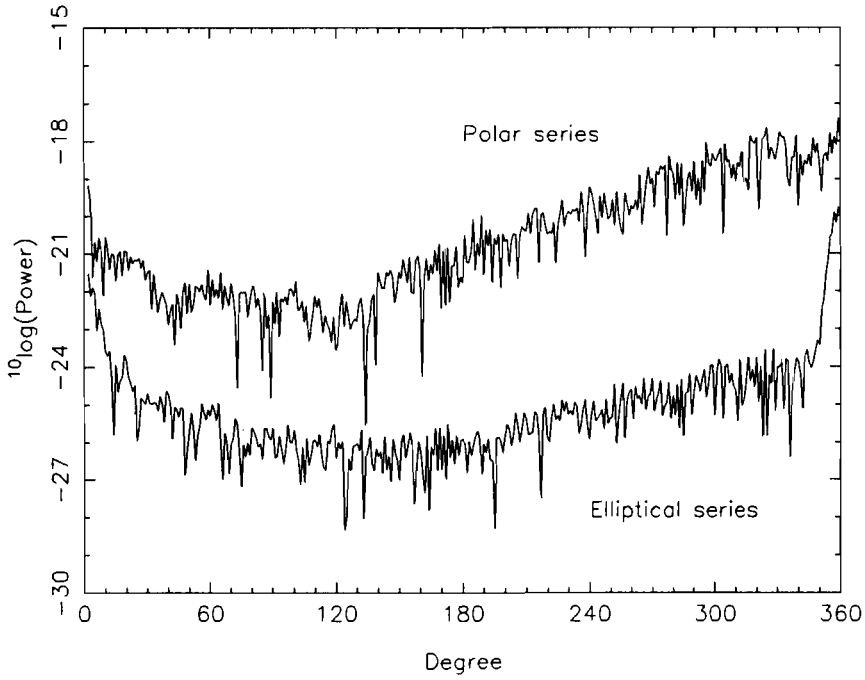

Figure 5.8 *The error power spectra of the solved potential coefficients from 720 potential and gravity observations with the linear model (IV) using polar or elliptical potential series.*

2. Regular data distribution. Very different data densities are still reality, especially because of the division of the earth into continents and oceans.
3. Data without noise. The observations always have a stochastic character.

The first point is considered briefly in this section. The second will not be tested in this thesis. One reason for this is the definition of irregularity. It is suspected that the solution presented above will break down if the data points are not very regularly distributed. But since a set of points can be distributed in infinitely many ways, it is difficult to judge the results from such tests. In the next section results are presented with noisy data, to satisfy point three.

We chose to use observations from a bandlimited potential to avoid aliasing. Although this an artifice not possible in reality, it gives the opportunity to separate aliasing errors from others, in order to be able to judge the results better. First it will be shown how the situation changes if no bandlimitation is taken. In table 5.10 the results for the fixed, scalar and vectorial problem are presented for observations with and without bandlimitation for 72 and 720 points. Actually the 'unbandlimited' data also have a bandlimit (degree 3600), but the power in these high frequencies is almost zero.

From the table the drastic effect of the higher frequencies is clearly visible. As could be expected, the result with only 72 points of observation becomes really bad,

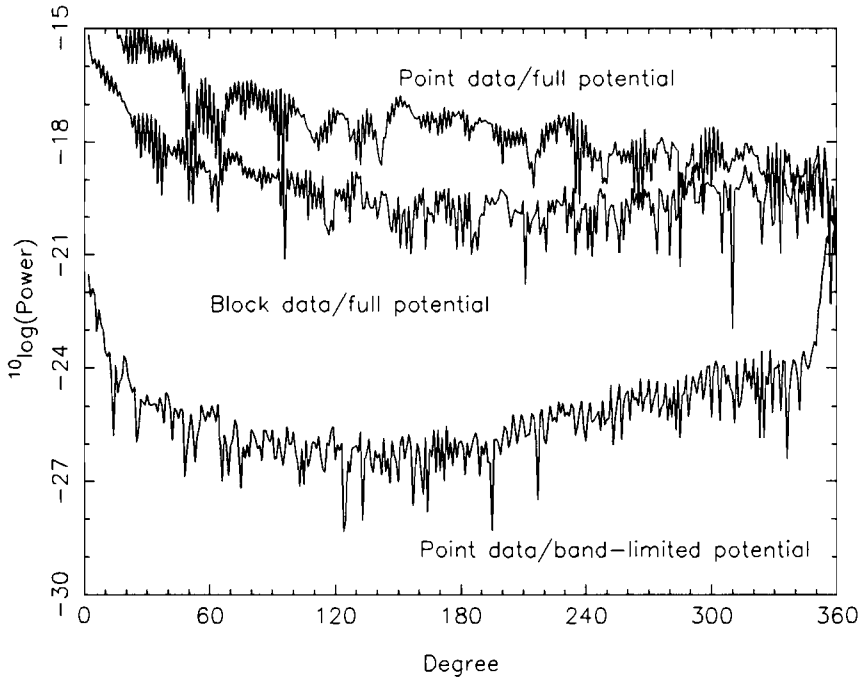

Figure 5.9 *The error power spectra of the solved potential coefficients from 720 potential and gravity observations with the linear model (IV).*

with 720 points the result is much better because of the higher sampling rate. The performance with the *bandlimited* data with 72 points with respect to 720 points is relatively poor. This is also caused by aliasing: the bandlimitation was taken with respect to the potential series in polar coordinates, whereas a series with elliptical coordinates was applied for the computation (see section 5.4).

The error spectra for the scalar problem with model IV is shown in figure 5.9. We observe that the difference between the potential solved from the 'real' data (with the complete signal) is several orders of magnitude worse than with the bandlimited data. But we have to be careful not to jump to conclusions. For these computations a *model* for the potential was postulated. It can be wrong orders of magnitude,

Table 5.10 *The relative total errors of the potential computed with the linear model (IV) with elliptical potential series after 7 iterations (fixed problem). The abbreviation 'b.l.' denotes bandlimited.*

	72 points		720 points	
	b.l.	no b.l.	b.l.	no b.l.
Fixed	0.000480	0.391376	0.000046	0.066718
Scalar	0.000481	0.591836	0.000046	0.094529
Vectorial	0.000673	0.592101	0.000471	0.094023

especially for the higher frequencies, in comparison to the real 3D potential.

The third line in the figure indicates the result in case *block mean values* are used. Each observation in one of the 720 points is computed as an average over eleven observations (two adjacent blocks have one observation in common in order to simplify the formulas). The estimated potential coefficients are de-smoothed by the inverse moving average operator. Except for the high frequencies, the use of block mean values instead of point values yields an accuracy improvement of about two orders.

5.7 Overdetermined vertical problem with noise

As dessert we choose for the overdetermined scalar vertical problem with the observations W, g, Γ_{zz} and z. We also will take a brief look onto data with noise and the use of an analytical model for error prediction.

5.7.1 The gradiometric observable

We start with the observation equation for the vertical gradient. The general linear observation equation is (3.9):

$$\Delta\Gamma_{zz} = (U_{zzz} - \frac{2}{\gamma}U_{zz}^2)\,\Delta z + T_{zz} - \frac{2}{\gamma}U_{zz}\,T_z.$$

In circular approximation this becomes with dimensionless quantities (3.15):

$$d\Gamma_{zz} = -\left(\frac{R}{r}\right)^3 dz + T_{rr}.$$

For the two models in elliptical approximation (models II and IV, the quadratic model is omitted here) equations (4.7–4.8) are used for the derivatives of the normal potential. For T_z we refer to section 5.2. For the second vertical derivative we compute with

$$T_{ij} = \frac{\partial x_I}{\partial x_i}\frac{\partial x_J}{\partial x_j}\frac{\partial x_\alpha}{\partial x_I}\frac{\partial x_\beta}{\partial x_J}\,T_{\alpha\beta}$$

$$T_{zz} = (\sin 2\bar{\phi}\sin 2\phi + \cos 2\bar{\phi}\cos 2\phi)T_{rr} + \\ +(\sin 2\bar{\phi}\cos 2\phi - \cos 2\bar{\phi}\sin 2\phi)(\frac{1}{r}T_{\bar{\phi}} - T_{r\bar{\phi}})\frac{1}{r}$$

on the ellipse (model II) and

$$T_{zz} = (\frac{uv}{L^2}\sin 2\bar{\phi}\sin 2\beta + \cos 2\bar{\phi}(1 - \frac{2v^2}{L^2}\sin^2\beta)T_{rr} + \\ +(\sin 2\bar{\phi}(1 - \frac{2v^2}{L^2}\sin^2\beta) - \frac{uv}{L^2}\cos 2\bar{\phi}\sin 2\beta)(\frac{1}{r}T_{\bar{\phi}} - T_{r\bar{\phi}})\frac{1}{r},$$

Table 5.11 *The relative total errors for the potential with polar series for the case of 72 points and elliptical series for 720 points after 7 iterations (fixed problem).*

	72 points			720 points		
model	g	Γ_{zz}	Γ^*_{zz}	g	Γ_{zz}	Γ^*_{zz}
I	0.003214	0.006150	0.005729	—	—	—
II	0.000834	0.003484	0.003692	0.002850	0.064270	0.068072
IV	0.000004	0.000819	0.000000	0.000046	0.001150	0.000047
V	0.000000	0.000000	0.000000	0.000046	0.000047	0.000047

generally (model IV). If the derivatives with respect to the elliptical coordinates are used it becomes:

$$T_{zz} = \frac{v^2}{L^2} T_{uu} + \frac{E^2}{L^4} \sin\beta \cos\beta \, T_\beta - \frac{uE^2}{L^4} \cos^2\beta \, T_u.$$

For the non-linear models (5.11) is used.

First we take the fixed problem with the gravity gradients and compare the accuracy with the result with gravity observations from tables 5.2 and 5.10. For model I with 72 points, where the polar potential series are used, the elliptic correction is applied, as explained in 5.3.

In this table the results of two kinds of Γ_{zz} are listed. The first with e_z in the direction opposite to the gravity vector, as was supposed in the foregoing definition of the model, and the second, discriminated by an asterisk, opposite the normal gravity vector. For the observations with the latter definition of the z-axis the linear model becomes

$$d\Gamma^*_{zz} = U_{zzz} \, dz + T_{zz}.$$

The reason for the consideration of this additional observation type is twofold: with e.g. satellite gradiometry the attitude of the instrument is known, so there is no need to use the (unknown) direction of the real gravity vector, secondly, the model for $d\Gamma^*_{zz}$ is more accurate in circular approximation than the model for $d\Gamma_{zz}$ because the additional terms required for the latter are zero in that case.

From table 5.11 it can be seen that for all linear models the results with gradiometry are worse than with gravity. This can be explained by the accuracy of the models. The relative error we commit by using circular approximation or neglecting the topography is larger in case of gradiometry than with gravimetry. This will be shown below.

With model IV the potential can be exactly reconstructed from the observations Γ^*_{zz} (except for the aliasing error with 720 points caused by the use of the elliptical series) because there is no non-linear term in the equation for these observations.

5.7.2 Accuracy of observation equations

The observation equations for dg and $d\Gamma_{zz}^{*}$ are closer examined here. Since their main difference lies in the disturbing term of the equations, the fixed problem is taken. The observation equations can be written as

$$dg = T_z + \varepsilon_g$$
$$d\Gamma_{zz} = T_{zz} + \varepsilon_\Gamma$$

where the derivatives of T are taken with some approximation and ε denotes the error introduced by this approximation. The solution of the potential coefficients becomes (in circular, constant radius approximation)

$$\Delta c_n \approx \frac{1}{|n|}(dg - \varepsilon_g)_n$$

or

$$\Delta c_n \approx \frac{1}{|n|(|n|+1)}(d\Gamma_{zz} - \varepsilon_\Gamma)_n.$$

The notation $(\ldots)_n$ denotes the Fourier coefficient of degree n of the expression between parentheses. The error in the solved coefficients becomes

$$\varepsilon(\Delta c_n) \approx \frac{\varepsilon_{g_n}}{|n|} \tag{5.24}$$

when computed from dg and

$$\varepsilon(\Delta c_n) \approx \frac{\varepsilon_{\Gamma n}}{|n|(|n|+1)} \tag{5.25}$$

in case the vertical gravity gradient is used. The error propagation is derived with circular, constant radius approximation, where the exact model should be used. But for an estimation of the error it is sufficient.

First the circular approximation is considered. The derivatives of T are linearized with respect to e^2:

$$T_z = \frac{v}{L}T_u \approx T_r + \frac{1}{2}e^2\cos^2\bar{\phi}\,T_r$$
$$T_{zz} = \frac{v^2}{L^2}T_{uu} + \frac{E^2}{L^4}\cos\beta\sin\beta\,T_\beta - \frac{uE^2}{L^4}\cos^2\beta\,T_u$$
$$\approx T_{rr} + e^2(\cos^2\bar{\phi}T_{rr} + \frac{1}{R^2}\cos\bar{\phi}\sin\bar{\phi}\,T_{\bar{\phi}} - \frac{1}{R}\cos^2\bar{\phi}\,T_r).$$

Since circular approximation means that $e = 0$, the error estimates for the coefficients become by insertion into (5.24–5.25):

$$\varepsilon(\Delta c_n) = \frac{(\frac{1}{2}e^2\cos^2\bar{\phi}T_r)_n}{|n|} < \frac{1}{2}e^2\Delta c_n$$

and

$$\varepsilon(\Delta c_n) = \frac{e^2(\cos^2\bar{\phi}T_{rr} + \frac{1}{R^2}\cos\bar{\phi}\sin\bar{\phi}\,T_{\bar{\phi}} - \frac{1}{R}\cos^2\bar{\phi}\,T_r)_n}{n^2} < e^2\Delta c_n;$$

approximately two times as large as with gravity observations. This can also be concluded from table 5.11, model I, the model in circular approximation. The error bounds derived above are not very strict, they are only a rough estimate of the expected accuracy of the equations.

Next we take a look at the neglect of the topography. Since the errors to be estimated are not very large, the model in circular approximation is used for the derivation. For T_z we have:

$$T_z \approx T_z|_{r=R} + h\,\frac{\partial T_z}{\partial r} \approx T_z|_{r=R} - h\,T_{rr},$$

and for the second vertical derivative

$$T_{zz} \approx T_{zz}|_{r=R} + h\,\frac{\partial T_z z}{\partial r} \approx T_z z|_{r=R} - h\,T_{rrr}.$$

Insertion into (5.24–5.25) yields for the error introduced by taking $h = 0$ (neglecting the sign):

$$\varepsilon(\Delta c_n) \approx \frac{(h.T_{rr})_n}{|n|},$$

for gravimetry and for gradiometry

$$\varepsilon(\Delta c_n) \approx \frac{(h.T_{rrr})_n}{n^2}.$$

We have to remember that the Fourier coefficients of the products of the topography function and the second, respectively third, derivative of T have to be computed for this error estimate, which implies a spectral convolution. Test computations show that above degree 50 the error for the potential coefficients is the same for both types of observations. Below degree 50 the gravity gradients give larger errors, up to about one order of magnitude. This yields considerable differences for the total accuracy of the solved potential, see table 5.11 with model II, the model on the ellipse.

5.7.3 The overdetermined problem

Together with the observation of the vertical position, z or dz, we now have four observables related to potential and/or vertical position, see section 3.6. In case dz observations are available, it is natural to use them for the computation of the coordinates of the approximate point (together with the ϕ, which is considered to be given for all scalar problems). But in order to make the software not more complicated than it already is, we choose to obtain the vertical coordinate of the approximate point by the mapping we also used for the uniquely determined problem. Test computations showed that the difference between the two procedures is

Table 5.12 *The relative total errors for the potential with polar series and 72 points after 7 iterations with the scalar problem.*

		Combination of observations				
Unknown	Model	$\{W,g\}$	$\{W,g,\Gamma\}$	$\{W,g,\Gamma^*\}$	$\{W,g,z\}$	$\{W,g,\Gamma^*,z\}$
T	I	0.003645	0.007367	0.006623	0.002673	0.005234
	II	0.001139	0.005300	0.005729	0.000835	0.004222
	IV	0.000007	0.001275	0.000002	0.000004	0.000001
	V	0.000000	0.000000	0.000000	0.000000	0.000000
h	I	0.093080	0.180060	0.167601	0.066582	0.137206
meter	II	0.021566	0.120804	0.130385	0.013628	0.095173
	IV	0.000175	0.029558	0.000075	0.000106	0.000069
	V	0.000000	0.000000	0.000000	0.000000	0.000000

negligible. Subsequently the dz observations are computed from the coordinates of the real and of the approximate point.

In table 5.12 the results are presented for several combinations of data. Again the two types of gradiometric observations are used (cf. section 5.7.1). We observe results that seem to be unreasonable at first sight: addition of the Γ observations to the potential and gravity data results in a less accurate estimate for the unknowns instead of more accurate, what we generally expect when observations are added. This is due to the inaccurate observation equation of the gravity gradient. Comparison with table 5.11 shows that the models that give a poor performance with the fixed problem with Γ_{zz}, yield here a worse result. Only in case the observation equation we add is of comparable or better accuracy than the existing, the estimate of the unknowns improves.

We have to keep in mind that we are still using data without noise. This means that only model errors can prevent a perfect solution of the unknowns. However, for the overdetermined cases we have to remind that the iteration procedure applied does not converge exactly to the right solution (see section 4.3.4). Observing the results of this table, we can conclude that this deviation is very small.

The unknown dz is formally solved by (3.51). But because the observation equation for the potential anomaly is superior to that of gravity and gravity gradient, the estimate

$$dz = -dW + T$$

is better than the least squares solution. The solution for dz in table 5.12 are computed in this way. In case dz is available as *observation*, we could directly 'estimate' dz without any error. To be able to compare the results for the different combinations of observations, the estimate using dW is applied for all situations.

5.7.4 Observations with noise

In this last paragraph we present some results for more realistic circumstances. It is not intended to obtain accuracy estimates that can be transferred to the 3D world, or to show which kind of approximation is allowed in case of some data availability, but we want to get an impression of how the accuracy estimates change in case data noise is added, and secondly to see how a simple model for analytical error prediction performs.

The noise on the data is obtained by a computer random number generator. It is uniformly distributed between on the interval $[-\sigma,\sigma]$, where σ denotes the used standard deviation. A normal distribution would have been better, it is more realistic, but that was not directly available.

For the *analytical error model* white noise is assumed. In the spectral domain this means that the power (variance of the noise) is equally distributed over all degrees. The error is propagated to the disturbing potential by (3.50), the relation between observations and potential in circular, constant radius approximation.

All examples we show here are error power spectra for the potential solved from the scalar problem with observations in 720 points, using elliptical potential series and several iterations. We start with an uniquely determined problem. For observations we chose potential and gravity, both with a relative accuracy of 10^{-8}. They are point values computed from a bandlimited potential as shown in figure 5.10. We conclude from this figure that the analytical error model represents the trend in the power spectrum very well for the non-linear model (V). In case model II is used the analytical model gives a far too optimistic perspective. Because the analytical model only represents the non-systematic observation noise, the approximation in the observation equations with II is not represented.

In the next plot (figure 5.11) we show four error spectra computed with an analytical model, each for a different combination of observations. The standard deviations where taken as: $\sigma_w = \sigma_z = 10^{-8}$, $\sigma_g = 10^{-6}$ and $\sigma_\Gamma = 10^{-4}$. We clearly see that the addition of z to $\{W,g\}$ improves the lower frequencies and Γ_{zz} the higher frequencies.

In figure 5.12 the real error spectra are computed (again with data from a bandlimited potential and the non-linear model) for the problem with $\{W,g\}$, and for the problem with the observations $\{W,g,\Gamma_{zz},z\}$. For both the analytic model yields realistic error spectra.

In the last plot, figure 5.13, three error spectra are plotted, all for the scalar problem with potential and gravity observations in 720 points, using the elliptical potential series and the non-linear model solved by iteration. The potential is observed with a relative standard deviation of 10^{-8} and gravity with 10^{-6} for all three cases. We see that with noisy data, the effect of taking block mean values from the full signal, instead of the unrealistic bandlimited point values, is less then without any noise, see figure 5.9. The observation noise is now the main error source. Hence, the analytical model yields also realistic results for the block mean data, only for

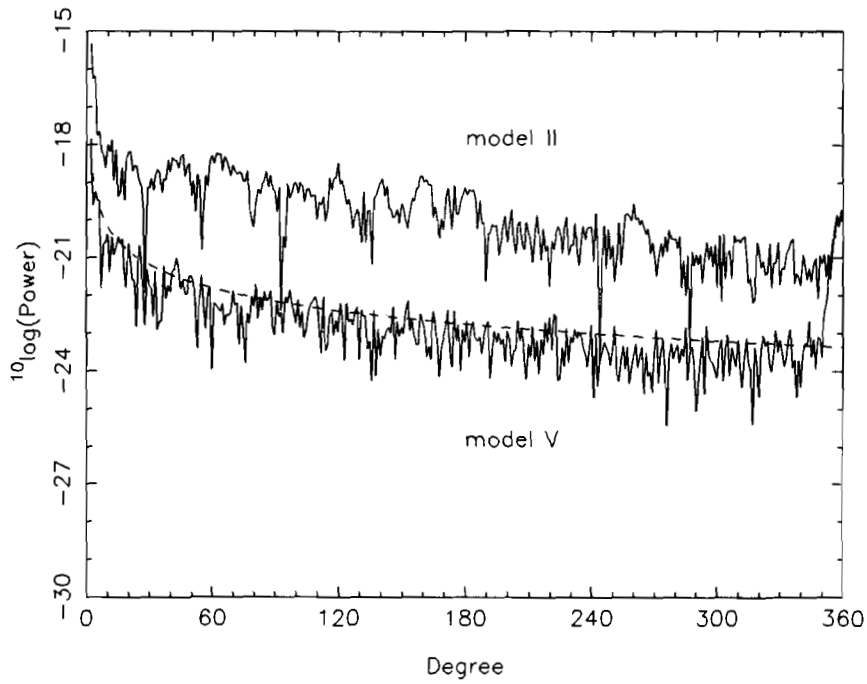

Figure 5.10 *The error power spectra of the solved potential coefficients from 720 potential and gravity observations. The dashed line indicates the analytical error model.*

the high frequencies aliasing introduces an noticeable additional error.

Although we do not present this results in order to draw any conclusion but just as an example, it will be clear that simple analytical models, such as the error power spectrum model used here, can be tested by simulations. This can serve as example for analytical models for the estimation of e.g. aliasing errors and the effect of data inhomogeneity.

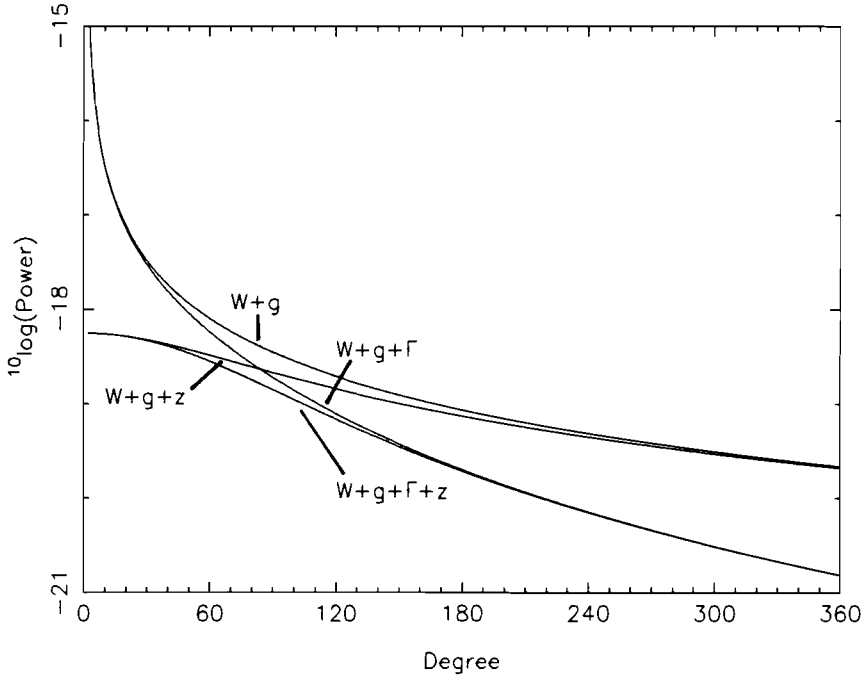

Figure 5.11 *The analytical error power spectra of the solved potential coefficients from 720 points.*

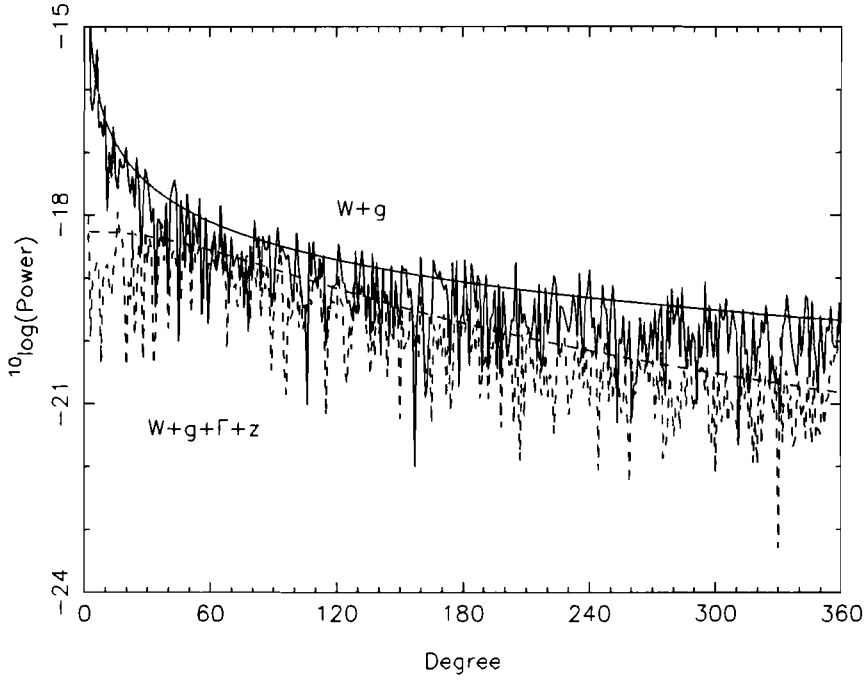

Figure 5.12 *The error power spectra of the solved potential coefficients from 720 points.*

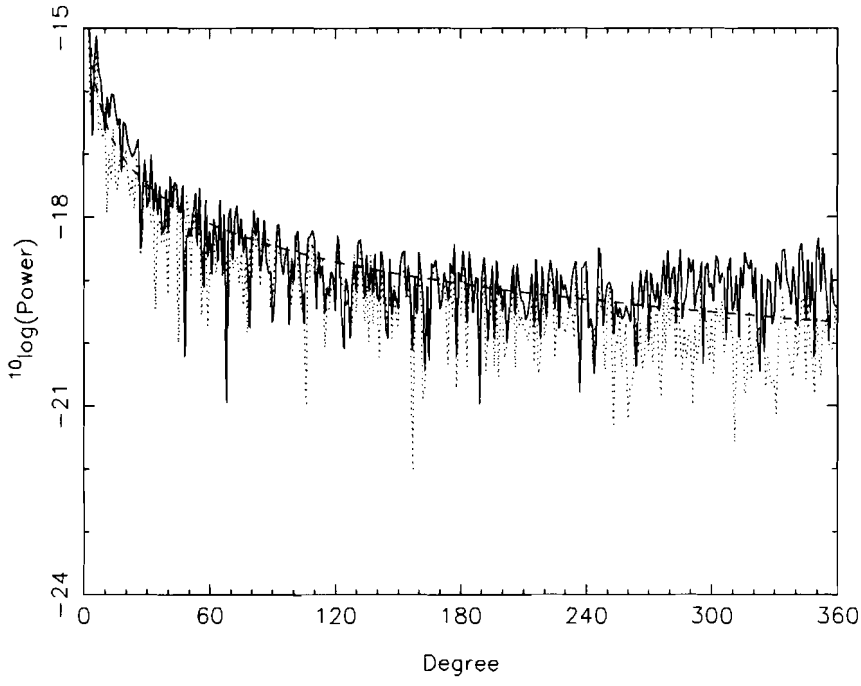

Figure 5.13 *The error power spectra of the solved potential coefficients from 720 potential and gravity observations with the non-linear model. The solid line for block mean values, the dotted line for point values from a bandlimited potential and the dashed line from the analytical model.*

Conclusions

A two dimensional world is an artifact without any physical connection to our real world. But the mathematical structure of its gravitational field, and the formulation of the equations of physical geodesy, show great resemblance with our real world. Therefore, it is not only out of curiosity that this investigation has been carried out, but it also serves to gain a better understanding of some aspects of (three dimensional) physical geodesy.

After the derivation of the basic formulas of the potential theory, the linearized observation equations were derived in circular, constant radius approximation. Their structure and solution by symmetric kernel integrals are almost the same as for the three dimensional case, the main difference being the replacement of the spherical harmonics by Fourier series. The latter are not only easier to handle, but offer also the opportunity of solving the potential from discrete data. The analytical solution for the various GBVP's in circular, constant radius approximation, gives a very easy opportunity for error prediction. From the noise model of the observations the accuracy of the solved potential and position unknowns can be directly computed. Also reliability analysis of an overdetermined GBVP can be performed analytically.

It it shown that there exists a direct relationship between the integral of astronomical leveling and the solution of the GBVP from astronomic latitude, a relation that could not be established so far for the 3D GBVP.

The solution of the GBVP by iteration is the key issue of this study. An iteration method is proposed for which criteria for convergence are given by means of eigenvalues of a matrix related to the design matrix of the system. For the solution step in the iteration, the (analytical) solution of the GBVP in circular, constant radius approximation is used, in order to avoid matrix inversion. Because of the use of analytical solutions, more advanced numerical methods are not likely to pay off because of the increase in computation time per step. The level of approximation in the backward substitution step of the iteration determines the accuracy of the final solution, in case convergence is guaranteed and no other error sources are present.

For the purpose of numerical tests, a synthetical earth is generated with a topography and a gravity field resembling the features of the real earth. By means of simulations it is shown that the iteration procedure works according to our expectations. For some cases the solution determined by the iteration can be compared to the solution by means of a direct numerical matrix inverse. They turn out to be the

same. This implies the iteration works correctly, and the derived criteria for convergence suffice. The solution of the the classical GBVP in circular approximation, the simple problem of Molodensky, can also be derived analytically using the iteration method. This solution is the same as given by other authors.

The iteration is applied to three uniquely determined GBVP's: the *fixed* problem (only potential is unknown), the *scalar* problem (only horizontal position is given) and the *vectorial* problem. Furthermore, the overdetermined scalar problem is considered. They are solved in several approximations: the GBVP in circular approximation (ellipticity neglected but with topography), the linear model on the ellipse (no topography but ellipticity taken into account), the linear model without further approximation, the GBVP in quadratic approximation and finally the original, non-linear model. As can be expected, the iteration is most beneficial if a problem without much approximation is used, and high quality data is available. In order to be able to separate the different error sources, several idealized data conditions were created, such as band limitation and zero noise level. In the ideal case, without any error sources, an exact solution, up to the level of the computer rounding-off errors, can be obtained of the non-linear problem. The accuracy of the solution of the unknowns mainly depends on the approximation level of the model, the accuracy of the observations, the number of observations and the gravity field.

When determining the potential coefficients to a high degree, the speed of convergence of the iteration slows down and diverges in our case for a maximum degree of about 300. By analysis of the convergence criteria, it can be concluded that the ellipticity of the earth causes the problem. This can be overcome by the use of a potential series expressed in elliptical coordinates, instead of polar coordinates.

The simulation can not only be used to show that an almost perfect solution from hypothetical data conditions is possible, but also to investigate the effects on the solution of e.g. aliasing, data distribution, noise and overdetermined problems. In this study only some of these aspects are considered. It is shown that aliasing can be a major error source. But one has to be careful with drawing conclusions from the simulations since the magnitude of the aliasing error strongly depends on the power in the high degrees of the potential, which is virtually unknown in reality.

The analytical error propagation mentioned before is tested by comparison with the errors obtained from the simulations. It is shown that this analytical error prediction works very well in case data noise is the major error source.

Also for some other effects, such as listed above, simple analytical models can be obtained, e.g. the use of the moving average operator in order to represent the smoothing of potential coefficients in case block averages are used. By using the same kind of models for our 2D world, and comparing them to the outcomes of the more realistic simulations, conclusions can be drawn about their validity.

appendix **A**

Coordinate frames and their transformations

WHEN FORMULATING THE GBVP in explicit formulas, coordinate frames have to be introduced. This also involves the need of the transformation equations between the different coordinate frames. In this appendix all the coordinate frames which are used in the text, are treated. Also the scheme of computation of the transformations between the coordinate frames is shown.

In the text tensor equations are used since they have the advantage of being the same in all possible coordinated frames. As notation the kernel-index notation is used as developed in (Schouten,1954). We choose this notation since it gives clear and compact formulas which can easily be transformed into a computer algorithm.

In the first part of this appendix some general properties and formulas for tensors are repeated. They will be used in the derivation of the formulas we need. A comprehensive treatment of tensors, and their application in geodesy, can be found in (Hotine, 1969).

A.1 Elementary formulas

We define the following kernel letters

x	coordinate
e	base vector
g	metric tensor
Γ	Christoffel symbol
δ	Kronecker delta

The Christoffel symbols are computed as

$$\Gamma^{\gamma}_{\alpha\beta} = \tfrac{1}{2} g^{\gamma\delta}(g_{\alpha\delta,\beta} + g_{\beta\delta,\alpha} - g_{\alpha\beta,\delta}). \tag{A.1}$$

If necessary for clarity, the index of the coordinates with respect to which the partial derivative is taken is preceded by a comma. The Einstein convention is used (summation over equal upper and lower indices) in all equations. The covariant derivative of a tensor of rank 0, 1 and 2 is:

$$\begin{aligned} W_{;\alpha} &= \tfrac{\partial W}{\partial x^\alpha} = W_{,\alpha} && \equiv W_\alpha \\ W_{\alpha;\beta} &= W_{\alpha,\beta} - \Gamma^\gamma_{\alpha\beta} W_\gamma && \equiv W_{\alpha\beta} \\ W_{\alpha\beta;\gamma} &= W_{\alpha\beta,\gamma} - \Gamma^\delta_{\alpha\gamma} W_{\delta\beta} - \Gamma^\delta_{\beta\gamma} W_{\delta\alpha} && \equiv W_{\alpha\beta\gamma}. \end{aligned} \tag{A.2}$$

The semicolon is used to indicate covariant differentiation. The tensors are transformed to another coordinate frame as

$$\begin{aligned} W_\alpha &= \frac{\partial x^a}{\partial x^\alpha} W_a \\ W_{\alpha\beta} &= \frac{\partial x^a}{\partial x^\alpha}\frac{\partial x^b}{\partial x^\beta} W_{ab} \\ W_{\alpha\beta\gamma} &= \frac{\partial x^a}{\partial x^\alpha}\frac{\partial x^b}{\partial x^\beta}\frac{\partial x^c}{\partial x^\gamma} W_{abc}. \end{aligned} \tag{A.3}$$

The relation between the contravariant and covariant components is

$$\begin{aligned} W^\alpha &= g^{\alpha\beta} W_\beta \\ W^{\alpha\beta} &= g^{\alpha\gamma} g^{\beta\delta} W_{\gamma\delta}. \end{aligned}$$

A.2 Coordinate frames

Several frames are used for the formulation of the GBVP. We start with two cartesian frames

$$\begin{aligned} \text{the equatorial frame} \quad & \{x^I, \quad I = 1,2\} \equiv \{X, Z\} \\ \text{the local frame} \quad & \{x^i, \quad i = 1,2\} \equiv \{x, z\} \ . \end{aligned}$$

As introduced here, and we will do the same for other frames, the coordinates $x^I, x^i, \ldots$ are also denoted by their more frequently used names. The equatorial frame is a Cartesian frame with its origin in the center of mass of the earth, the Z-axis pointing towards the North pole and the X-axis coinciding with the Z-axis rotated 90° degrees clockwise. The local frame is a Cartesian frame, with its origin in some local (terrestrial) point, the z-axis pointing outwards and the x-axis north. The exact orientation depends on the application. Generally, it will be aligned with the gravity vector $\boldsymbol{g}$ or with the normal gravity vector $\boldsymbol{\gamma}$. If necessary different local frames are discriminated by $x^i, x^{i'}$, etc. The general parameter ω is used to define the orientation of x^i w.r.t. x^I. In the applications of x^i the appropriate angle will be substituted. The two coordinate frames are shown in figure A.1.

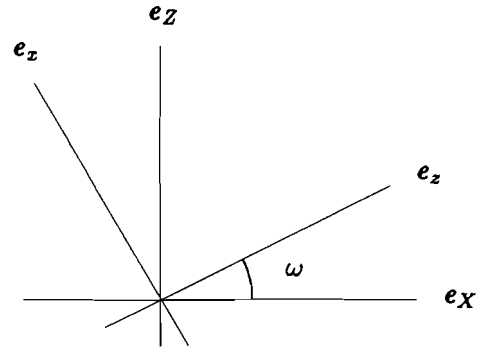

Figure A.1 *The equatorial and the local frame. The local frame here has an arbitrary orientation ω. For simplicity the origin of the local frame coincides with the equatorial frame, which will usually not be the case.*

Because of the circular, or more accurately the elliptical, structure of the earth and its gravity field, the following curvilinear coordinates are often used

$$\begin{aligned} \text{polar} \quad & \{x^\alpha, \quad \alpha = 1,2\} \equiv \{r, \bar{\phi}\} \\ \text{elliptical} \quad & \{x^a, \quad a = 1,2\} \equiv \{h, \phi\} \\ & \{x^A, \quad A = 1,2\} \equiv \{u, \beta\} \end{aligned}$$

The first two are directly connected with the approximation of the earth's potential: their first coordinates are directed along the lines of force of the circular respectively elliptical normal gravity field. The second elliptic coordinate system is primarily well suited for the normal potential and its derivatives. The particular convenience of the x^A is due to the fact that $x^{A=1} = constant$ defines an ellipse which is an equipotential line of the elliptic normal potential. The graphical interpretation of the three systems is given in figure A.2.

A.3 Transformation of the coordinates

When working with different coordinate frames transformations between the coordinates are indispensable. These relations will also be used for the derivation of the transformations of the tensors of the gravity field. The easiest connection of the frames is the computation of x^I from the coordinates refering to the other four frames. The relations are (see (Heiskanen & Moritz, 1967) or (Bakker et al., 1989)

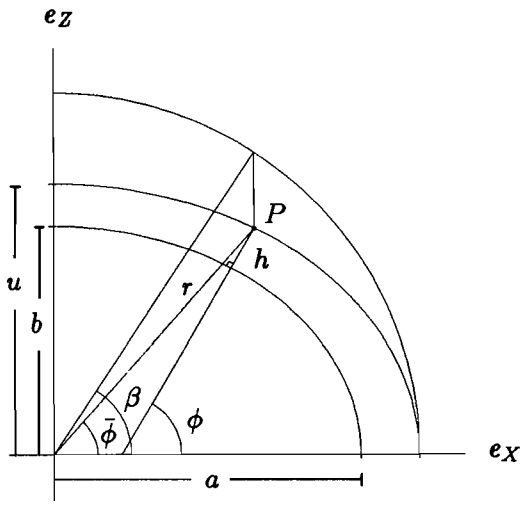

Figure A.2 *The three curvilinear frames.*

and figures A.1 and A.2)

$$\begin{array}{llll} x^I & x^\alpha & x^a & x^A \\ \hline X = r\cos\bar{\phi} = & & (N+h)\cos\phi = \sqrt{u^2+E^2}\cos\beta & \\ Z = r\sin\bar{\phi} = & (N(1-e^2)+h)\sin\phi = u\sin\beta. & & \end{array} \tag{A.4}$$

The local frame is connected to x^I by:

$$\begin{aligned} X &= -x\sin\omega + z\cos\omega \\ Z &= \quad x\cos\omega + z\sin\omega. \end{aligned} \tag{A.5}$$

In (A.4) the symbols N, E and e represent the corresponding quantities of the three dimensional coordinates:

$$N = \frac{a}{\sqrt{1-e^2\sin^2\phi}},$$

$$E = \sqrt{a^2-b^2}, \qquad e = \sqrt{\frac{a^2-b^2}{a^2}}. \tag{A.6}$$

Thereby a and b denote respectively the semi-major and semi-minor axis of the reference ellipse. The inverse relations of (A.4) are more complicated. For x^α and x^A we have

$$r = \sqrt{X^2+Z^2}, \quad \bar{\phi} = \arctan\frac{Z}{X},$$

$$u = \tfrac{1}{2}\sqrt{2}\sqrt{X^2 + Z^2 - E^2 + \sqrt{(X^2 + Z^2 - E^2)^2 + 4E^2Z^2}},$$
$$\beta = \arctan \frac{Z\sqrt{u^2 + E^2}}{uX}.$$

The transformation $x^I \rightarrow x^a$ can not be computed directly. It is computed by the iteration procedure

$$\begin{aligned} \phi_0 &= \arctan \frac{Z}{X}, \\ \phi_{n+1} &= \arctan \frac{Z + E^2 a \sin\phi_n}{X\sqrt{1 - E^2 \sin^2\phi_n}}, \\ h &= \frac{Z}{\sin\phi} - N(1 - e^2) \quad \text{or} \quad h = \frac{X}{\cos\phi} - N. \end{aligned} \tag{A.7}$$

Two formulas for h are given in (A.7). The choice depends on ϕ. Since this procedure does not give sufficient accuracy in all quadrants, the transformation is always computed in the first quadrant, and then rotated.

The backward transformation of the local coordinates is easy: the transformation matrix between these systems equals its own inverse.

A.4 Partial derivatives, metric tensors and Christoffel symbols

From the transformation equation (A.4) the partial derivatives of x^I with respect to the other frames can be computed straightforward as

$$\begin{aligned} \frac{\partial x^I}{\partial x^\alpha} &= \begin{pmatrix} \frac{\partial X}{\partial r} & \frac{\partial X}{\partial \bar{\phi}} \\ \frac{\partial Z}{\partial r} & \frac{\partial Z}{\partial \bar{\phi}} \end{pmatrix} = \begin{pmatrix} \cos\bar{\phi} & -r\sin\bar{\phi} \\ \sin\bar{\phi} & r\cos\bar{\phi} \end{pmatrix}, \\ \frac{\partial x^I}{\partial x^a} &= \begin{pmatrix} \frac{\partial X}{\partial h} & \frac{\partial X}{\partial \phi} \\ \frac{\partial Z}{\partial h} & \frac{\partial Z}{\partial \phi} \end{pmatrix} = \begin{pmatrix} \cos\phi & -(N+h)\sin\phi + N_\phi\cos\phi \\ \sin\phi & (N(1-e^2)+h)\cos\phi + N_\phi(1-e^2)\sin\phi \end{pmatrix}, \\ \frac{\partial x^I}{\partial x^A} &= \begin{pmatrix} \frac{\partial X}{\partial u} & \frac{\partial X}{\partial \beta} \\ \frac{\partial Z}{\partial u} & \frac{\partial Z}{\partial \beta} \end{pmatrix} = \begin{pmatrix} \frac{u}{v}\cos\beta & -v\sin\beta \\ \sin\beta & u\cos\beta \end{pmatrix}. \end{aligned} \tag{A.8}$$

We use the symbols

$$N_\phi = \frac{\partial N}{\partial \phi} = \frac{Ne^2 \sin\phi\cos\phi}{1 - e^2\sin^2\phi},$$
$$v = \sqrt{u^2 + E^2}.$$

These two by two matrices can be inverted easily. It is

$$\frac{\partial x^\alpha}{\partial x^I} = \begin{pmatrix} \frac{\partial \bar{r}}{\partial X} & \frac{\partial \bar{r}}{\partial Z} \\ \frac{\partial \bar{\phi}}{\partial X} & \frac{\partial \bar{\phi}}{\partial Z} \end{pmatrix} = \begin{pmatrix} \cos\bar{\phi} & \sin\bar{\phi} \\ -\frac{1}{\bar{r}}\sin\bar{\phi} & \frac{1}{\bar{r}}\cos\bar{\phi} \end{pmatrix},$$

$$\frac{\partial x^a}{\partial x^I} = \begin{pmatrix} \frac{\partial h}{\partial X} & \frac{\partial h}{\partial Z} \\ \frac{\partial \phi}{\partial X} & \frac{\partial \phi}{\partial Z} \end{pmatrix} = \frac{1}{(N+h) - e^2 N \cos^2\phi - \sin\phi\cos\phi e^2 N_\phi} \cdot$$

$$\begin{pmatrix} (N(1-e^2)+h)\cos\phi + N_\phi(1-e^2)\sin\phi & (N+h)\sin\phi - N_\phi\cos\phi \\ -\sin\phi & \cos\phi \end{pmatrix},$$

$$\frac{\partial x^A}{\partial x^I} = \begin{pmatrix} \frac{\partial u}{\partial X} & \frac{\partial u}{\partial Z} \\ \frac{\partial \beta}{\partial X} & \frac{\partial \beta}{\partial Z} \end{pmatrix} = \frac{v}{L^2} \begin{pmatrix} u\cos\beta & v\sin\beta \\ -\sin\beta & \frac{u}{v}\cos\beta \end{pmatrix}, \tag{A.9}$$

with

$$L = \sqrt{u^2 + E^2 \sin^2\beta}.$$

For the local frame we have from (A.5)

$$\frac{\partial x^I}{\partial x^i} = \begin{pmatrix} \frac{\partial X}{\partial x} & \frac{\partial X}{\partial z} \\ \frac{\partial Z}{\partial x} & \frac{\partial Z}{\partial z} \end{pmatrix} = \frac{\partial x^i}{\partial x^I} = \begin{pmatrix} \frac{\partial x}{\partial X} & \frac{\partial x}{\partial Z} \\ \frac{\partial z}{\partial X} & \frac{\partial z}{\partial Z} \end{pmatrix} = \begin{pmatrix} -\sin\omega & \cos\omega \\ \cos\omega & \sin\omega \end{pmatrix}. \tag{A.10}$$

From the partial derivatives the metric tensors can be computed. When we know the components of the metric tensor in one coordinate system, the components in the other systems can be computed using the transformation equation (A.3). Since x^I and x^i are Cartesian coordinates their metric tensors are

$$g^{IJ} = \delta^{IJ}, \qquad g^{ij} = \delta^{ij}.$$

Using g^{IJ} and g_{IJ} as starting-point we have

$$g^{\alpha\beta} = \frac{\partial x^\alpha}{\partial x^I}\frac{\partial x^\beta}{\partial x^J}\, g^{IJ} = \begin{pmatrix} 1 & 0 \\ 0 & \frac{1}{r^2} \end{pmatrix},$$

$$g_{\alpha\beta} = \frac{\partial x^I}{\partial x^\alpha}\frac{\partial x^J}{\partial x^\beta}\, g_{IJ} = \begin{pmatrix} 1 & 0 \\ 0 & r^2 \end{pmatrix}, \tag{A.11}$$

$$g^{ab} = \frac{\partial x^a}{\partial x^I}\frac{\partial x^b}{\partial x^J}\, g^{IJ} = \begin{pmatrix} 1 & 0 \\ 0 & \left(\frac{N(1-e^2)+h(1-e^2\sin^2\phi)}{1-e^2\sin^2\phi}\right)^2 \end{pmatrix},$$

$$g_{ab} = \frac{\partial x^I}{\partial x^a}\frac{\partial x^J}{\partial x^b}\, g_{IJ} = \begin{pmatrix} 1 & 0 \\ 0 & \left(\frac{1-e^2\sin^2\phi}{N(1-e^2)+h(1-e^2\sin^2\phi)}\right)^2 \end{pmatrix},$$

$$g^{AB} = \frac{\partial x^A}{\partial x^I}\frac{\partial x^B}{\partial x^J}\, g^{IJ} = \begin{pmatrix} \frac{v^2}{L^2} & 0 \\ 0 & \frac{1}{L^2} \end{pmatrix}, \tag{A.12}$$

$$g_{AB} = \frac{\partial x^I}{\partial x^A}\frac{\partial x^J}{\partial x^B}\, g_{IJ} = \begin{pmatrix} \frac{L^2}{v^2} & 0 \\ 0 & L^2 \end{pmatrix}.$$

The next step is the computation of the Christoffel symbols. The only components different from zero are, according to (A.1),

$$\begin{aligned}
\Gamma^\gamma_{\alpha\beta}: \quad & \Gamma^2_{12} = \Gamma^2_{21} = \tfrac{1}{r}, && \Gamma^1_{22} = -r, \\
\Gamma^c_{ab}: \quad & \Gamma^2_{12} = \Gamma^2_{21} = \frac{1-e^2\sin^2\phi}{N(1-e^2)+h(1-e^2\sin^2\phi)}, \\
& \Gamma^1_{22} = -\frac{N(1-e^2)+h(1-e^2\sin^2\phi)}{1-e^2\sin^2\phi}, \\
& \Gamma^2_{22} = \frac{3(1-e^2)\sin\phi\cos\phi e^2 N}{(1-e^2\sin^2\phi)(N(1-e^2)+h(1-e^2\sin^2\phi))}, \\
\Gamma^C_{AB}: \quad & \Gamma^1_{11} = \tfrac{u}{v^2L^2}E^2\cos^2\beta, && \Gamma^2_{11} = -\tfrac{E^2}{v^2L^2}\cos\beta\sin\beta, \\
& \Gamma^1_{12} = \Gamma^1_{21} = \tfrac{E^2}{L^2}\cos\beta\sin\beta, && \Gamma^2_{12} = \Gamma^2_{21} = \tfrac{u}{L^2}, \\
& \Gamma^1_{22} = -\tfrac{uv^2}{L^2}, && \Gamma^2_{22} = \tfrac{E^2}{L^2}\cos\beta\sin\beta.
\end{aligned} \tag{A.13}$$

As last step the covariant derivatives can be computed using (A.2). Since that gives rather lengthy expressions they are not written down here.

At the beginning of this appendix it was already noted that the kernel-index notation used here is especially suitable for computer implementation. We did compute most of the expressions presented here with a program for algebraic manipulations called REDUCE.

Before closing this appendix one remark about notation. As stated before the coordinates are now and then replaced by another single symbol. Also for the derivatives such a shorthand notation is used. For example we have for the components

of the gravity vector g with respect to the local frame

$$
\begin{aligned}
g &= \frac{\partial W}{\partial x^i}\, e_i = W^i\, e_i && \text{formal notation (with Einstein convention)} \\
&= W_i\, e_i && \text{numerical value of } W_i \text{ equals } W^i \\
&= \frac{\partial W}{\partial x}\, e_x + \frac{\partial W}{\partial z}\, e_z = W_x\, e_x + W_z\, e_z && \text{replacement of index by coordinate symbol.}
\end{aligned}
$$

We have to be careful with this simplification. Using the notation W_x or W_i for the contravariant components $W^{i=1}$ is not proper. But its use can be justified here by the fact that for Cartesian frames the contravariant and covariant components coincide. Whenever these components are identical we prefer to use the covariant (lower index) since its notation looks better (a kernel letter with only high indices looks like it can tumble down every moment). When working with curvilinear coordinates, the proper use of high and low indices is naturally maintained.

appendix **B**

Elliptical harmonics

AS WAS DONE IN POLAR COORDINATES in chapter 2, a series representation of the potential in elliptical coordinates can be obtained by solving Laplace's equation. We would prefer to have this series with the coordinates $\{h, \phi\}$. Unfortunately this gives a Laplace equation which can not be solved by separation (i.e. a solution of the form $V(h,\phi) = f(h) \cdot g(\phi)$). This makes it unsuitable for the solution of Dirichlet's problem: the computation of the potential from the prescribed values on the elliptical boundary. The coordinates $\{u, \beta\}$ are used instead. After the derivation of a series representation of the potential with the elliptical coordinates, a connection between the coefficients of these series and the series in polar coordinates is derived.

In (Gerontopoulos, 1978) and (Morse & Feshbach, 1953) the equation of Laplace is given as:

$$u\frac{\partial V}{\partial u} + (u^2 + E^2)\frac{\partial^2 V}{\partial u^2} + \frac{\partial^2 V}{\partial \beta^2} = 0. \tag{B.1}$$

The solution is sought by the substitution

$$V(u,\beta) = f(u) \cdot g(\beta).$$

This leads to

$$u\frac{f'(u)}{f(u)} + (u^2 + E^2)\frac{f''(u)}{f(u)} = -\frac{g''(\beta)}{g(\beta)} \equiv n^2 \qquad (n \in \mathrm{Z}). \tag{B.2}$$

This equation consists of two independent differential equations, each equal to the same constant. For this constant we took already a specific choice since other constants will lead to solutions for $g(\beta)$ not periodic with 2π. First the differential equation on the left hand side of (B.2) is solved. It is first transformed to other variables by

$$\eta = \ln(u + \sqrt{u^2 + E^2}) - \ln E \;\Rightarrow\; \sinh\eta = \frac{u}{E}, \quad \cosh\eta = \frac{\sqrt{u^2 + E^2}}{E}.$$

The transformation reduces the differential equation to

$$f''(\eta) - n^2 f'(\eta) = 0,$$

which is solved by

$$f(\eta) = \begin{cases} a_0 + a\eta & n = 0 \\ \\ a_n e^{n\eta} & n \neq 0 \end{cases}.$$

The other differential equation of (B.2) has the solution

$$g(\beta) = e^{in\beta}, \qquad n \in \mathrm{Z}$$

(omitting solutions not periodic with 2π). Now for V the solutions of (B.2) are

$$V_n = a_n e^{n(\eta + i\beta)}, \qquad n \neq 0,$$
$$V_0 = a_0 + a\eta.$$

A linear combination of particular solutions is also a solution of Laplace's equation, following from its linearity and homogeneity. This gives for the exterior domain:

$$V = -a\ln(u+v) + \sum_{n=-\infty}^{\infty} a_n \frac{1}{(u+v)^{|n|}} e^{in\beta}, \tag{B.3}$$

with $v = \sqrt{u^2 + E^2}$. Only the negative powers of $(u+v)$ are solutions for the exterior domain because we demand that the potential in the exterior domain tends asymptotically to the potential of a points mass for $u \to \infty$, see section 2.2.2. On the ellipse the variable u is equal to the length of the semi-minor axis of the ellipse; the series (B.3) become ordinary Fourier series, for which the coefficients can be computed easily. With dimensionless coefficients the series (B.3) are written as

$$V = -c\ln(u+v) + \sum_{n=-\infty}^{\infty} c_n \left(\frac{a+b}{u+v}\right)^{|n|} e^{in\beta}. \tag{B.4}$$

If the series (2.6) and (B.3) both converge to the same potential in the exterior domain, the coefficients of the series have to related. This relationship will be derived by expressing $\ln \frac{1}{\ell}$ in a series with polar coordinates and in a series with elliptical coordinates, as was shown in (Jekeli, 1988) for the three dimensional harmonics. The former series is derived in section 2.2.1, the latter below.

The distance between two points P and Q is computed as

$$\ell_{PQ} = \sqrt{(X_P - X_Q)^2 + (Z_P - Z_Q)^2}.$$

Insertion of the elliptical coordinates from (A.4) yields

$$\ell_{PQ} = (u_P^2 + u_Q^2 + E^2(\cos^2\beta_P + \cos^2\beta_Q) - 2(v_P v_Q \cos\beta_P \cos\beta_Q + u_P u_Q \sin\beta_P \sin\beta_Q))^{\frac{1}{2}}.$$

After some manipulations, this can be rewritten as

$$\ell_{PQ} = \frac{1}{2}\sqrt{1 + \left(\frac{u_Q + v_Q}{u_P + v_P}\right)^2 - 2\frac{u_Q + v_Q}{u_P + v_P}\cos(\beta_P - \beta_Q)} \cdot$$
$$\sqrt{1 + \left(\frac{v_Q - u_Q}{u_P + v_P}\right)^2 - 2\frac{v_Q - u_Q}{u_P + v_P}\cos(\beta_P + \beta_Q)} \cdot (u_P + v_P).$$

For the logarithm of the inverse distance it is

$$\ln\frac{1}{\ell_{PQ}} = -\frac{1}{2}\ln(1 - \frac{u_Q + v_Q}{u_P + v_P}e^{i(\beta_P - \beta_Q)}) - \frac{1}{2}\ln(1 - \frac{u_Q + v_Q}{u_P + v_P}e^{-i(\beta_P - \beta_Q)})$$
$$-\frac{1}{2}\ln(1 - \frac{v_Q - u_Q}{u_P + v_P}e^{i(\beta_P + \beta_Q)}) - \frac{1}{2}\ln(1 - \frac{v_Q - u_Q}{u_P + v_P}e^{-i(\beta_P + \beta_Q)}) - \ln\frac{u_P + v_P}{2}.$$

The logarithmic functions are expanded into a Taylor series, as we did for the polar coordinates. Convergence is guaranteed if $r_P > r_Q$. We obtain:

$$\ln\frac{1}{\ell_{PQ}} = -\ln\frac{u_P + v_P}{2} + \frac{1}{2}\sum_{\substack{n=-\infty \\ n\neq 0}}^{\infty}\frac{1}{|n|}\left(\frac{u_Q + v_Q}{u_P + v_P}\right)^{|n|}e^{in(\beta_P - \beta_Q)} +$$
$$+\frac{1}{2}\sum_{\substack{n=-\infty \\ n\neq 0}}^{\infty}\frac{1}{|n|}\left(\frac{v_Q - u_Q}{u_P + v_P}\right)^{|n|}e^{in(\beta_P + \beta_Q)}.$$

Or, with $\dfrac{v - u}{E} = \dfrac{E}{u + v}$,

$$\ln\frac{1}{\ell_{PQ}} = -\ln\frac{u_P + v_P}{2} +$$
$$+\frac{1}{2}\sum_{\substack{n=-\infty \\ n\neq 0}}^{\infty}\frac{E^{|n|}}{|n|}\left\{\left(\frac{u_Q + v_Q}{E}\right)^{|n|}e^{-in\beta_Q} + \left(\frac{E}{u_Q + v_Q}\right)^{|n|}e^{in\beta_Q}\right\}\frac{1}{(u_P + v_P)^{|n|}}e^{in\beta_P}.$$

Insertion of this expansion into (2.2) yields

$$V(P) = \sum_{\substack{n=-\infty \\ n\neq 0}}^{\infty}\frac{GE^{|n|}}{2|n|}\int_\Sigma \rho(Q)\left\{\left(\frac{u_Q + v_Q}{E}\right)^{|n|}e^{-in\beta_Q} + \left(\frac{E}{u_Q + v_Q}\right)^{|n|}e^{in\beta_Q}\right\}d\sigma_Q \cdot$$
$$\cdot\frac{1}{(u_P + v_P)^{|n|}}e^{in\beta_P} - G\int_\Sigma \rho(Q)d\sigma_Q \cdot \ln\frac{u_P + v_P}{2} + constant$$
$$= -\mu\ln\frac{u_P + v_P}{2} + \sum_{n=-\infty}^{\infty}a_n^{ell}\frac{1}{(u_P + v_P)^{|n|}}e^{in\beta_P}, \qquad \text{(B.5)}$$

with

$$\mu = G\int_\Sigma \rho(Q)d\sigma_Q,$$

$$a_n^{ell} = \frac{GE^{|n|}}{2|n|}\int_\Sigma \rho(Q)\left\{\left(\frac{u_Q+v_Q}{E}\right)^{|n|}e^{-in\beta_Q} + \left(\frac{E}{u_Q+v_Q}\right)^{|n|}e^{in\beta_Q}\right\}d\sigma_Q, \quad (B.6)$$

$$(n \neq 0),$$

a_0^{ell} arbitrary.

The Fourier series (B.5) are the same as (B.3). They only differ by the constant $\mu \ln 2$. The coefficient μ is equal to the μ used for the expansion in terms of polar coordinates.

To establish the relationship between the coefficients with respect to the series in polar coordinates, a_n^{cir}, and those for the elliptical coordinates, a_n^{ell}, the functions appearing in the integrals (2.8) and (B.6) have to be related. This is done by deriving a series expression for the basefunctions in one system with respect to the other system.

First two general series expressions are derived, which will be used to obtain the required relation. For two complex variables q and z the following relation is assumed:

$$q = \frac{1}{2}(z + z^{-1}). \quad (B.7)$$

The inverse of this relation is

$$z = q \pm \sqrt{q^2-1}, \qquad z^{-1} = q \mp \sqrt{q^2-1}. \quad (B.8)$$

From (B.7) and (B.8) a series is derived for q^n and z^n for $n > 0$. From (B.7) we obtain, using a binomial expansion,

$$q^n = \frac{1}{2^n}\sum_{k=0}^{n}\binom{n}{k}z^{n-k}z^{-k} = \frac{1}{2^n}\sum_{k=0}^{n}\binom{n}{k}z^{n-2k}$$

$$= \frac{1}{2^n}\sum_{k=0}^{w}\binom{n}{k}\left\{z^{n-2k}+z^{2k-n}\right\} + \underbrace{\frac{1}{2^n}\binom{n}{\frac{1}{2}n}}_{\text{only if } n \text{ even}}, \quad (B.9)$$

with $w = (n-1)/2$ (n odd) or $w = (n-2)/2$ (n even). From (B.8) is obtained

$$z^n + z^{-n} = \sum_{k=0}^{n}\binom{n}{k}\left\{q^{n-k}\sqrt{q^2-1}^{k} + q^{n-k}(-1)^k\sqrt{q^2-1}^{k}\right\}$$

$$
\begin{aligned}
&= \sum_{k=0}^{t} \binom{n}{2k} q^{n-2k}(q^2-1)^k \\
&= \sum_{k=0}^{t} \binom{n}{2k} q^{n-2k} \sum_{l=0}^{k} \binom{k}{l} q^{2k-2l}(-1)^l \\
&= \sum_{l=0}^{t} q^{n-2l} \underbrace{(-1)^l \sum_{k=l}^{t} \binom{n}{2k} \binom{k}{l}}_{\equiv A_{nl}},
\end{aligned}
\tag{B.10}
$$

with $t = (n-1)/2$ (n odd) or $t = n/2$ (n even).

The basefunctions in polar coordinates and those in elliptical coordinates are linked by

$$
\frac{r}{E}e^{-i\phi} = \frac{X - iZ}{E} = \frac{v\cos\beta - iu\sin\beta}{E} = \frac{1}{2}\left(\frac{E}{u+v}e^{i\beta} + \frac{u+v}{E}e^{-i\beta}\right). \tag{B.11}
$$

When putting

$$
q = \frac{r}{E}e^{-i\phi}, \qquad z = \frac{u+v}{E}e^{-i\beta},
$$

(B.7) is equivalent to (B.11) and the following relations hold:

$$
r^{|n|}e^{-in\phi} = \begin{cases} E^n q^n & n \geq 0 \\ E^{|n|}\overline{q}^{|n|} & n \leq 0 \end{cases},
$$

$$
\left(\frac{u+v}{E}\right)^{|n|} e^{-in\beta} = \begin{cases} z^n & n \geq 0 \\ \overline{z}^{|n|} & n \leq 0 \end{cases},
$$

$$
\left(\frac{E}{u+v}\right)^{|n|} e^{in\beta} = \begin{cases} z^{-n} & n \geq 0 \\ \overline{z}^{-|n|} & n \leq 0 \end{cases}.
$$

Thereby the overbar denotes the complex conjugate. With the definitions of q and z, and the relations stated above, the basefunctions in polar coordinates are expressed with (B.10) as

$$
r^{|n|}e^{-in\phi} = \left(\frac{E}{2}\right)^{|n|} \sum_{k=0}^{w} \binom{|n|}{k} \left[\left(\frac{u+v}{E}\right)^{|n|-2k} \begin{cases} e^{-i(n-2k)\beta} \\ e^{i(|n|-2k)\beta} \end{cases} + \right.
$$

$$+\left(\frac{E}{u+v}\right)^{|n|-2k}\left\{\begin{array}{c} e^{i(n-2k)\beta} \\ \\ e^{-i(|n|-2k)\beta}\end{array}\right\}\Bigg]\underbrace{+\left(\frac{E}{2}\right)^{|n|}\binom{n}{\frac{1}{2}n}}_{n\text{ even}}\quad\left\{\begin{array}{l} n>0 \\ \\ n<0\end{array}\right. \tag{B.12}$$

with the definition of w as before. Insertion of (B.12) into (2.8) yields

$$a_n^{cir}=\frac{G}{2|n|}\int_\Sigma \rho(Q)\left[\left(\frac{E}{2}\right)^{|n|}\sum_{k=0}^{w}\binom{|n|}{k}\left\{\begin{array}{l}\left(\frac{u+v}{E}\right)^{|n-2k|}e^{-i(n-2k)\beta}+ \\ \left(\frac{u+v}{E}\right)^{|n+2k|}e^{-i(n+2k)\beta}+\end{array}\right.\right.$$

$$\left.\left.\begin{array}{l}+\left(\frac{E}{u+v}\right)^{|n-2k|}e^{i(n-2k)\beta} \\ +\left(\frac{E}{u+v}\right)^{|n+2k|}e^{i(n+2k)\beta}\end{array}\right\}\underbrace{+\left(\frac{E}{2}\right)^{|n|}\binom{n}{\frac{1}{2}n}}_{n\text{ even}}\right]d\sigma_Q\quad\left\{\begin{array}{l} n>0 \\ \\ n<0\end{array}\right. .$$

With (B.6), this finally gives for the relation between the coefficients

$$a_n^{cir}=\frac{1}{|n|}\left(\frac{E}{2}\right)^{|n|}\sum_{k=0}^{w}\binom{|n|}{|k|}\frac{1}{E^{|n-2k|}}a_{n-2k}^{ell}\underbrace{+\frac{1}{2n}\left(\frac{E}{2}\right)^{|n|}\binom{|n|}{\frac{1}{2}|n|}\mu}_{n\text{ even}}. \tag{B.13}$$

Where $w=(n-1)/2$ (n odd) or $w=(n-2)/2$ (n even) for positive n and $w=(n+1)/2$ (n odd) or $w=(n+2)/2$ (n even) for negative n. In that case, k runs from zero down to w. For normalized and dimensionless coefficients the relation becomes with (2.15) and (B.4),

$$c_n^{cir}=\left(\frac{a+b}{2R}\right)^{|n|}\sum_{k=0}^{w}\binom{|n|}{|k|}\left(\frac{E}{a+b}\right)^{|2k|}\frac{|n-2k|}{|n|}c_{n-2k}^{ell}\underbrace{+\frac{1}{2n}\left(\frac{E}{2R}\right)^{|n|}\binom{|n|}{\frac{1}{2}|n|}c}_{n\text{ even}}. \tag{B.14}$$

For the elliptical functions it is found by (B.10)

$$\left(\frac{u+v}{E}\right)^{|n|}e^{-in\beta}+\left(\frac{E}{u+v}\right)^{|n|}e^{in\beta}=\sum_{l=0}^{t}\left(\frac{r}{E}\right)^{|n|-2l}\left\{\begin{array}{c} e^{-i(n-2l)\phi} \\ \\ e^{i(|n|-2l)\phi}\end{array}\right\}A_{nl}\quad\left\{\begin{array}{l} n>0 \\ \\ n<0\end{array}\right. . \tag{B.15}$$

Substitution of (B.15) into (B.6) yields

$$a_n^{ell}=\frac{G}{2|n|}\int_\Sigma \rho(Q)\left[\sum_{l=0}^{t}\left\{\begin{array}{l}\left(\frac{r}{E}\right)^{|n-2l|}e^{-i(n-2l)\phi} \\ \left(\frac{r}{E}\right)^{|n+2l|}e^{-i(n+2l)\phi}\end{array}\right\}A_{nl}\right]d\sigma_Q\quad\left\{\begin{array}{l} n>0 \\ \\ n<0\end{array}\right. .$$

With (2.7) we find

$$a_n^{ell} = E^{|n|} \sum_{l=0}^{t} \frac{1}{E^{|n-2l|}} \frac{|n-2l|}{|n|} A_{|n|,|l|}\, a_{n-2l}^{cir}. \tag{B.16}$$

With $t = (n-1)/2$ (n odd) or $t = n/2$ (n even) for positive n and $t = (n+1)/2$ (n odd) or $t = n/2$ (n even) for negative n. For A_{nl} we have

$$A_{nl} = (-1)^l \sum_{k=l}^{t} \binom{n}{2k} \binom{k}{l}.$$

In the summation of (B.16) k assumes negative values for n negative. The relation for normalized and dimensionless coefficients becomes, with (2.15) and (B.4),

$$c_n^{ell} = \left(\frac{R}{a+b}\right)^{|n|} \sum_{l=0}^{t} \left(\frac{E}{R}\right)^{|2l|} \frac{|n-2l|}{|n|} A_{|n|,|l|}\, c_{n-2l}^{cir}. \tag{B.17}$$

A potential which is bandlimited in the elliptical series, does not have this property in the circular series (and vice versa). It is easily seen from (B.14) that there is no upper limit for n such that c_n^{cir} vanishes. Although this is somewhat inconvenient, it does not give serious problems in computation of the coefficients c_n^{cir} . This can be seen be writing (B.14) as (for $n > 0$)

$$c_n^{cir} = c_n^{ell} + \frac{1}{4}(n-2)e^2 c_{n-2}^{ell} + \frac{1}{32}(n-1)(n-4)e^4 c_{n-4}^{ell} + \cdots + \underbrace{\frac{e^n}{n2^{2+1}} \binom{n}{\frac{1}{2}n}}_{n \text{ even}}.$$

This series converges fast for low degree c_n^{cir} if there is not very much power in the high degree coefficients. For higher degree coefficients the convergence can be much slower. In figure B.1 this is elucidated by plotting the magnitude of the first five terms of summation (B.12), where $c_n^{ell} = 1/n$ was assumed. As the real power in the coefficients is lower, this result is somewhat pessimistic.

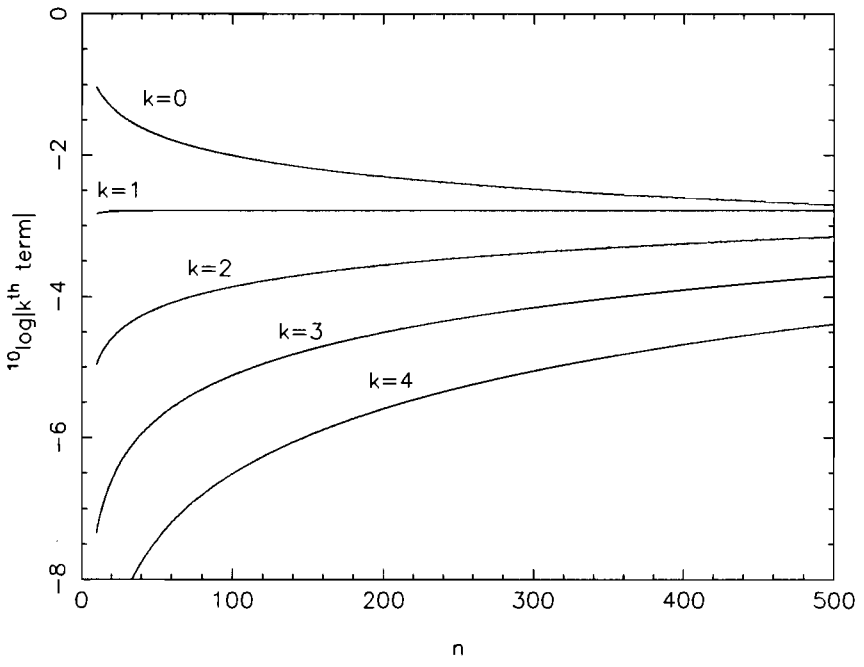

Figure B.1 *The magnitude of the first five terms of the transformation from elliptical to circular potential coefficients. For the elliptical coefficients,* $c_n^{ell} = 1/n$ *was taken.*

References

Baarda, W. (1968), A testing procedure for use in geodetic networks, Netherlands geodetic commission, new series, vol. **2**, nr. 5

Baarda, W. (1979), A connection between geometric and gravimetric geodesy, a first sketch, Netherlands Geodetic Commission, Publ. on geodesy, new series, vol. 6, number **4**

Backus, G.A. (1968), Application of a non-linear boundary value problem for Laplace's equation to gravity and geomagnetic intensity survey, *Quar. Jour. Mech. and Appl. Math.*, **21**, 195–221

Baeyer, J.J. (1861), *Grösse and Figur der Erde*, Georg Reimer, Berlin

Bakker, G., G. Strang van Hees (1989), *A course on radio positioning*, Delft University Press

Clarke, A.R. (1880), *Geodesy*, Clarendon Press, Oxford

Courant, R., D. Hilbert (1957), *Methods of mathematical physics*, Princeton University Press

Cruz, J.Y. (1986), Ellipsoidal corrections to potential coefficients obtained from gravity anomaly data on the ellipsoid, Ohio State University, Department of Geodetic Science, report **371**

Dermanis, A. (1984), The geodetic boundary value problem linearized with respect to the Somigliana-Pizetti normal field, *Man. Geod.*, **9**, 77–92

Gerontopoulos, P. (1978), Molodensky's problem in the plane, Mitteilungen der geodätischen Institute der TU Graz, Folge **32**

Gleason, D.M. (1988), Comparing ellipsoidal corrections to the transformation between the geopotential's spherical and ellipsoidal spectrums, *Man. Geod.*, **13**, 114–129

Gradshteyn, I.S., I.M. Ryzhik (1980), *Table of integrals, series and products*, Academic Press, New York

Grafarend, E.W., W. Niemeier (1971), The free nonlinear boundary value problem, *Bull. Géod.*, **45**, 243–262

Grafarend, E.W., B. Schaffrin (1986), The overdetermined geodetic boundary value problem, Proc. int. symp. figure and dynamics of the earth, moon and planets, Prague

Haasbroek, N.D. (1968), Gemma Frisius, Tycho Brahe and Snellius and their triangulations, Publication of the Netherlands geodetic commission

Heck, B. (1988), The non–linear geodetic boundary value problem in quadratic approximation, *Man. Geod.*, **13**, 337–348

Heck, B., (1989a), On the non-linear geodetic boundary value problem for a fixed boundary surface, *Bull. Géod.*, **63**, 57–67

Heck, B. (1989b), A contribution to the scalar free boundary value problem of physical geodesy, *Man. Geod.*, **14**, 87–99

Heck, B. (1991), On the linearized boundary value problems of physical geodesy, Ohio State University, Department of Geodetic Science, report **407**

Heiskanen, W.A., H. Moritz (1967), *Physical geodesy*, Freeman

Holota, O. (1982), Mixed boundary value problems in physical geodesy, proceedings of the symposium 'Figure and dynamics of the earth, moon and planets', Prague

Holota, P. (1989), Higher order theories in the solution of bvp's of physical geodesy by means of succesive approximations, Presented at II Hotine-Marussi symposium

Hörmander, L. (1976), The boundary problems of physical geodesy, *Arch. Rat. Mech. Anal.*, **62**, 1–52

Hotine, M. (1969), *Mathematical Geodesy*, ESSA Monograph **2**, US Dept. of commerce, Washington

Jekeli, C. (1988), The exact transformation between ellipsoidal and spherical harmonic expansions, *Man. Geod.*, **13**, 106–113

Jenkins, W., D.G. Watts (1968), *Spectral analysis and its applications*, Holden-Day

Kellogg, O.D. (1929), *Foundations of potential theory*, Ungar

Knickmeyer, E.H. (1984), Eine approximative Lösung der allgemeinen linearen geodätischen Randwertaufgabe durch Reihenentwicklungen nach Kugelfunktionen, DGK reihe C, **304**, München

Koch, K.R., A.J. Pope (1972), Uniqueness and existence for the geodetic boundary value problem using the known surface of the earth, **Bull. Géod., 46**, 467–476

Krarup, T. (1971), Molodensky letters, unpublished

Krarup, T. (1981), A convergence problem in collocation theory, *Boll. Géod. e Sci. Aff.*, **3**, 225–241

Lelgemann, D. (1970), Untersuchungen zu einer genaueren Lösung des Problems von Stokes, DGK reihe C, **155**, München

Mainville, A. (1986), The altimetry-gravimetry boundary value problem, Ohio State University, Department of Geodetic Science, report **373**

Mayer, E. (1876), Gestalt und Grösse der Erde, *Mitteilungen aus dem Gebiete des Seewesens*

Mikhlin, S.G. (1970), *Mathematical physics, an advanced course*, North-Holland

Molodensky, M.S., V.F. Eremeev, M.I. Yurkina (1962), *Methods for the study of the external gravitational field and figure of the earth*, Israel program for scientific translations, Jerusalem

Moritz, H., (1968), Linear solutions of the geodetic boundary value problem, DGK Reihe A, **58**, München

Moritz, H. (1969), Nonlinear solutions of the geodetic boundary-value problem, Ohio State University, Department of Geodetic Science, report **126**

Moritz, H. (1972), Convergence of Molodensky's series, Ohio State University, Department of Geodetic science, report **183**

Moritz, H. (1980), *Advanced physical geodesy*, Wichmann, Karlsruhe

Moritz, H. (1990), *The figure of the earth*, Wichmann, Karlsruhe

Morse, P.M., H. Feshbach (1953), *Methods of mathematical physics*, McGraw-Hill, New York

Papoulis, A. (1962), *The Fourier-transform and its applications*, McGraw-Hill

Rapp, R.H., N.K. Pavlis (1990), The development and analysis of geopotential coefficient models to spherical harmonic degree 360, *J. of Geoph. Res.*, **95**, B13, 21,885–21,911

Rikitake, T., R. Sato, Y. Hagiwara (1987), *Applied mathematics for earth scientists*, Reidel

Rummel, R., P.J.G. Teunissen (1982), A connection between geometric and gravimetric geodesy – some remarks on the role of the gravity field, In:*Daar heb ik veertig jaar over nagedacht*, vol. II, Delft

Rummel, R., P.J.G. Teunissen (1986), Geodetic boundary value problem and linear inference, proceedings of the symposium 'Figure and dynamics of the earth, moon and planets', Prague

Rummel, R. (1988), Zur iterativen Lösung der geodätischen Randwertaufgabe, in: Festschrift Rudolf Sigl, DGK reihe B, heft **287**

Rummel R., R. Rapp, H. Sünkel, C. Tscherning (1988), Comparison of global topographic/isostatic models to the earth's observed gravity field, Ohio State University, Department of geodetic science, report **388**

Rummel, R., P. Teunissen, M. v. Gelderen (1989a), Uniquely and overdetermined geodetic boundary value problems by least squares, *Bull. Géod.*, **63**, 1–33

Rummel, R., P. Teunissen (1989b), Horizontal boundary value problems, LS collocation and astronomic levelling, Medd. nr. **58**, Festschrift to Torben Krarup, ed.: E. Kejlso

Sansò, F., F. Sacerdote (1983), A contribution to the analysis of the altimetry-gravimetry problem, proceedings of the symposium 'Figure and dynamics of the earth, moon and planets', Prague

Sacerdote, F., F. Sansò (1985), Overdetermined boundary value problems in physical geodesy, *Man. Geod.*, **10**, 195–207

Sacerdote, F., F. Sanso (1986), The scalar boundary value problem of physical geodesy, *Man. Geod.*, **11**, 15–28

Sansò, F. (1977), The geodetic boundary value problem in gravity space, *Atti della Accademia Nazionale dei Lincei*, serie VIII, volume **XIV**

Sansò, F. (1988), The Wiener integral and the overdetermined boundary value problem's of physical geodesy, *Man. Geod.*, **13**, 75–98

Schouten, J.A. (1954), *Ricci calculus*, 2nd ed., Springer Verlag, Berlin

Stokes, G.G. (1849), On the variation of gravity at the surface of the earth, *Trans. Camb. Phil. Soc.*, **8**, 672–695

Stokes, G.G. (1854), *A Smith's prize paper*, Cambridge University Calendar

Strang, G. (1986), *Introduction to applied mathematics*, Wellesley-Cambridge press, Wellesley

Svensson, S.L. (1983), Solution of the altimetry-gravimetry problem, *Bull. Géod.*, **57**, 332–353

Varga, R.S. (1962), *Matrix iterative analysis*, Prentice–Hall, Englewood Cliffs

Vening Meinesz, F.A. (1928), A formula expressing the deflection of the plumb-line in the gravity anomalies and some formulae for the gravity-field and the gravity-potential outside the geoid, Proceedings of the Koninklijke Akademie van Wetenschappen, **31**, 3, Amsterdam

Walter, W. (1971), *Einfürung in die Potentialtheorie*, Bibliographisch Institut, Berlin

Wilford, J.N. (1981), *The mapmakers*, Knopf, New York

Witsch, K.J. (1985), On a free boundary value problem of physical geodesy, I (uniqueness), *Math. Meth. in the Appl. Sci.*, **7**, 269–289

Witsch, K.J. (1986), On a free boundary value problem of physical geodesy, II (existence), *Math. Meth. in the Appl. Sci.*, **8**, 1–22